Graphene-based flexible sensors towards electronic wearables

by

Seval Ören

A dissertation submitted to the graduate faculty

in partial fulfillment of the requirements for the degree of

DOCTOR OF PHILOSOPHY

Major: Electrical Engineering
(Microelectronics and Photonics & Electromagnetics Microwave and Nondestructive Evaluation)

Program of Study Committee:
Liang Dong, Co-major Professor
Halil Ceylan, Co-major Professor
Jiming Song
Nathan M. Neihart
Meng Lu

The student author, whose presentation of the scholarship herein was approved by the program of study committee, is solely responsible for the content of this dissertation. The Graduate College will ensure this dissertation is globally accessible and will not permit alterations after a degree is conferred.

Iowa State University

Ames, Iowa

2018

TABLE OF CONTENTS

NOMENCLATURE iv
ACKNOWLEDGEMENTS v
ABSTRACT vii
CHAPTER 1 GENERAL INTRODUCTION 1
1.1 Background 1
1.2 Introduction 3
1.2.1 Graphene patterning and transferring methods 4
1.2.2 Stretchable and flexible graphene strain sensors 9
1.2.2 Graphene-oxide film formation on flexible substrates for RH sensing applications 12
1.3 Problem Statement 15
1.4 Thesis Organizations 18
CHAPTER 2 HIGH-RESOLUTION PATTERNING AND TRANSFERRING OF GRAPHENE-BASED NANOMATERIALS ONTO TAPE TOWARD ROLL-TO-ROLL PRODUCTION OF TAPE-BASED WEARABLE SENSORS 19
2.1 Abstract 19
2.2 Introduction 20
2.3 Results and Discussion 25
2.3.1 Micro Scale Patterning and Transferring 25
2.3.2 Application Demonstrations 33
2.3.2.1 On-Tape Strain Sensors 33
2.3.2.2 On-Tape Pressure Sensors 35
2.3.2.3 Smart Glove 37
2.3.2.4 On-Tape Plant Leaf Sensors 39
2.4 Conclusion 42
2.5 Acknowledgements 43
2.6 References 43
CHAPTER 3 HELICAL- SHAPED GRAPHENE TUBULAR SPRING FORMED WITHIN MICROCHANNEL FOR WEARABLE STRAIN SENSOR WITH WIDE DYNAMIC RANGE 52
3.1 Abstract 52
3.2 Introduction 52
3.3 Method 54
3.4 Results and Discussion 57
3.5 Conclusions 62
3.6 Acknowledgements 62
3.7 References 62
CHAPTER 4 TRACKING OF WATER MOVEMENT DYNAMICS INSIDE PLANTS USING LEAF SURFACE HUMIDITY SENSORS 66
4.1 Abstract 66
4.2 Introduction 66
4.3 Device Principle and Design 68
4.4 Device Fabrication and Installation 70
4.5 Experimental Results 73
4.6 Conclusions 75

4.7 Acknowledgements 75
4.8 References 75
CHAPTER 5 CONCLUSIONS AND OUTLOOK 77
5.1 Conclusions 77
5.2 Outlook 79
REFERENCES 80
APPENDIX SUPPORTING INFORMATION 88

NOMENCLATURE

AC	Alternating Current
CNT	Carbon Nanotubes
CVD	Chemical Vapor Deposition
D^2SP	Drop Cast Dry Stick
DC	Direct Current
FQM	Fluorescence Quenching Microscopy
GNRs	Graphene Nanoribbons
GO	Graphene Oxide
GQDs	Graphene Quantum Dots
IDEs	Interdigitated Electrodes
PDMS	Polydimethylsiloxane
PEN	Polyethylene Naphthalate
rGO	Reduced Graphene Oxide
RH	Relative Humidity
SEM	Scanning Electron Microscopy
ST	Stick and Transfer
UV	Ultraviolet
WUE	Water Use Efficiency
$\Delta R/R$	Relative Resistance Change of the sensor
2D	Two-dimensional

ACKNOWLEDGEMENTS

It has been fortunate to be a graduate student and meet so many lovely people at Iowa State University. I would like to thank all the people who have helped and supported me for my dissertation and further.

First of all, I want to express my deepest gratitude to my advisors Professors Liang Dong and Halil Ceylan for their guidance and continuous encouragement throughout my Ph.D. journey. I would also like to specially thank them for their invaluable support and encouragement to continue my Ph.D. during my harsh times I had, which changed direction of my life a lot. I will be forever grateful for their strong support, guidance, and encouragement in my research and my personal life.

Thanks to all members of my thesis committee, Dr. Jiming Song, Dr. Nathan. M. Neihart, and Dr. Meng Lu for discussing my thesis and providing invaluable feedback to make it better.

I would like to thank my colleagues at Laboratory for Mems and Biochips research group, Dr. Huawei Jiang, Dr. Peng Liu, Dr. Qiugu Wang, Dr. Md Azahar Ali, Dr. Zhen Xu, Yifei Wang, Yuncong Chen, Xinran Wang, Xuan Qiao, Yueyi Jiao, Junhao Zhu, Shawana Tabassum, and Praveen Gurrala for their friendship and assistance. It was a great pleasure to be included in this research team. I would also like to thank Shuo Yang for his collaboration regarding graphene strain sensors experiments on concretes. Thanks to Leland Harker for his strong help in terms of manufacturing parts and circuits and to Lisa Coffey for growing the plants for experimental studies. I wish you all the best in all aspects of your life.

I would like to acknowledge the funding support from Iowa Department of Transportation, Iowa Highway Research Board, Iowa Corn Promotion Board, and Plant Sciences Institute at Iowa State University through PSI Faculty Scholar program, and U.S. National

Science Foundation (Award #: DBI 1353819), and U.S. Department of Agriculture (Award #: 2017-67013-26463).

Special thanks to Turkish Council of High Education and Anadolu University in Turkey for financial support that enabled this research.

My heartfelt thanks go to my beloved family. To my lovely parents, Mehmet Oren and Zeynep Oren, for taking care of, supporting, and encouraging me towards difficulties ever since the day I was born. Special thanks to my lovely sister, my best friend, Duygu Oren, for making me always strong with her precious, ever-lasting support. My thanks also go to my little cousin, Rabia Kocagoz, who was born when I was far away. Watching her videos made me blissful and gave incredible motivation to work even harder. Finally, I would like to thank to my precious grandparents, Ulfet Kocagoz and Mustafa Kocagoz, who always motivated me with their endearments and lovely prayers.

ABSTRACT

Flexible electronics and wearable devices have attracted considerable attention due to their mechanical liberty, in terms of flexibility and stretchability that can enable the possibility of a wide range of new applications. The term “wearable electronics” can be used to define devices that can be worn or mated with the sensed surface to continuously monitor signals without limitations on mechanical deformability of the devices and electronic performance of the functional materials. The use of polymeric substrates or other nonconventional substrates as base materials brings novel functionalities to sensors and other electronic devices in terms of being flexible and light weight. As functional materials, conductive nanomaterials, such as carbon nanotubes and graphene have been utilized for flexible electronics and wearable devices. Graphene has specifically been considered for producing next-generation sensors due to its impressive electrical and mechanical properties. As a result, incorporation of flexible substrates and graphene-based nanomaterials has been widely utilized to form versatile flexible sensors and other wearable devices through use of different fabrication processes.

Creation of a large-scale, simple, high-resolution and cost-effective technique that overcomes fabrication limitations and supports production of flexible graphene-based sensors with high flexibility and stretch ability is highly demanding. Soft lithography can be merged with a mechanical exfoliation process using adhesive tape followed by transfer printing to form a graphene sensor on a desired final substrate. *In situ* microfluidic casting of graphene into channels is another promising platform driving the rapid development of flexible graphene sensors and wearable devices with a wide dynamic detection range. Selective coating of graphene-based nanomaterials (e.g. graphene oxide (GO)) on flexible electrode tapes can,

because of its flexibility and adhesive features, be used to track relative humidity (RH) variations at the surface of target surfaces. This thesis describes the design and development of flexible and wearable strain, pressure and humidity sensors based on a novel tape-based cost-effective patterning and transferring technique, an *in situ* microfluidic casting method, and a novel selective coating technique for graphene-based nanomaterials.

First of all, we present a tape-based graphene patterning and transferring approach to production of graphene sensors on adhesive tapes. The method utilizes the work of adhesion at the interface between two contacting materials as determined by their surface energies to pattern graphene on PDMS substrate and transfer it onto a target tape. We have achieved patterning and transferring method with the features of high pattern spatial resolution, thickness control, and process simplicity with respect to functional materials and pattern geometries. We have demonstrated the usage of flexible graphene sensors on tape to realize interaction with structures, humans, and plants for real-time monitoring of important signals.

Secondly, we present a helical spring-like piezo resistive graphene sensor formed within a microfluidic channel using a unique and easy *in situ* microfluidic casting method. Because of its helical shape, the sensor exhibits a wide dynamic detection range as well as mechanical flexibility and stretch ability.

Finally, we present a flexible GO-based RH sensor on an adhesive polyimide thin film realized by selectively coating and patterning GO at the surface of Au Interdigitated electrodes (IDEs) and subsequently peeling the device from a temporary polydimethylsiloxane (PDMS) film. Real-time monitoring of the water movement inside the plant has been demonstrated by installing GO-based RH sensor at the surfaces of different plant leaves.

CHAPTER 1

GENERAL INTRODUCTION

1.1 Background

Recent advances in electronic devices have broadened the scope of flexible electronics from earlier flexible/stretchable, foldable storage devices to the more advanced stretchable and wearable devices that lie outside the operational scope of conventional rigid material-based electronics. By integrating them with complex curved surfaces and maintain their functionality even when subjected to a deformation, they open a new route for applications for closely monitoring and recording various vital signals such as those found in structural and human health monitoring [1-2], prototypes of skin patches [3], robotic grasping [4], and real-time motion tracking [5]. For wearable electronics, since sensors should be easily attached onto the irregular surfaces of the sensed objects with good curvature, so high flexibility of sensors are highly demanding in different kinds of sensing applications. Flexible sensors and wearable devices are often fabricated by integration between nanomaterials and flexible substrates. For convenient choice of base and functional materials, flexible substrates (e.g., polyethylene terephthalate, polyimide, and PDMS, Ecoflex, adhesive tape, fabric, and paper) [6-13] have been used as the base materials and conductive nanomaterials, such as carbon nanotubes, metal oxide nanowires, nanoparticles, and graphene have been utilized as a functional material of flexible sensors [14-18]. One of the most popular choice of functional materials to realize flexible sensors is graphene. Graphene is a two-dimensional (2D) material, is made up of carbon atoms linked together in a honeycomb lattice [19], and appealing owing to its unique properties, including atomic thickness, large surface area, fast electron mobility, good piezoresistivity, and

high mechanical flexibility [20-21]. To date, mechanical exfoliation method is the first method used to peel single or few-layer graphene from bulk graphite by using sticky tape and transfer it to another surface. However, it is rather uncontrollable in terms of the number of graphene layers, location, and size of the peeled graphene [22]. Graphene can also be grown by chemical vapor deposition (CVD), but such graphene possesses many defects that lead to weaker mechanical properties than those required for many mechanical sensors [23]. Graphene film can be transferred from a growth substrate (e.g., copper foil) onto a target substrate using polymer-assisted transfer but during this process some cracks may form, and the graphene can be contaminated by both etchant and polymer residues, resulting in an unwanted doping effect that may reduce the graphene carrier mobility [24-26]. Photolithography-based microfabrication for graphene patterning is another useful method, but it is relatively complex and requires multiple steps such as film deposition, lithography, and etching [27-29]. In addition to these methods, various other graphene patterning and transferring techniques have been developed. Laser enabled printing of graphene offers a highly promising platform, but it requires expensive laser-based machines and is limited to fabricating patterns with minimum feature sizes of several tens of micrometers. Ink-jet printing methods can be used to produce reduced graphene oxide (rGO) patterns, but their resolution is poor, and an additional laser-printing process is necessary to increase the electrical conductivity of rGO. Despite all these efforts, many problems remain unsolved before a large-scale and cost-effective graphene-based nanomaterials patterning method with high feature resolution and process simplicity can be realized. By taking the advantage of different materials surface energies graphene patterns at a few micrometers can be formed on a mold and transferred to flexible substrate for different sensing applications.

Most conventional graphene sensors built on rigid substrates or even formed on an elastomer substrate have a planar structure, and even though an elastomer substrate may still be functional under large strain, planar graphene film has a high tendency to break. There is also no capability for compressive sensing on most planar graphene sensors. To improve sensor stiffness, sub-micrometer single-crystal elements can be structured into shapes with microscale, periodic, and wavelike geometries [30], and the facile CVD growth of carbon nanotubes (CNT) array double helices has been used as a sensitive film on elastomer substrates to realize a highly stretchable sensor [31]. *In situ* microfluidic casting method of a graphene layer directly inside a helical channel can overcome the limitations of traditional techniques of graphene strain sensor fabrication and also can provide sensors capable of responding to both compression and tension due to a helical spring-like design.

Easy installation of sensors onto irregular surfaces of a sensed object is also highly demanding for RH sensing applications. By utilizing different GO patterning techniques on flexible substrates, GO-based sensors have been deployed for RH sensing applications [32-37]. Selectively coating and patterning GO film at the surface of Au IDEs on an adhesive polyimide thin film can produce a GO-based RH sensor for tracking water movement inside a plant via real-time monitoring of RH variations at the surfaces of leaves. Such a low-cost GO patterning method-based sensor can be used to explore water transport dynamics in plants by installation of such flexible sensors onto leaf surfaces.

1.2 Introduction

The previous section introduced the concepts of a graphene patterning and transferring technology, flexible and stretchable graphene sensors, and GO film formation methods for RH

sensing applications. This section will give details of relevant work, including: 1. Graphene patterning and transferring methods, 2. Stretchable and flexible graphene strain sensors. 3. GO film formation on flexible substrates for RH sensing applications.

1.2.1 Graphene patterning and transferring methods

Graphene is a 2D material with an atomic thickness of ~0.345 nm in which carbon atoms are patterned hexagonally in a single plane resembling a honeycomb structure. Building blocks in graphite, formed by stacking graphene in different ways, have led to discovery of various important properties. Rapid steps forward in graphene development have led to formation of several types of graphene-based materials, including monolayer to multilayer Graphene, Graphene quantum dots (GQDs), Graphene nanoribbons (GNRs), Nano mesh, Nanosheets, and GO [38]. Mechanical exfoliation, where bulk graphite is first attached to a clean scotch tape, and another scotch tape is adhered on the other side, has been the first method used to peel single or a small number of layers of graphene from bulk graphite, after which the two tapes are separated to reduce the number of graphene layers on each tape. The graphene layers obtained from this method generally have non-uniform thicknesses, irregular shapes, and very small size [22].

CVD has been considered as another efficient, inexpensive, and feasible method for producing single-layer or multi-layer graphene [39]. CVD grown on Cu is one of the fastest methods of produce single-layer graphene due to the low solubility of carbon in Cu that leads to a self-limited process [40]. Figure 1.1 illustrates the proposed growth mechanism of graphene on Cu. The annealing at high temperature in an H_2 environment is used to remove the native oxide layer on the Cu surface. With the exposure of Cu foil in a CH_4 /H_2 environment, nucleation of graphene islands begins taking place randomly but preferentially at the grain boundary of the Cu

surface. As exposure to CH_4 continues, the graphene domains grow in size to cover the whole area of a Cu substrate and eventually aggregate into a continuous graphene film [41].

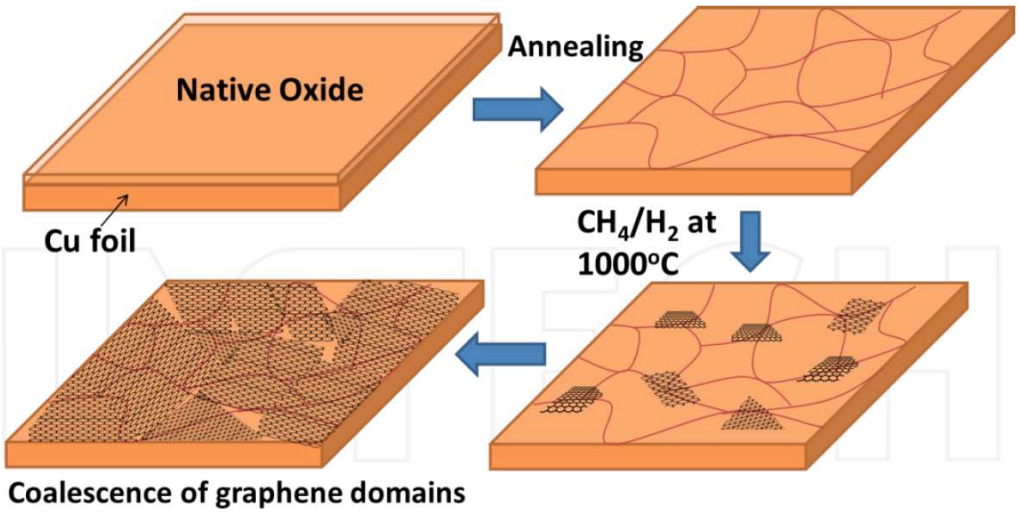

Figure 1.1 Schematic illustrating the proposed growth mechanism of graphene on Cu substrates by CVD: (a) copper foil with native oxide; (b) Native Cu oxide is reduced while Cu develops grains on the surface after annealing at high temperature in H2 environment; c) The exposure of the Cu foil to CH4/H2 atmosphere at 1000 ˚C leading to the nucleation of graphene islands; (d) enlargement of the graphene flakes and coalescence of graphene domains with different lattice orientation [41].

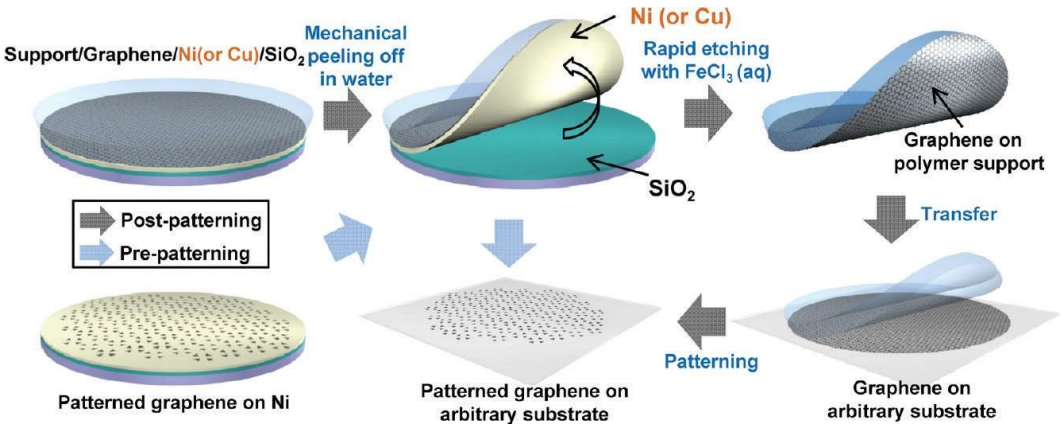

Figure 1.2 Schematic illustration for synthesis, etching, and transfer of large-area graphene films. Transferring and patterning of graphene films grown on a metal/SiO2/Si wafer. Graphene/metal layers supported by polymer films are mechanically separated from a SiO2/Si wafer. After fast etching of metal, the graphene films can be transferred to arbitrary substrates and then patterned using conventional lithography [42].

After graphene film has been produced on a grown substrate, it must be transferred onto a target substrate. To date, the most commonly used technique for doing this is to chemically etch the grown substrate (e.g. Cu) away to obtain a free-standing graphene membrane, followed by scooping the membrane onto a desired substrate. A general transfer technique of CVD-graphene onto a target substrate is illustrated in Figure 1.2 [42].

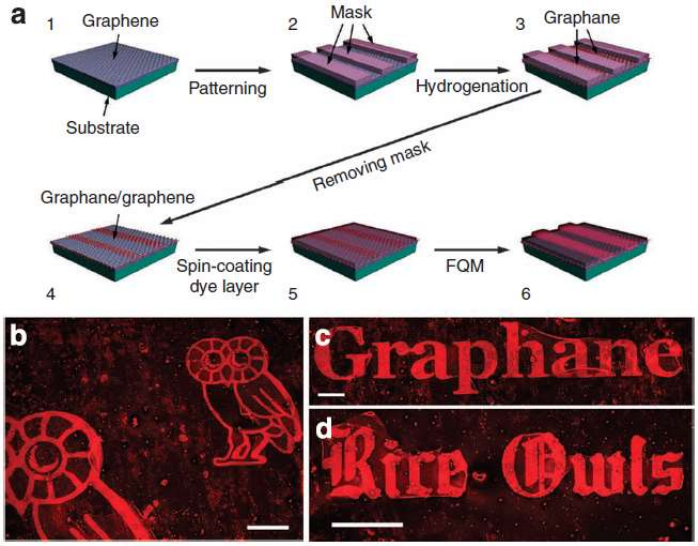

Figure 1.3 Graphane/graphene superlattices fabrication and imaging. (a) Schematic illustration to fabricating the graphane/graphene superlattices and subsequent fluorescence quenching microscopy (FQM) imaging. (b to d) FQMimaging of the graphene with different graphane/graphene patterns. The scale bars in b to d are 200 μm [43].

There also has been intensive study of using photolithography-based microfabrication for graphene patterning [43]. First large-area graphene, grown from Cu substrates by CVD or solid carbon methods, is transferred to an insulating substrate, after which conventional photolithography using a photoresist mask is employed to define patterns atop the graphene films. The exposed area of graphene is then hydrogenated. Finally, the photoresist mask is removed to yield a conductive graphene sheet patterned with domains of insulating graphene-containing regions (Fig. 1.3).

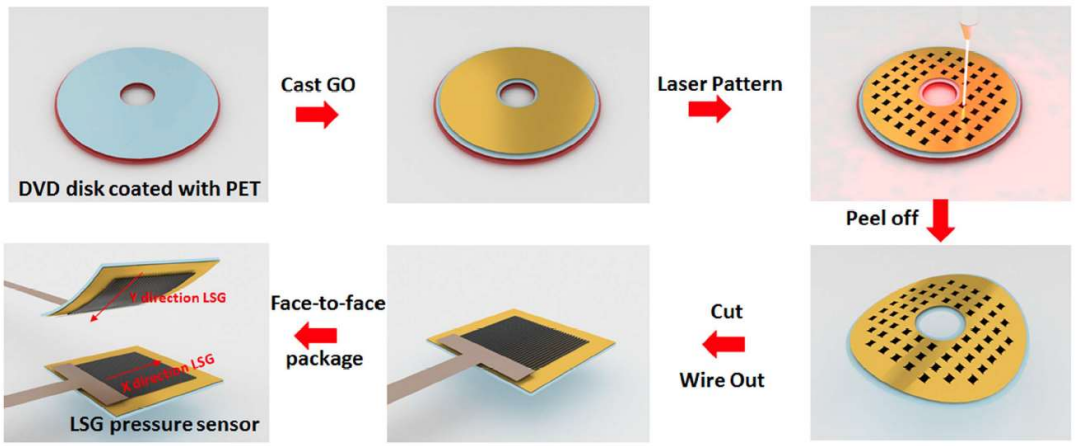

Figure 1.4 The main fabrication processing steps of the laser scribed graphene based (LSG) pressure sensor. A DVD burner with a laser-scribing function is used to convert GO into LSG [44].

Laser-scribe patterning and ink-jet printing techniques support graphene pattern formation based on the reduction of GO. For example, the work described in Fig. 1.4. shows laser-scribed graphene patterns used as functional material for pressure sensing [44]. Unlike the denser GO films, the laser-scribed graphene is composed of loosely stacked graphene layers and it has a 3D profile that makes the pressure sensor sensitivity higher.

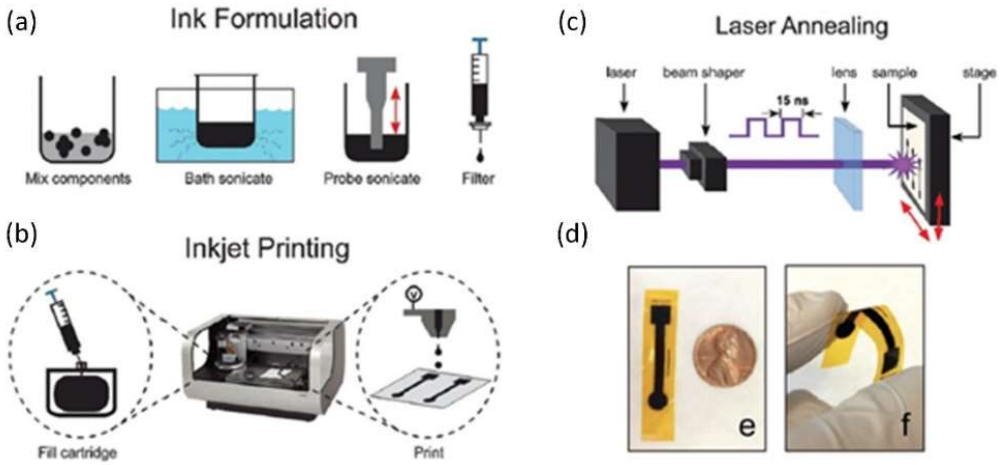

Figure 1.5 (a) Schematic diagram of graphene ink formulation. (b) Printing process of graphene patterns with Dimatix Materials printer. (c) Additional pulsed-laser processing of the graphene electrodes for improved conductivity using a Nd:Yag laser. (d) Graphene inkjet printed electrode on a flexible polyimide substrate [45].

In addition to laser-scribe patterning, inkjet printing is another platform that can be used to form graphene patterns on different substrates. Fig. 1.5 represents a pulsed laser process that can selectively irradiate inkjet printed rGO and consequently improve electrical conductivity (R_{sheet} ~0.7 kΩ $\square^{-1}$) of printed graphene with an additional laser annealing process [45]. This additional laser annealing no only improvees the electrical conductivity, but also converts the 2D planar printed graphene into 3D petal-like graphene nanostructures.

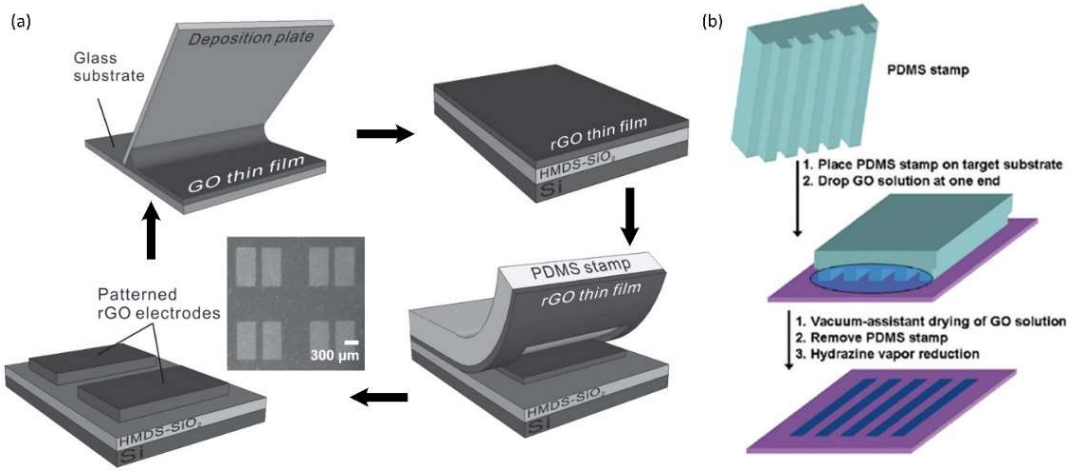

Figure 1.6 (a) Schematic illustration of fabricating rGO source-drain electrodes based on transfer printing method [46]. (b) Schematic illustration of patterning GO films by the micromolding in capillary method with a GO aqueous solution, followed by chemical reduction with hydrazine vapor [47].

Finally, transfer printing and micro transfer molding methods used to create graphene patterns on different subtrates can be seen in Fig. 1.6. Transferprinting technique involves first creating graphene patterns on an initial substrate, then utilizing a stamping process to transfer them onto a final substrate [46]. Micro transfer molding is based on filling the carved patterns of a stamp placed on top of a target substrate with graphene-based suspensions, followed by vacuum drying and removing the stamp from the final substrate [47].

1.2.2 Stretchable and flexible graphene strain sensors

Graphene can respond to applied mechanical strain without any degradation in its electrical properties due to its high flexibility [51], so it has been considered as an ideal candidate to realize highly stretchable and flexible sensors and electronic devices. Suspended multilayer graphene flakes exhibit an intrinsic tensile strength between 118 and 121 GPa and a Young's modulus of 0.5 TPa [48]. At room temperature, its fast electron mobility can reach 15,000 $cm^2 . V^{-1} . s^{-1}$ [49], and the sheet resistance of multilayer graphene has been reported to lie between 8.8 – 200 Ω. sq^{-1} [50]. Many intensive studies have reported using graphene as a sensitive film on stretchable substrates for strain and pressure sensing applications.

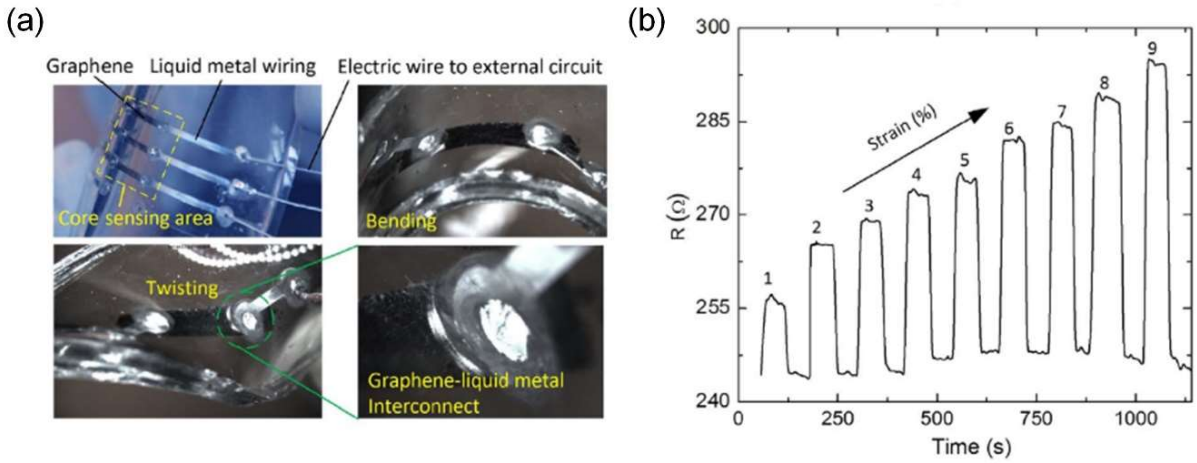

Figure 1.7 (a) Images showing the structural flexibility of the fabricated unidirectional graphene strain sensors. (b) Sensor resistance change during the applied cyclic stretch-and-release time-varying strain [52].

For example, flexible strain sensors made of piezo-resistive graphene, microfluidic liquid metal, and stretchable elastomer have been developed, as can be seen in Fig. 1.7 [52]. To achieve flexible electrical contacts with graphene sensing elements, liquid metal can be introduced into microfluidic channels as interconnect material, resulting in sensor resistance that varies between 245 and 295 Ω as the applied strain is increased to 9 %. A gauge factor value of 1.51 is found for

the graphene sensing element itself, while the liquid metal wire has a gauge factor close to zero, so the liquid metal wires inside the device makes little contribution to the total sensor response.

Fig. 1.8 presents a resistance-type strain sensor made of hollow tubing graphene fiber maintained cylindrical tubing and PDMS for strain/bending detection applications [53]. The cylindrical geometry provides a capability for detecting bidirectional strain, curvature, and torsional strain as well as being easy to install. Its gauge factor is in the range of 34.3-48.9 for to tensile strain of up to 8%.

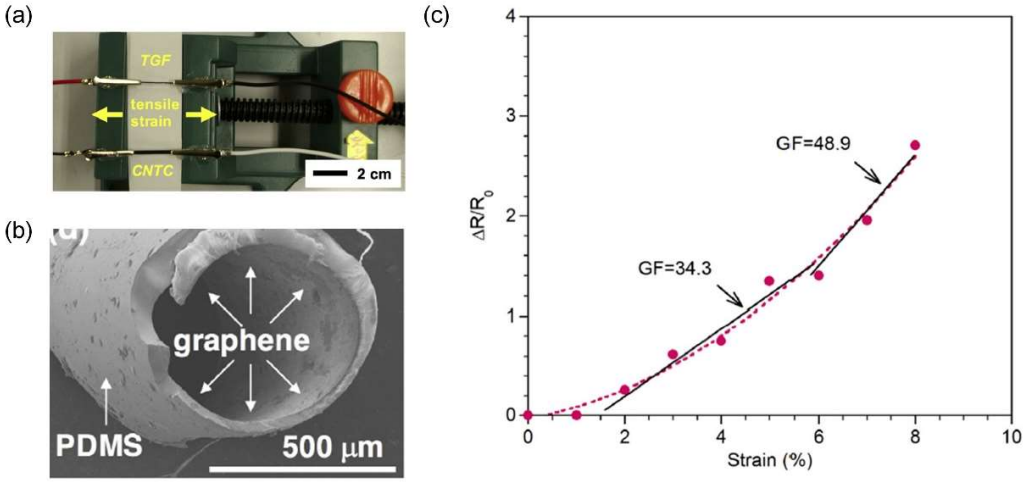

Figure 1.8 (a) Picture of testing equipment of the tensile strain testing machine. (b) SEM image of the cross-sectional view of graphene/PDMS hollow tubing after Ni etched removal (b). (c) Relative resistance variation of the TGF with applied tensile strain [53].

Another scheme for achieving a highly-stretchable sensor consists of sub-micrometer single-crystal elements structured into shapes with microscale, periodic, and wavelike geometries as shown in Fig. 1.9 [30]. Thin elements of single-crystal Si are fabricated by conventional lithographic processing, followed by etching of the top Si and SiO_2 layers of a SOI wafer, with the ribbon structures supported by the underlying wafer. A pre-strained elastomeric substrate,

PDMS is in contact with the ribbons, providing bonding between these materials. The PDMS is peeled back with the ribbons bonded to its surface and releasing the pre-strain structure causes the PDMS to relax back to its unstrained state, leading to highly periodic and stretchable wavy structures in the ribbons. Controlling the level of pre-strain allows the range of strains (nearly 30%) to balance the desired degrees of compressive and tensile deformability of the structure. For example, a pre-strain of 3.5% (the maximum they examined) yields a range of –24% to 5.5%.

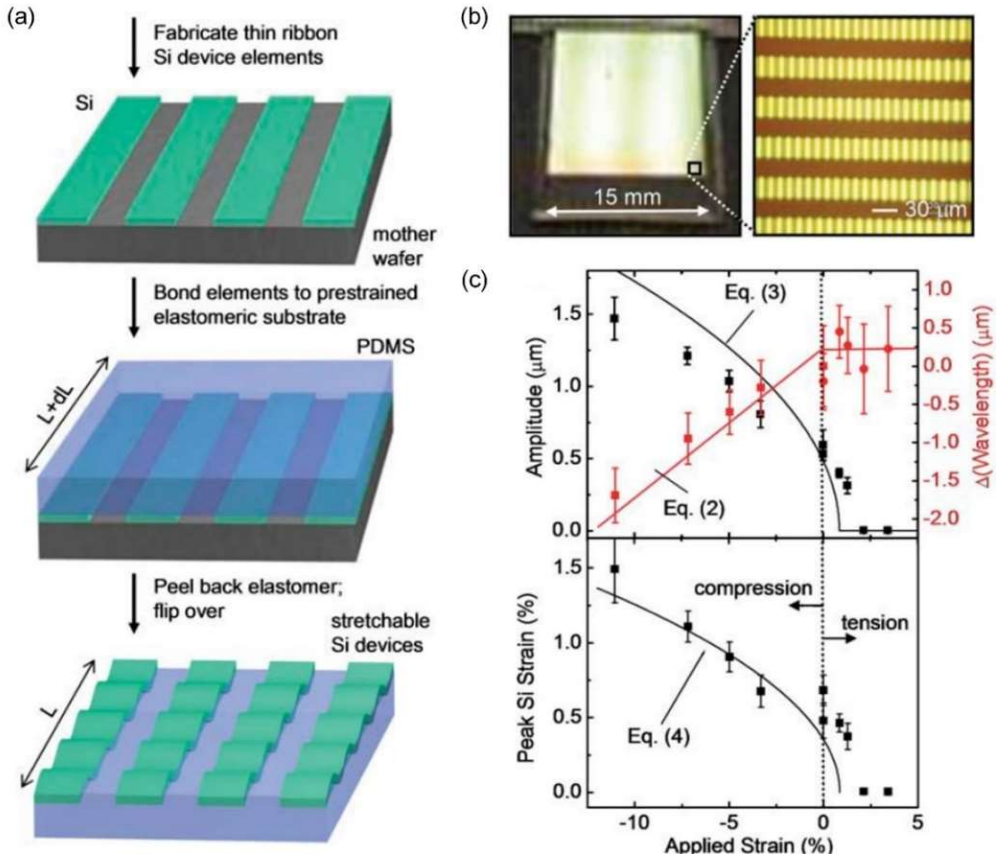

Figure 1.9 (a) Schematic illustration of the process for building stretchable single-crystal Si devices on elastomeric substrates. (b) Optical images of a large-scale aligned array of wavy, single-crystal Si ribbons (widths = 20 mm, spacings = 20 mm, thicknesses = 100 nm) on PDMS. (c) Average amplitudes (black) and changes in wavelength (red) of wavy Si ribbons as a function of strain applied to the PDMS substrate (top panel). For the wavelength measurements, different substrates were used for tension (circles) and compression (squares). Peak Si strains as a function of applied strain is shown in the bottom panel [30].

1.2.2 Graphene-oxide film formation on flexible substrates for RH sensing applications

GO has recently emerged as a new carbon-based nanoscale material that provides an alternative to graphene. GO is a two-dimensional network of hybridized carbon atoms arranged in a dense honeycomb crystalline structure with many oxygen groups, including hydroxyl, epoxy, and carboxylic acid bonded to the two-dimension network [54]. These functional groups provide GO with a high hydrophilicity, allowing the intercalation of different types of molecules, especially polar molecules [55]. The solubility of GO in water and other solvents allows it to be uniformly deposited onto a wide range of substrates in the form of thin films or networks, making it potentially useful for sensing applications [32-37].

Fig. 1.10 depicts the study of the RH sensing properties of GO film deposited on Au interdigitated electrodes using a drop-casting method [32]. The effect of water adsorption on electrical properties of the GO film was observed through electrical characterizations that included both direct-current (DC) measurements and alternating-current (AC) complex impedance spectroscopy. DC measurements indicated that the electrical properties of the GO film depend on both the RH and the amplitude of applied voltage, while the AC complex impedance spectroscopy analysis revealed that the conductivity of the GO film increases along with the RH level. At low RH (<54%), the conductivity of the GO is film is poor due to functional groups, while when RH increases, the conductivity of the GO film increases sharply owing to strong water adsorption that induces ion conduction.

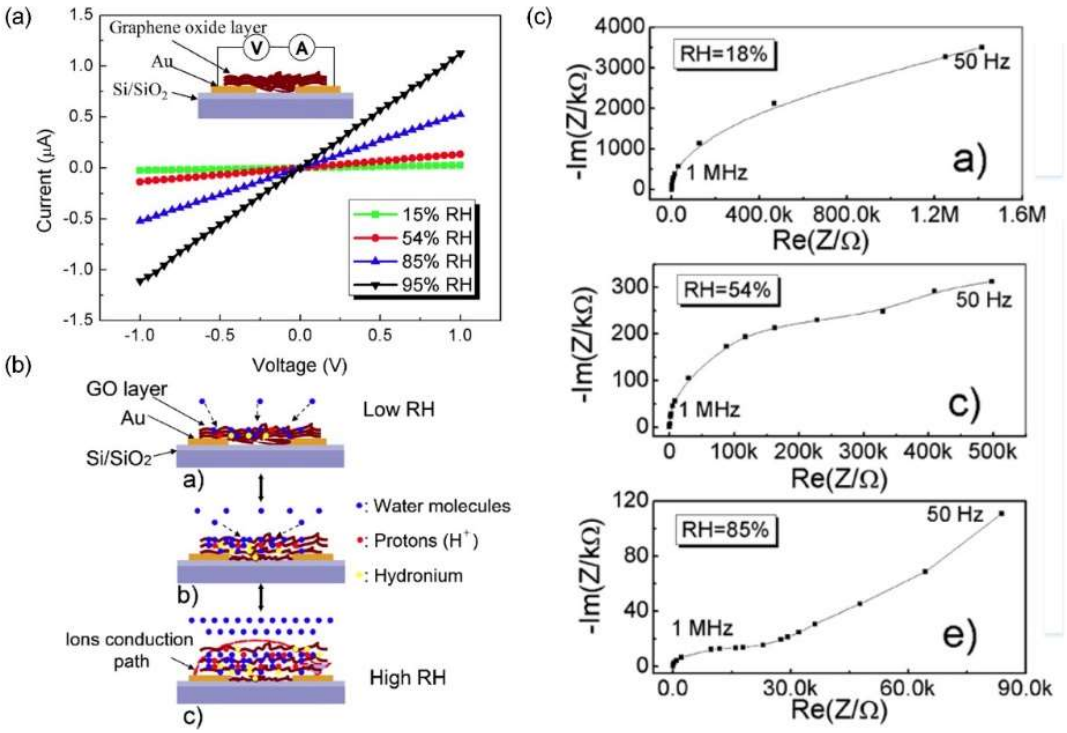

Figure 1.10 (a) I-V characteristic of the GO-film-functionalized IDE with a low sweeping voltage (-1 to 1 V) at various RH levels. (b) The electrical interaction mechanism between GO films and water molecules at low RH, medium RH, and high RH. (c) Measured complex impedance spectroscopy of the GO-film-functionalized IDE [32].

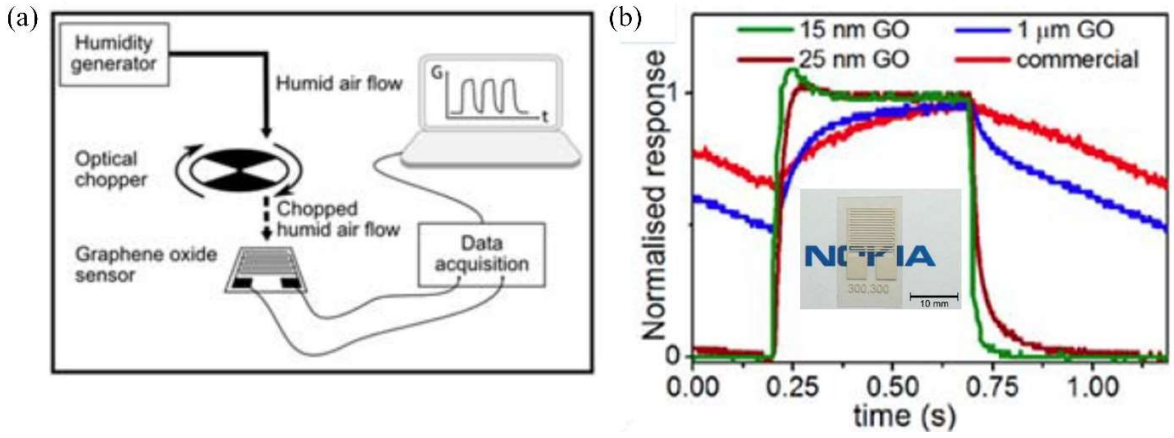

Figure 1.11 (a) Diagram of the experimental setup used to study the humidity sensors speed. A wire bonded graphene pressure sensor. (b) Normalized response of the different sensors to a modulated humid air flow at 1 Hz. Inset shows a sprayed GO film on the printed Ag electrodes. [33].

Another group, shown in Fig.1.11, exhibits the super permeability to water of GO films deposited by either drop casting or spray coating on silver screen-printed interdigitated electrodes formed on a polyethylene naphthalate (PEN) substrate [33]. The effect of the GO film thickness to modulated humid flow on response time was explored by varying the thickness of the GO film from 15 nm (ultra-thin spray coated) to 1μm (thick drop casted). When the thickness of GO film decreased to 15 nm, the response of the sensor to a modulated humid flow became ultrafast (~30 ms response and recovery times).

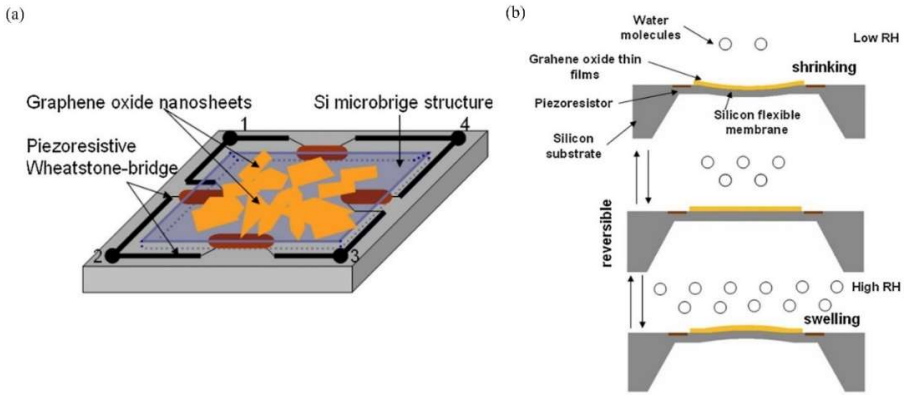

Figure 1.12 (a) Schematic figure of GO-Si bi-layer structure. (b) Schematic illustration of humidity sensing mechanism of GO thin film piezo resistive Si membrane [37].

In addition to these studies, a different approach, depicted in Fig. 1.12, using a GO-Si bi layer flexible structure as a stress-based humidity sensor has been reported [37]. A GO thin film is deposited onto a Silicon micro bridge as a humidity-sensing layer. The GO film swells, leading to bending of the Si membrane when it is exposed to a humid environment. A piezo-resistive Wheatstone bridge embedded into the Si micro bridge is used to transform the deformation into a measurable voltage output. The sensor exhibits high performance, with a maximum sensitivity of 79.3 μV/ RH %, over a wide detection range of 10-98 % RH. It is also found that the proposed GO-Si bi-layer structure is subject to humidity-induced deformation of the GO film, providing formation of a multi-information sensor.

1.3 Problem Statement

Up to now, we have discussed the concepts of using graphene patterning and transferring technology, flexible and stretchable graphene sensors, and GO film formation for RH sensing applications. The remaining problems needing to be solved for graphene patterning and transferring techniques are related to large-scale and cost-effective graphene patterning with high feature resolution and process simplicity. The main areas of challenge here are high cost, process complexity, and lack of capability in terms of large scale fabrication, good flexibility, and high stretchability of the graphene-based sensors. It is impossible to discuss the challenges solely without considering their applications. Depending on the feature of each graphene-based sensor, challenges and approaches will be discussed separately from the application perspective.

1.3.1 Graphene patterning and transferring

While different techniques have recently been developed for patterning graphene-based nanomaterials and transferring them onto final substrate, there are still many unsolved issues that must be resolved to perfect a large-scale, cost-effective graphene patterning method producing high feature resolution, process simplicity, and diversity with respect to functional materials and pattern geometries. While a mechanical exfoliation technique can be applied to fabrication of graphene film electrodes at centimeter scale, the film obtained has non-uniform thickness and irregular shape [56]. To achieve high pattern spatial resolution, photolithography-based microfabrication for graphene patterning [27-29] can also be used, but it lacks process simplicity since it requires multiple fabrication steps that include film deposition, lithography, and etching.

Another method using laser and ink-jet printing techniques can be useful in fabricating graphene patterns onto different substrates, but these methods require sophisticated lasers and are limited to producing patterns with minimum feature size of several tens of micrometers. In addition, in ink-jet printing, additional laser treatment may be required to produce conductive

patterns. Transfer printing and molding methods have also been proposed, but to achieve process simplicity, special care is required to modify the surface properties of the device substrates and functional materials. Our work will develop a simple, high-resolution, and scalable graphene patterning and transferring method oriented toward roll-to-roll production of flexible graphene sensors, and it will outperform many other approaches with respect to functional materials and pattern geometries in terms of pattern spatial resolution, thickness control, process simplicity, and diversity.

1.3.2 Stretchable and flexible graphene strain sensors

While highly-flexible and stretchable sensors with a wide dynamic range can be used for wearable strain sensor applications where large strains are applied, most of the existing graphene-based strain sensors have a planar structure and are generally realized on surfaces of elastomer substrates. Planar graphene structures have a high tendency to break at larger strains and have no capability for being compressed. To increase the flexibility and dynamic sensing range of such sensors, wrinkled structures at micro/nano scale [30] and Carbon nanotube (CNT) array double helices have been proposed as main building blocks of sensitive film [57] formed on elastomer substrate. Despite these efforts, most recently-developed sensors are lacking in an improved dynamic sensing range of the applied strain and are also unable to respond to both compression and tension.

Our work demonstrates unique design and manufacturing of novel helical-shaped tubular graphene strain sensors to allow a wide dynamic sensing range, from 24% compressive strain to 20% tensile strain. The *in situ* microfluidic casting method of the graphene film has been developed to create a helical-shaped tubular hollow structure composed of graphene. This allows easy coating of a graphene layer on the inner wall of the helical channel in all radial directions

and embedded inside a PDMS substrate. Because of the helical spring-like design, the sensor offers an improved dynamic range of strain along the axis of the spring and is also able to respond to both compression and tension.

1.3.3 GO film formation on flexible substrates for RH sensing applications

In the field of agriculture, the relationship between plants and water usage has given rise to quantification of water use efficiency (WUE) and the amount of water transported from soil to plant parts. A variety of sensors have recently been developed, including; soil moisture sensors [58], dew sensors [59], leaf thickness sensors [60-61], and leaf water content sensors [62-63]. Although these sensors are widely used, they cannot give a direct measure of the water transpiration process that regulates water content in a plant, and some of them are suitable only to laboratory environment. Thermal imaging systems have also been developed for monitoring the water stress level of plants by observing change in leaf temperature due to stomatal closure [64]. However, these systems are not cost-effective, and the resulting measurements might be influenced by environmental factors. Our work focuses on a new method for monitoring water movement within a plant using GO-based RH sensors that are uniquely formed on a flexible, thin, and adhesive polyimide film. They are mounted on different leaves to monitor real-time RH levels at the leaf surfaces upon irrigation. A simple assembly fixture was designed for easy installation of the sensor on the leaf to avoid any damage and let the plant grow as normal.

This RH sensor-enabled approach can provide information associated with water use efficiency and on how water moves within a plant, an important selection trait for evaluating crop quality.

1.4 Thesis Organizations

The following chapters represent an accumulation of two published journal papers and one conference paper.

Chapter 2 describes methods for simple, cost-effective, scalable, and versatile patterning and transferring of graphene-based nanomaterials onto various types of tape to realize roll-to-roll production of graphene-based flexible sensors on tape. The study suggests applications of wearable graphene-based sensors to mechanical and RH sensing on human and crop plant surfaces. The paper, entitled "High-Resolution Patterning and Transferring of Graphene-Based Nanomaterials onto Tape Toward Roll-to-Roll Production of Tape-Based Wearable Sensors" has been published in *Advanced Materials Technologies,* **2**, 1700223 (2017).

Chapter 3 reports on a helical spring-like piezo-resistive graphene strain sensor formed within a microfluidic channel. The study may find application in real-time motion tracking because of its wide dynamic range due to high mechanical flexibility and stretchability of the sensor. The paper, entitled "Helical-Shaped Graphene Tubular Spring Formed within Microchannel for Wearable Strain Sensor with Wide Dynamic Range", has been published in *IEEE Sensors Letters,***1**, 6 (2017).

Chapter 4 describes a new method for monitoring water movement within a plant using GO-based RH sensors that can provide information on how water associated with WSE moves within the plant, an important selection trait in evaluating crop quality. The paper, entitled "Tracking of Water Movement Dynamics inside Plants Using Leaf Surface Humidity Sensors" has been published in the Proceedings of the12th International Conference on Nano/Micro Engineered and Molecular Systems (IEEE-NEMS 2017).

CHAPTER 2

HIGH-RESOLUTION PATTERNING AND TRANSFERRING OF GRAPHENE-BASED NANOMATERIALS ONTO TAPE TOWARD ROLL-TO-ROLL PRODUCTION OF TAPE-BASED WEARABLE SENSORS

A paper published in Journal of Advanced Materials Technologies

Seval Oren, Halil Ceylan, Patrick S. Schnable, and Liang Dong

2.1 Abstract

This paper reports on a simple and versatile method for patterning and transferring graphene-based nanomaterials onto various types of tape to realize flexible microscale sensors. The method involves drop-casting a graphene film on a prepatterned polydimethylsiloxane (PDMS) surface containing negative features by graphene suspensions, applying Scotch tape to remove the excess graphene from the nonpatterned areas of the PDMS surface, and then transferring the patterned graphene from the inside of the negative features at the PDMS surface onto a target tape. The feature size of transferred graphene patterns on the final tape is as small as a few micrometers. This method is easy to implement, but does not require the use of expensive equipment, except for needing a PDMS substrate containing negative features. This method has a high versatility in producing micropatterns of graphene-based nanomaterials on different types of adhesive tape. For the purpose of application demonstration, flexible mechanical sensors and sensor arrays, smart gloves, and plant leaf sensors on tapes to realize real-time monitoring of important signals indicating human motion and plant water transport behavior have been developed. This technology will open a new route for low-cost, scalable, and roll-to-roll production of graphene-based sensors on tape.

2.2 Introduction

Flexible plastic substrates (e.g., polyethylene terephthalate, polyimide, and polydimethylsiloxane or PDMS) [1–6] and other nonconventional substrates (e.g., paper, tape, and cloth) [7–10] have been widely utilized as the base materials of flexible electronic devices. Conductive nanomaterials, such as carbon nanotubes, metal oxide nanowires, and graphene, have also attracted considerable attention as functional materials for applications ranging from transistors, to sensors, to energy harvesting and storage devices [11–22]. Among these conductive nanomaterials, graphene plays a key role in producing next-generation sensors owing to its unique properties, including atomic thickness, large surface area, fast electron mobility, good piezo resistivity, and high mechanical flexibility.[23–27] As a result, integrations between flexible substrate materials and graphene-based nanomaterials have led to a variety of sensors and other electronic devices through development of novel fabrication processes, advancing emerging and significant fields such as real-time motion tracking [28], structural and human health monitoring [29–31], electronic skin sensing [32–36], and humanized robotic manipulation [37]. It is well known that repeated mechanical exfoliation to peel single- or few-layer graphene from bulk graphite using sticky tape and transfer it to another surface is rather uncontrollable in terms of the number of graphene layers, location, and size of the peeled graphene [38]. Recently, graphene film electrodes at centimeter scale have been fabricated by peeling tape from a commercial graphite foil for the detection of glucose [39], but the obtained electrodes did not have well-defined shapes or control over thickness. Physically rubbed graphene electrodes have also been produced by directly placing solid-state graphene powders at a channeled adhesive surface and then rubbing against the surface [40]. The resulting graphene patterns, however, have poor feature resolution. Photolithography-based microfabrication for graphene patterning [41–

49] is relatively complex and requires multiple steps such as film deposition, lithography, and etching. Recently, various interesting methods have been developed for patterning and transferring graphene-based materials onto different substrates. For example, laser printing of graphene has been studied with variable laser energy, spot size, and pulse duration [50–54]. This method, however, requires sophisticated lasers and is limited to producing patterns with minimum feature size of several tens of micrometers. An ink-jet printing method has also produced patterns of reduced graphene oxide (rGO), but resolution is poor, and, for practical applications, additional laser processing is required to improve electrical conductivity of rGO [55]. A transfer printing method involves first creating graphene patterns on an initial substrate, and then utilizing a stamping process to transfer them onto a final substrate [56]. Micro transfer molding is based on filling the carved patterns of a stamp emplaced on top of a target substrate with graphene-based suspensions, followed by vacuum drying and removing the stamp from the final substrate [57]. Both the transfer printing and molding methods require a special care to modify the surface properties of the device substrates and functional materials. In addition, most existing graphene-based sensors cannot be easily installed onto the irregular surfaces of the sensed objects so, despite the efforts made, many problems remain unsolved before a large-scale, cost-effective graphene patterning method with high feature resolution and process simplicity can be realized.

In this paper, we report on a simple, high-resolution, and scalable graphene patterning and transferring method toward roll-to-roll production of flexible graphene sensors. This method involves (i) creating graphene patterns inside prepatterned negative features at the surface of a polydimethylsiloxane (PDMS) substrate using a unique “Drop Cast-Dry-Stick-Peel” (D^2SP)

method, and subsequently (ii) transferring the resulting graphene patterns onto a final sticky tape via an easy-to-implement “Stick-and-Transfer” (ST) process. The feature size of the transferred graphene structure on the final tape can be as small as a few micrometers. This method does not require the use of any expensive equipment, except for needing a PDMS substrate containing negative features. The versatility of this approach is demonstrated by producing complex graphene and rGO micro patterns onto different tapes commercially available (e.g., polyimide, Scotch, 3M electrically conductive, and aluminum foil adhesive tapes). Furthermore, tape-based flexible graphene pressure and strain sensors, sensor-enabled smart gloves, and plant leaf humidity sensors are realized to interact with humans and plants for real-time monitoring of important signals. We have demonstrated that smart gloves with multiple strain and pressure sensors allow real-time tracking of finger motion behavior during capturing a moving object, while graphene- based humidity sensors can be made to adhere to leaf surfaces to monitor water movement within plants upon irrigation. These sensors are flexible enough to highly conform to various irregular shapes of the sensed objects. The patterning and transferring method presented outperforms many other counterpart approaches in terms of pattern spatial resolution, thickness control, process simplicity, and diversity with respect to functional materials and pattern geometries.

The main procedures for forming graphene patterns on the tape surface are illustrated in Figure 2.1. Briefly, a master Si mold with positive patterns made of SU-8 photoresist was first formed on the surface of a silicon wafer, and negative patterns were then formed on a PDMS substrate from the Si mold via soft lithography (Figure 2.1a). Here, the "negative" patterns or features refer to the "channels" or cut out areas at the PDMS surface. Subsequently, aqueous suspensions of graphene nanoplatelets were loaded onto the PDMS surface (Figure 2.1b). After drying on a hotplate in air, a thin graphene film was formed, covering the entire PDMS surface (Figure 2.1c). Next, Scotch tape was manually applied and stick to the top surface, and then peeled the excess graphene from the nonpatterned areas on the surface. This stick-and-peel process was repeated to ensure complete removal of the unwanted graphene from the top surface (Figure 2.1d), while the graphene inside the PDMS negative patterns remained intact because it was set below the top surface. Therefore, the D^2SP process was completed, resulting in the graphene structures inside the negative patterns on the PDMS surface (Figure 2.1e). After that, transfer of the formed graphene patterns onto a final target tape was implemented by manually applying and pressing the target tape, and then peeling it from the PDMS surface (Figure 2.1f, g). The ST process was thus completed, and the microscale graphene patterns were formed onto the surface of the final tape. Figure 2.1h–l displays the images for the main procedures of the D^2SP and ST processes. The details of fabrication are described in the Experimental Section.

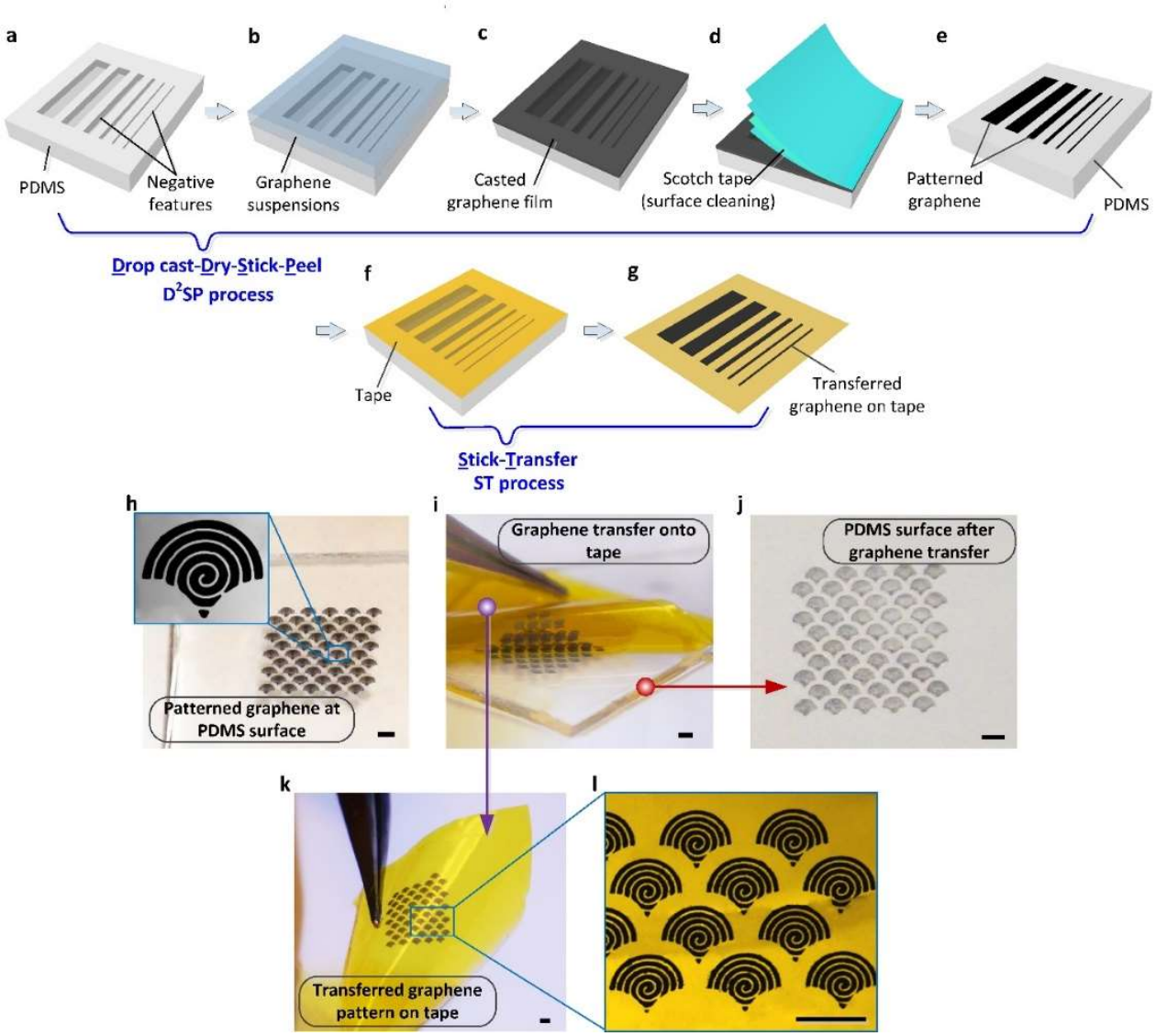

Figure 2.1 (a)–(g) A schematic representation of the graphene pattern formation on tape. (a) Negative patterns created on the PDMS substrate via soft lithography. (b) Graphene suspensions drop-coated onto the entire surface of the PDMS slab. (c) A graphene film formed on the PDMS surface. (d) The graphene film outside the negative patterns removed using Scotch tape. (e) Graphene patterns formed inside the negative patterns at the PDMS surface. (f) A target tape adhered onto the PDMS surface. (g) Graphene patterns transferred onto the target tape. (h)–(i) Optical images showing the main steps of graphene patterning and transferring process. The scale bars represent 1 mm. (h) Graphene patterns obtained in the PDMS structures. The negative patterns on the PDMS substrate were 15.4 µm deep. The graphene inside the PDMS negative patterns were 10.3 µm thick. (i) Application of the ST process for graphene pattern transfer onto the polyimide tape. (j) PDMS surface after graphene transfer. (k)–(i) Graphene patterns transferred onto the polyimide tape.

Essentially, the tape-based graphene patterning and transfer technique utilizes the work of adhesion $W_{A\text{-}B}$ at the interface between two contacting materials A and B as determined by their surface energies [59,60], with $W_{A\text{-}B}$ given by [61]

$$W_{A-B} = 4\left(\frac{{\gamma_A}^d {\gamma_B}^d}{{\gamma_A}^d + {\gamma_B}^d} + \frac{{\gamma_A}^p {\gamma_B}^p}{{\gamma_A}^p + {\gamma_B}^p}\right) \quad (1)$$

where d and p correspond to the dispersion and polar components of surface energy ($\gamma = d + p$). Table A1 (Appendix) provides the surface energies of the materials used in this work [68–70] and the calculated values of $W_{graphene\text{-}PDMS}$ at the interfaces between graphene and PDMS and $W_{graphene\text{-}tape}$ between graphene and tape. The fact that $W_{graphene\text{-}tape} > W_{graphene\text{-}PDMS}$ for different types of tape make it possible to remove the excess graphene from the PDMS top surface using the cleaning Scotch tape during the D^2SP process and transfer the patterned graphene onto the target tape during the ST process. See the Appendix for the values of $W_{A\text{-}B}$ for different material combinations.

2.3 Results and Discussion

2.3.1 Micro Scale Patterning and Transferring

Figure 2.2 shows several examples of microscale graphene patterns transferred onto a 25 μm thick polyimide tape with silicone adhesive. The PDMS substrate used here contained 15.4 μm deep negative features prefabricated at its surface. The graphene structures inside these negative patterns were 10.3 ± 2.7 μm thick, which was determined by a surface profilometer (see the measurement method in the Experimental Section). The transferred patterns were of high spatial resolution (≈5 μm), and mostly retained the features of the original patterns at the PDMS surface. This method also allowed producing graphene patterns on a tape roll, as shown in Figure 2.2f–h (see Figure A1, Appendix, for the fabrication process).

Figure 2.2 (a)–(e) Versatile graphene patterns formed on the polyimide tape using the proposed method. (f)–(h) Formation of graphene patterns on the relatively large polyimide tape roll with liner. The transferred graphene patterns are protected by a non-sticky liner.

It should be noted that, to realize these graphene patterns on a tape, several critical geometrical and processing parameters, including the volume of graphene suspensions over the unit surface area, the depth, and width of the preformed negative features at the PDMS surface, and the number of repeating D^2SP times, should be carefully considered. The following section will discuss the influences of these parameters on the quality of pattern formation and transfer.

First, although a thick graphene film could easily be produced by loading a large volume of graphene suspensions per unit surface area onto the PDMS surface, patterning of a thick film was difficult using the D^2SP method. The experiment here utilized a PDMS substrate containing 15.4 μm deep and 500 μm wide channels at its surface and was covered by a 10.3 μm thick graphene film. This thick film was formed by drop-casting with 20 mg mL^{-1} concentration graphene suspensions at a large volume per unit surface area of 710 μL cm^{-2} (Figure 2.3a, top). Then, Scotch tape was applied and stick to the PDMS surface, with an intent to clean the PDMS surface by removing the unwanted graphene from the PDMS top surface. However, as shown schematically in Figure 2.3a and experimentally in Figure 2.3b, some portions of the graphene inside the channels were also removed by the Scotch cleaning tape.

A possible explanation for this is that the tape peeling could not easily break such a thick graphene film at the step and sidewall of the channel completely covered by the continuous graphene film. Therefore, to successfully produce thick graphene patterns in the PDMS channels, sequential D2SP processes were applied multiple times (each time producing a thin film until the desired film thickness was achieved (Figure 2.3c). Specifically, our experiment shows that when the drop-casted graphene film was no more than ≈1.5 μm thick, Scotch tape worked perfectly to break the film at the step of the channel, almost regardless of the channel depth, as long as the tape was not in direct contact with the graphene inside the channel. Therefore, in the subsequent experiments, graphene suspensions (concentration: 20 mg mL^{-1}) were loaded to the PDMS surface (the volume of graphene suspensions per unit surface area: 100 μL cm^{-2}) to form an ≈1.45 μm thick graphene film (Figure 2.3c, top). Next, this thin film was patterned to form the graphene structures inside the channel using the stick-and-peel process with Scotch

tape (Figure 2.3c, middle). To increase the thickness of the graphene patterns inside the channel, the whole D^2SP process (described in Figure 2.1a–e) was repeated multiple times until a desired thickness was obtained (Figure 2.3c, bottom). Figure 3d shows the PDMS channel filled by an ≈10.3 μm thick graphene film after seven times repeated D^2SP processes. Figure 2.3e shows the optical images for the graphene patterns in the PDMS channels obtained with 1–7 times repeated D^2SP processes. Figure 2.3f shows that the graphene patterns exhibit a linear increase in thickness and a linear decrease in electrical resistance with the number of repeated D^2SP processes (or the number of coatings).

Next, to transfer the patterned graphene from the PDMS channels onto a final tape via the ST process, we investigated the influences of the channel width and depth on the transfer quality. The experiment here utilized the PDMS channels with depths of 5, 15.4, and 41.6 μm, and widths of 20, 40, and 100 μm. By performing sequential D^2SP processes, the channels were almost fully filled by graphene, with a few micrometers gap distance to the channel top. Polyimide tapes with silicone adhesive were used to transfer the graphene patterns, with results indicating that, after the graphene structures were transferred onto the tape, the 41.6 μm deep channels of all the different widths contained graphene residues as shown in Figure 2.3g. This may be because the van der Waals force within the drop-casted graphene film was not large enough to hold the ≈36.7 μm thick graphene structure together during transferring using the tape. The other plausible cause may be due to an increased drag force occurring at the large-area sidewalls of the deep channel and acting on the graphene during peeling. When the channel depth decreased to 15.4 μm and contained ≈10.3 μm thick graphene, the tape transfers of graphene became easier and only a very minor residue remained in the channels. With decreasing channel width from 100 to 20 μm, the increased aspect ratio of the channel led to

somewhat increased amounts of residue at the channel edges, but overall the transferred graphene on the tape retained the original pattern features of the graphene structures in the channels. Furthermore, in the case of transferring ≈2.3 μm thick graphene from the 5 μm deep channels, no residues were observed to remain in the channels for all widths.

To increase electrical conductivity of the transferred graphene, the transferred graphene patterns on the polyimide tape were annealed in air. Essentially, thermal treatment may improve contacts between graphene nanoplatelets, and thus increase electrical conductance of the formed graphene patterns [58]. Because polyimide tapes are dimensionally stable below 400 °C [62] the annealing was carried out at temperatures ranging from 150 to 300 °C (Figure 2.3h) over different treating times ranging from 60 to 210 min (Figure 2.3i). The results show that the sheet resistance of the transferred graphene (≈10.3 μm thickness) was decreased by about seven times after the treatment at 250 °C for 180 min. Increased annealing time did not help to further decrease the sheet resistance. As the annealing temperature increased toward 300 °C, the sheet resistance was found to decrease, but, the optimum annealing temperature was chosen as 250 °C because of the above-mentioned critical temperature restriction of polyimide tape [62].

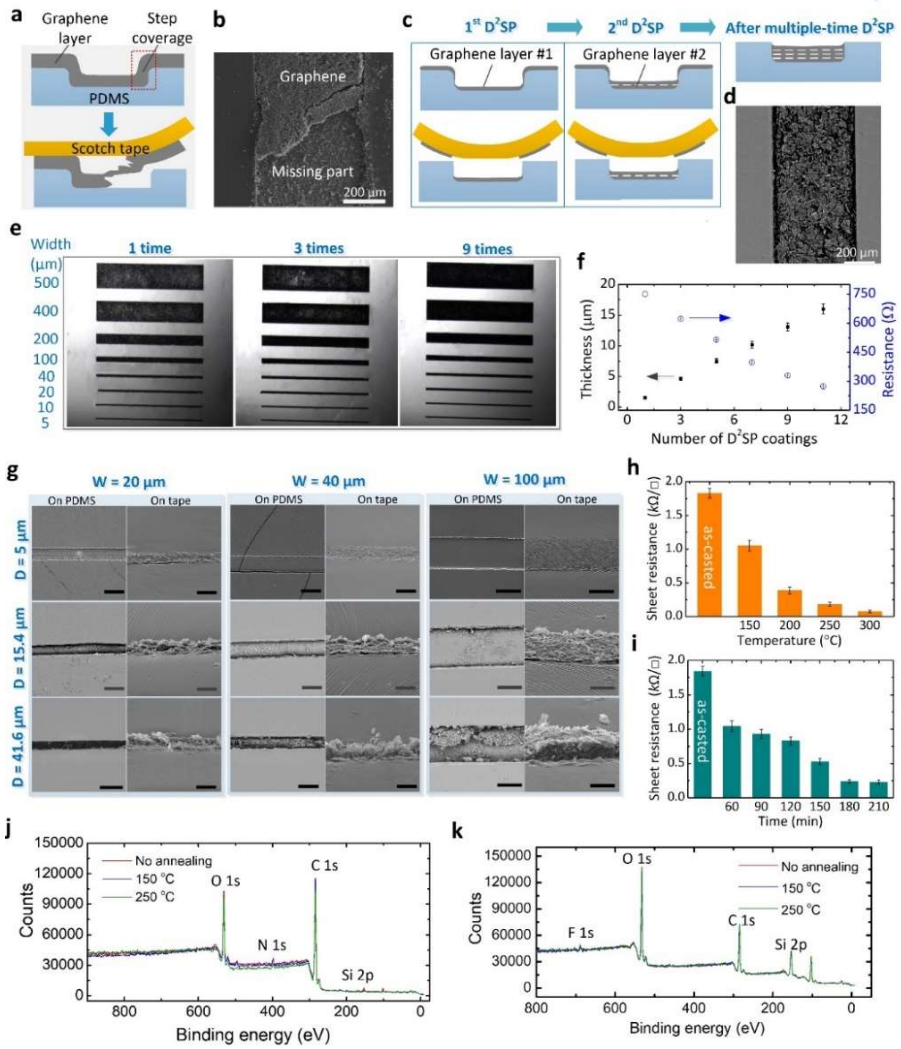

Figure 2.3 (a) A schematic representation of forming a thick graphene film over the entire PDMS surface by one time drop-casting, followed by using Scotch cleaning tape to remove the unwanted graphene from outside the patterned areas. (b) SEM image of the PDMS channel containing the incomplete graphene pattern. (c) A schematic representation of forming a thick graphene film over the entire PDMS surface via multi-time D^2SP processes. (d) SEM images of the PDMS channel filled with the complete graphene pattern after multiple D^2SP processes were applied. (e) Optical images for three groups of graphene patterns inside the PDMS channels. The numbers "5 μm–500 μm" and "1–3–9" represent PDMS channel widths, and numbers of graphene layers formed inside the PDMS channel by repeated D^2SP processes, respectively. (f) Thickness and electrical resistance of the graphene filled in the PDMS channel as a function of the number of D^2SP coatings. Each coating here is 1.45 ± 0.32 μm thick. (g) Analysis of influences of channel width and depth on the transfer process. The magnitudes of 20 μm, 40 μm, and 100 μm represent the channel widths, while the values of 5 μm, 15.4 μm, and 41.6 μm denote the channel depths. The scale bars represent 50 μm. Sheet resistance of transferred graphene patterns (~10.3 μm thickness) on the polyimide tape at different annealing temperatures (h) and durations (i). XPS survey spectra for graphene patterns transferred onto polyimide tapes (j) and the polyimide tape alone (k), without thermal treatment and annealed at 150 °C and 250 °C for 180 min.

X-ray photoelectron spectroscopy (XPS) was used to characterize the composition of the transferred graphene structures on tape before and after thermal treatment. Figure 2.3j, k depicts the XPS survey spectra for two groups of samples, that is, the transferred graphene (thickness: ≈ 10.3 μm) on a 25 μm thick polyimide tape, and the polyimide tape alone. There were three samples in each group, including one treated at 150 °C for 180 min, one 250 °C for the same time, and another not treated. The results show that all the on-tape graphene samples contain peaks assigned to C 1s (284 eV), O 1s (531.3 eV), N 1s (398.6 eV), and Si 2p (101.4 eV) (Figure 2.3j), and all the polyimide tape samples exhibited peaks belongs to C 1s (284.6 eV), O 1s (532.7 eV), F 1s (688.6 eV), and Si 2p (102.4 eV) (Figure 3k). For the on-tape graphene samples, O 1s peak occurs due to the physically adsorbed oxygen;[63] Si 2p peak might originate from the adhesive of the polyimide tape; and N 1s peak was observed because the graphene used here is N-doped graphene nanoplatelets.[64] Further, high-resolution spectra analysis (Figures A2 and A3, Appendix) confirms that the thermal treatment did not make distinct changes to the chemical structure of the graphene and polyimide tape samples, although the intensity of C 1s peak decreased slightly at 250 °C. The intensity of Si 2p peak of the graphene pattern decreased as the temperature increased up to 250 °C (Figure A2c, Appendix).

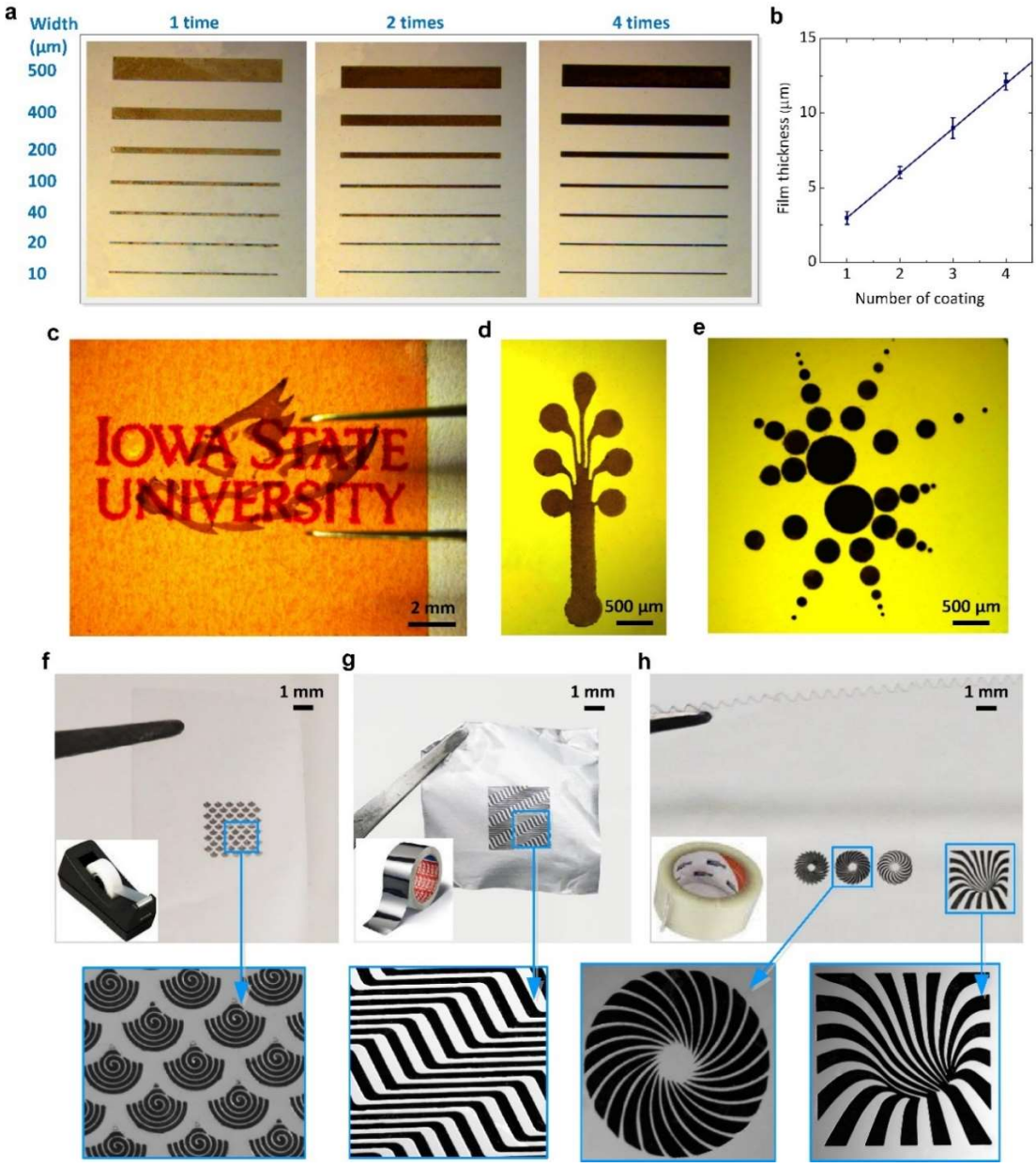

Figure 2.4 (a) Optical images of the rGO patterns inside the PDMS channels with a channel depth of 15.4 μm. The numbers "10 μm–500 μm" and "1– 2–4" denote the channel widths and numbers of graphene layers inside the PDMS channels, respectively. (b) Thickness of the GO patterns measured at different D^2SP times. (c–e) Various rGO patterns obtained on the polyimide tapes using a one-time (c), two-time (d), and five-time (e) D^2SP repeated process, followed by the ST process. (f–h) Optical images of the graphene patterns fabricated on various tape substrates, including Scotch tape with acrylic adhesive (f), aluminum foil tape (g), and Scotch tape with synthetic rubber adhesive (h).

The present patterning and transferring method could also be employed to obtain rGO patterns on tape. Figure 2.4a shows some rGO strip patterns formed inside the PDMS channels at different coating (or D^2SP) times, and Figure 2.4c–e shows the rGO patterns transferred onto the polyimide tape, using essentially the same method as described in Figure 2.1. The film thickness of the rGO linearly increased with coating time (Figure 2.4b). The experiments here utilized a PDMS substrate with 15.4 μm deep negative features at its surface. Five repeated D^2SP processes were sequentially applied to obtain the rGO patterns inside the negative features. For each coating, 100 μL cm^{-2} of rGO suspensions (20 mg mL^{-1} in the mixture of ethanol and DI water at a volume ratio of 7:3) were drop-coated over the entire PDMS surface.

In addition, the present method can also be used to produce graphene patterns on different adhesive substrates such as Scotch and aluminum foil tapes, both with acrylic adhesive (Figure 2.4f, g), and Scotch tape with synthetic rubber adhesive (Figure 2.4h). All the graphene patterns in Figure 2.4f–h was formed with five repeated D^2SP times and transferred onto the target tapes with the ST process.

2.3.2 Application Demonstrations

2.3.2.1 On-Tape Strain Sensors

A graphene strip pattern (6 mm length, 800 μm width, and 10.3 μm thickness) was transferred onto the polyimide tape as a strain sensor. The sheet resistance of the patterned graphene was 0.22 ± 0.12 kΩ sq−1. Electrical contacts between the graphene pattern and external tin copper electronic wires (Gauge 20) were realized with silver paste.

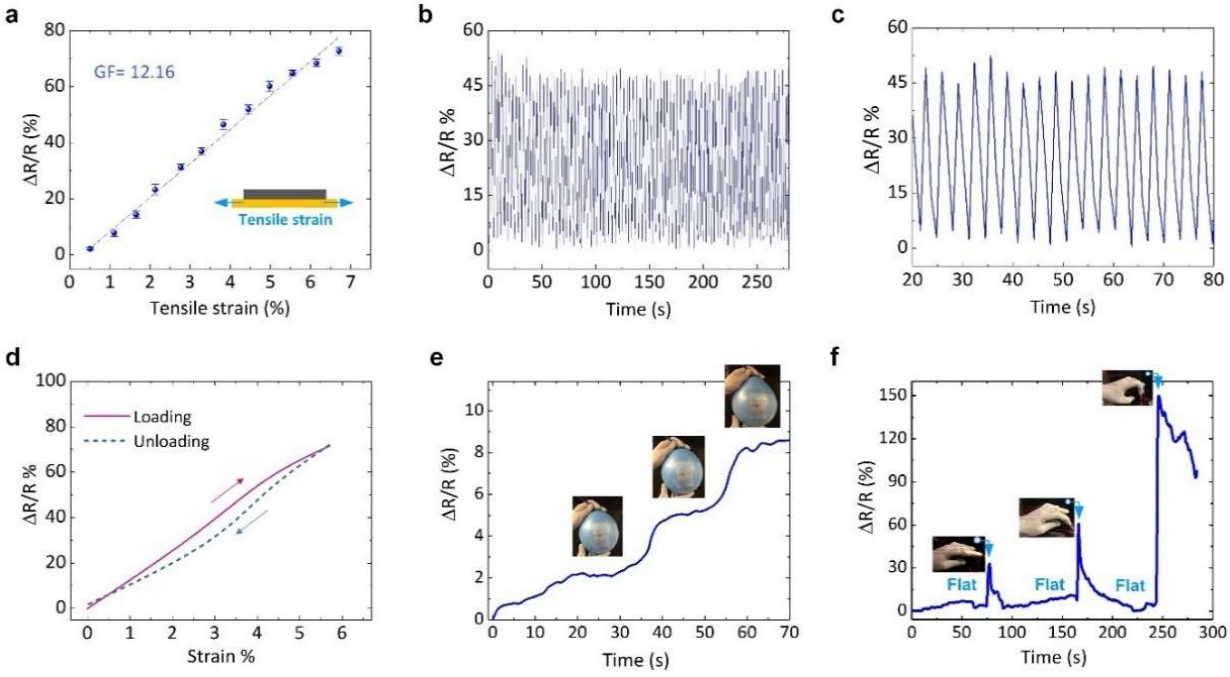

Figure 2.5 Demonstration of using a transferred graphene pattern as a strain sensor. (a) Relative change in resistance as a function of the tensile strain applied along the length direction of the graphene pattern. (b) Relative resistance of the sensor with the repetition of 100 loading/ unloading cycles by 4.4 % strain. (c) Enlarged view of (b), exhibits a stable sensor performance. (d) Hysteresis curve of the strain sensor. (e) Monitoring of tension changes on the balloon surface during inflation. (f) Monitoring of bending motions of the index finger.

Figure 2.5a shows the resistance response of the sensor to a tensile strain applied along the length direction of the graphene pattern. The relative resistance changes of the sensor (ΔR/R) increased linearly with applied tensile strain. The gauge factor of the sensor was found to be 12.16 from the slope of the linear fitting curve in Figure 2.5a. Figure 2.5b, c demonstrated the stability of the sensor by loading and unloading a 4.4% tensile strain for 100 times. The hysteretic behavior of the sensor was also investigated. The sensor was stretched up to 6% strain at the rate of 1.2% s^{-1}, and then released back to the initial position at the same rate (Figure 2.5d), exhibiting a low hysteretic behavior, which may be attributed to the elastic deformation of the sensor materials [65]. When the sensor was attached to the surface of a growing balloon, the value of ΔR/R increased due to the stretching of the graphene strip (Figure 2.5e). When the

balloon was in a temporarily static state, the sensor resistance remained constant. The tape-based strain sensor was therefore capable of monitoring strain variations at an object's surface.

In another test, the same type of sensor was attached to the middle joint of an index finger to measure the tensile strain formed during finger bending (Figure 2.5f). As the degree of bending increased from 5° to 90°, the value of ΔR/R of the sensor increased from 33.8 to 147.5%. After the finger returned to its original position, the sensor resistance immediately resumed its initial value, demonstrating good reversibility of the sensor response.

2.3.2.2 On-Tape Pressure Sensors

The above-mentioned strain sensor was adopted as an on-tape pressure sensor in this demonstration. Figure 2.6a shows that the ΔR/R value produced by the sensor increased with increasing pressure applied normal to the surface of the sensor. Based on the slopes of the linear fitting curves in different pressure ranges, the sensitivity of the sensor was found to be S = 0.13 kPa^{-1} for applied pressures below 300 kPa, and S = 0.053 kPa^{-1} in a higher pressure range up to 575 kPa. To verify durability of the sensor, the device was loaded (pressure normal to the sensor surface: 330 kPa) and unloaded for 100 cycles. No obvious degradation of the sensor response was observed after the testing (Figure 2.6b, c). In addition, the sensor exhibited a response time of ≈0.3 s (Figure 2.6d). This sensor was used to measure the pulse in the wrist. Figure 2.6e shows that the wrist pulses, 75 beats min−1, were counted via the time-varying relative resistance changes. Next, the sensor monitored repetitive finger clicking of a computer mouse. When the mouse was clicked, the ΔR/R value of the interacting sensor increased. Figure 2.6f demonstrates that the sensor continuously tracked various clicking pressures and frequencies.

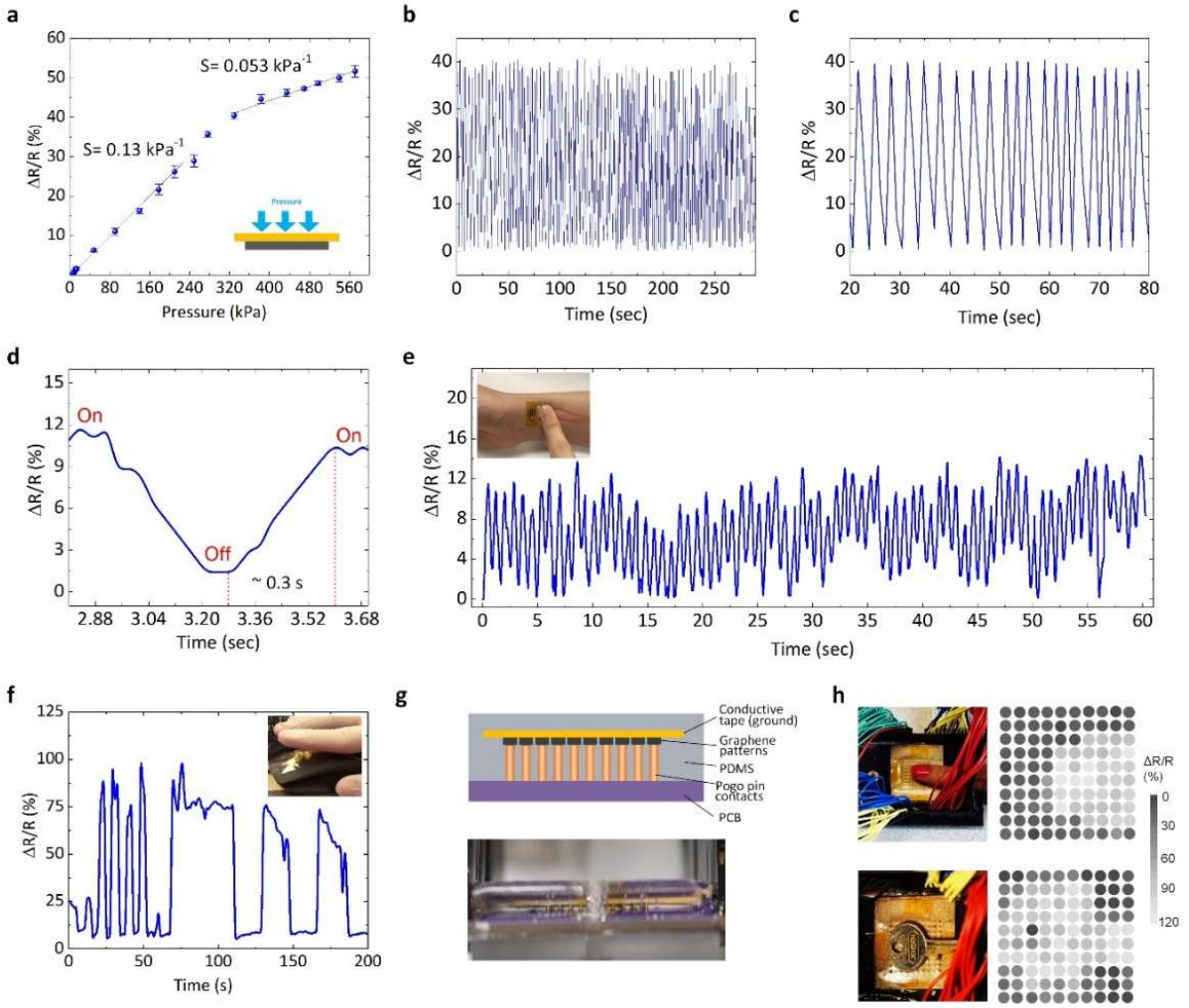

Figure 2.6 Demonstration of using transferred graphene pattern as a pressure sensor. (a) Relative change in resistance as a function of pressure uniformly applied to the polyimide tape surface. (b) Relative resistance changes of the sensor with repetition of 100 loading/unloading cycles by 330 kPa. (c) Enlarged view of (b), exhibiting a stable sensor performance. (d) Response curve of the sensor with an applied pressure of 80 kPa at a response time of 0.3 s. (e) Monitoring of the pulse rate of human wrist. (f) Monitoring of the frequency of mouse clicking. (g) Cross-sectional view of an array of 10 × 10 round-shaped graphene sensors for a pressure-mapping application. Top: schematic representation; bottom: fabricated device. (h) Top view of a finger (top) and a key (bottom) positioned on the surface of the pressure sensor array and ΔR/R mapping of the pressure distributions.

As another example application, an array of 10 × 10 round shaped graphene sensors was formed on 3M electrically conductive tape (Conductive adhesive transfer tape 9707) (Figure 2.6g). Each sensing element had a diameter of 1 mm, a thickness of ≈10.3 μm, and a pitch of 1.5 mm. Because this type of tape could sustain temperatures up to 85 °C [66], the transferred graphene was further annealed in air at 80 °C for 4 h to reduce its sheet resistance to 4.05 ± 0.18 kΩ sq^{-1}. These sensing elements were connected to an external detection circuit through an array of 10 × 10 vertical pogo pins (No. 575-09510152071, Mouser Electronics) formed on a printed circuit board and arranged in the same manner as the sensing elements (Figure 2.6g). The conductive tape served as a common ground for the sensing elements. To facilitate pressure application to the sensor array, the tape and pogo pins were embedded in a PDMS layer. After applying external pressure, changes in resistance were recorded by a multimeter through a multiplexer. Figure 2.6h shows that when a finger was pressed, or a key was positioned on the surface of the device, the embedded sensor array could monitor its interaction with the object and identify the shape and pressure (or resistance) profile of the object.

2.3.2.3 Smart Glove

Figure 2.7 depicts a smart glove equipped with on-tape strain and pressure sensors for monitoring mechanical response of fingers when interacting with an object. Specifically, each finger was equipped with a pressure sensor at its fingertip and a strain sensor at the top of the finger joint, respectively (Figure 2.7b, c). These sensors enabled real-time monitoring of changes in important mechanical parameters due to hand movements. As an example, the glove was worn while catching a tennis ball bounced from a hard floor (Figure 2.7d). The pressure (Figure 2.7e) and strain (Figure 2.7f) variations during preparing, adjusting, catching, and holding were obtained by the smart glove. As the ball bounded upward, the fingers adjusted to

bend more, increasing the tension on the sensors. When the ball was about to reach the palm, the fingers acted to catch the ball, producing immediate increases in the applied pressure. The flexibility of these tape-based graphene sensors allowed for conformable contact with the fingers. Such a smart glove would be useful in measuring hand mechanical function and control in many applications, such as providing real-time data streams for medical rehabilitation therapies and human-computer interaction.

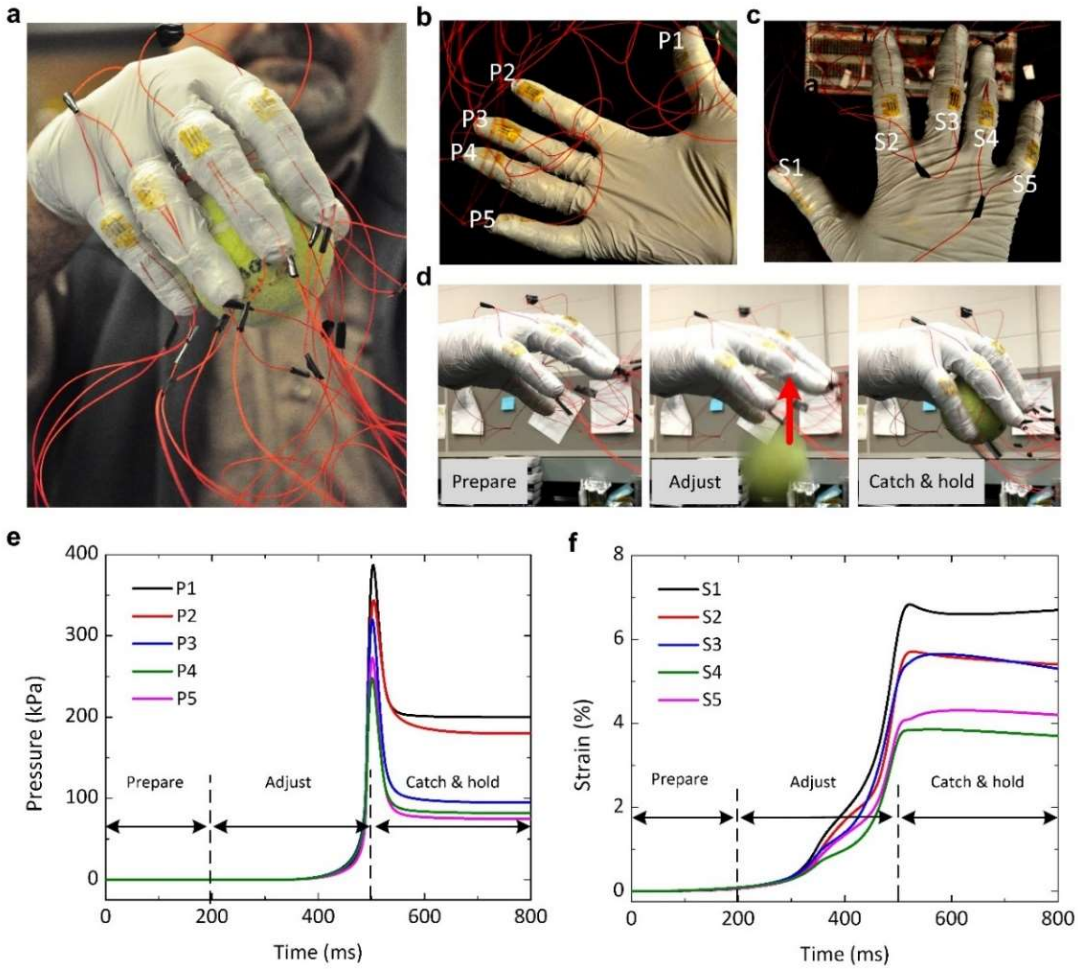

Figure 2.7 Demonstration of using a smart glove to monitor the pressure and strain levels during catching a tennis ball. (a) An optical image of the graphene sensors attached to the finger joints. (b–c) Positions of the five pressure sensors (P1–P5) and five strain sensors (S1–S5). (d) Time-lapse images of catching the tennis ball using the smart glove. The three images represent the three states: preparation (left), adjustment (middle), and catching (right). (e–f) Responses of the smart glove during catching the tennis ball, including pressure (e) and strain (f) responses.

2.3.2.4 On-Tape Plant Leaf Sensors

When Water uptake by roots, transport through the xylem, and transpiration from the stomata of leaves to the atmosphere are an important physiological process in plants. Using tape-based graphene RH sensors, we demonstrated a unique capability to estimate the time required for water movement within a plant from the roots to the lower and upper leaves (Figure 2.8a). When the stomata are open, water vapor escapes from the leaves, increasing the local humidity level on the leaf surface (Figure 2.8b). Consequently, by installing multiple RH sensors on different leaves to dynamically monitor RH variation at the leaf surfaces, it is possible to track the key time points at which significant water loss occurs at the leaves, thus quantifying water transport time via the xylem from the roots to each of the measured leaves. The RH sensors were structured as graphene strips (6 mm length, 800 μm width, and 10.3 μm thickness) transferred onto the polyimide tape and are the same as those used in the above-mentioned pressure and strain sensing applications. The sensing mechanism is based on changes in the electrical resistance of graphene in different moisture environments. Figure 2.8c shows the resistance response of the fabricated sensor exposed to different RH levels at room temperature. To facilitate the installation of the sensor onto the leaf surface, two additional tape strips (acrylic adhesive; No. 6915001 from Gorilla) were adhered to the two sides of the graphene pattern (see the inset of Figure 8c). This also created a 170 μm thick air gap between the sensor surface and the leaf, as well as two side openings that allow air exchange between inside and outside of the gap space for avoiding accumulation of water vapor. The air gap was determined by the thickness of the additional tape strips.

Figure 2.8d, e describes real-time monitoring of RH using the sensors installed on the back surfaces of the fourth and ninth leaf of two-month old maize plants. Here, one type of plant

(Figure 2.8d) was inbred line B73 [67]. The other type (Figure 2.8e) was a mixed genetic stock (having a more complicated pedigree in which the female parent was a hybrid with no close relationship to B73, and the male parent was in a B73 background; they were grown in Dr. Patrick Schnable's lab at Iowa State University). The testing was initiated 15 min before irrigation. After irrigation, for B73, the lower and upper sensors exhibited a resistance increment and thus an increase in RH at 55 and 135 min, respectively. Similarly, for the mixed genetic stock, the sensor outputs of the show that the lower and upper leaves had an increase in RH at 82 and 110 min, respectively. Therefore, in both the B73 plants and plants with mixed genetic backgrounds, it took less time for water to be transported from the roots to the fourth leaf than from the roots to the ninth leaf. Significantly, these two genetic stocks exhibited differences in the delta between the fourth and ninth leaves (80 ± 11 min, mean ± standard deviation obtained from the measurements on three plants for B73 versus 28 ± 10 min, mean ± standard deviation obtained from the measurements on three plants for the plants with a mixed genetic background). Because water transport is a critical process for plants, the on-tape RH sensor technology would be useful to select plants with a desirable water transport character or improved tolerance to increasing water stress, a major objective of crop breeding.

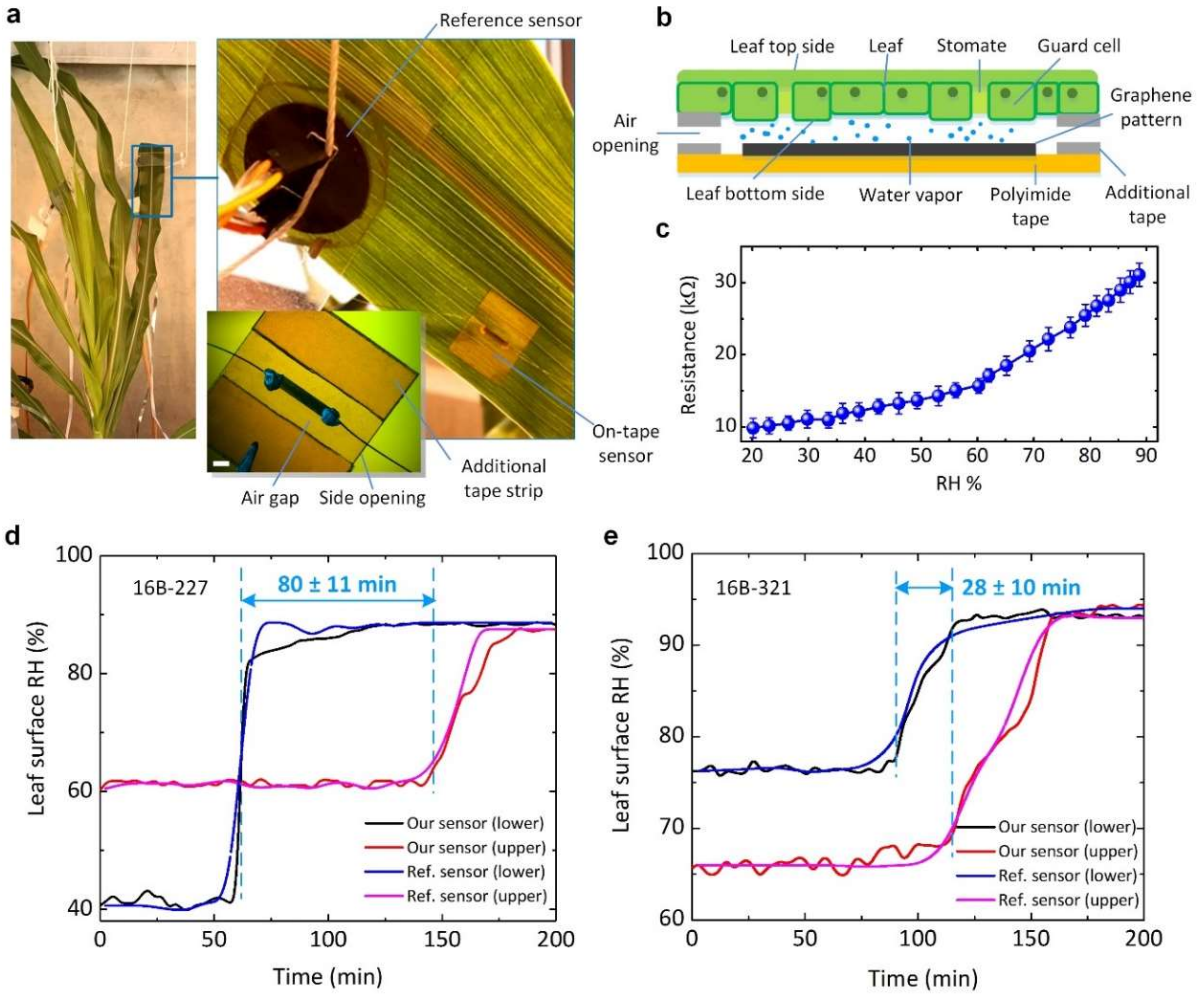

Figure 2.8 Demonstration of using the on-tape RH graphene sensors for the estimation of the times required for water movement within the plant from the roots to the lower and upper leaves. (a) A photo of the graphene RH sensor and a commercial RH reference sensor located at the back of the maze leaf. The placement of the two sensors is magnified in the right-hand image to clarify the structure. The scale bar represents 1 mm. (b) A schematic illustration of the sensor placement and detection mechanism. (c) Resistance of the graphene sensor as a function of RH. The resistance is measured using a RLC meter at 100 Hz operation frequency. (d)–(e) Real-time monitoring of the RH level on the leaf surface after plant irrigation at two maize plants: B73 (d) and a mixed genetic stock (e).

The above demonstrations provide only a few application examples of using tape-based flexible sensors, and many other graphene sensors could be designed and manufactured on tape for use in a variety of emerging applications. For example, the graphene pressure and strain

sensors could be fastened to the surfaces of mechanical and infrastructure systems for structural health monitoring purposes. By functionalizing the patterns of graphene-based nanomaterials on the tape with an enzyme substrate or a receptor ligand that respond to a specific receptor or enzyme, or by transferring materials already functionalized inside the PDMS negative features onto a tape, it would be possible to develop many wearable and disposable biological and chemical sensors on tape for applications in biomedical diagnostics (e.g., sweat glucose and electrolyte sensing), environmental monitoring (e.g., gas sensing), and agricultural monitoring (e.g., nutrient and pesticide sensing). In addition, this fabrication approach allows formation of high resolution patterns on the surfaces of versatile tapes as long as their free surface energies are different enough to enable strong adhesion to one another. This advantage, in conjunction with the ability to control the patterns along three dimensions with high spatial resolution, would further extend the application potential of this method. Further work will aim at using the presented technology to develop on-tape sensors with different nanomaterials. We believe that this technology will open a new route for low-cost, scalable, and roll-to-roll production of various types of nanomaterials-based sensors.

2.4 Conclusion

In summary, a novel tape-based graphene patterning and transfer approach has been developed. It is simple and effective and has potential to support realization of roll-to-roll production of various graphene sensors. Once PDMS negative patterns are formed via conventional soft lithography, only adhesive tapes are required to produce graphene patterns with feature resolution of a few micrometers. The method can be applied to many tapes to realize various flexible sensors, such as the demonstrated wearable graphene-based sensors for mechanical and RH sensing on surfaces of humans and crop plants.

2.5 Acknowledgements

This work was supported in part by the Iowa Department of Transportation, the Iowa Highway Research Board, the Plant Sciences Institute at Iowa State University through the PSI Faculty Scholar program, and the U.S. National Science Foundation under Grant No. DBI-1353819. S.O. thanks the Turkish Council of High Education and Anadolu University, Turkey, for partial financial support. The authors thank Lisa Coffey for growing plants for testing, Leland Harker for assistance in PCB design and manufacturing, Shawana Tabassum and Mehmet Oren for assistance in testing of sensors, and Dr. Kasthurirangan Gopalakrishnan, Dr. Sunghwan Kim, and Dr. Peter Taylor for helpful discussions. All the above names are affiliated with the Iowa State University, except for Mehmet Oren.

2.6 References

[1] Madaria, A. R., Kumar, A., Ishikawa, F. N. & Zhou, C. Uniform, highly conductive, and patterned transparent films of a percolating silver nanowire network on rigid nd flexible substrates using a dry transfer technique. *Nano Research* **3**, 564-573, doi:10.1007/s12274-010-0017-5 (2010).

[2] Wiria, F. E. *et al.* Improving surface quality of polyethylene terephthalate film for large area flexible electronic applications. *Journal of Solid State Electrochemistry* **20**, 1895-1902, doi: 10.1007/s10008-015-3021-6 (2016).

[3] Kizil, H., Pehlivaner, M. O. & Trabzon, L. Surface plasma characterization of polyimide films for flexible electronics. *Advanced Materials Research* **970**, 132-135, doi: 10.4028/www.scientific.net/AMR.970.132 (2014).

[4] Wang, C. *et al.* Extremely bendable, high-performance integrated circuits using semiconducting carbon nanotube networks for digital, analog, and radio-frequency applications. *Nano Letters* **12**, 1527-1533, doi: 10.1021/nl2043375 (2012).

[5] Wang, Y. *et al.* Super-elastic graphene ripples for flexible strain sensors. *ACS Nano* **5**, 3645-3650, doi: 10.1021/nn103523t (2011).

[6] Schwartz, G. *et al.* Flexible polymer transistor with high pressure sensitivity for application in electronic skin and health monitoring. *Nature Communications* **4**, 1859-1866, doi: 10.1038/ncomms2832 (2013).

[7] Zheng, Y., He, Z., Gao, Y. & Liu, J. Direct desktop printed-circuits on paper flexible electronics. *Scientific Reports* **3**, 1786-1793, doi: 10.1038/srep01786 (2013).

[8] Ishikawa, F. N. *et al.* Transparent electronics based on transfer printed aligned carbon nanotubes on rigid and flexible substrates. *ACS Nano* **3**, 73-79, doi: 10.1021/nn800434d (2009).

[9] Lee, Y.-H. *et al.* Wearable textile battery rechargeable by solar energy. *Nano Letters* **13**, 5753-5761, doi: 10.1021/nl403860k (2013).

[10] Pu, X. *et al.* A self-charging power unit by integration of a textile triboelectric nanogenerator and a flexible lithium-ion battery for wearable electronics *Advanced Materials* **27**, 2472-2478, doi: 10.1002/adma.201500311 (2015).

[11] Kim, Y. H. *et al.* Self-activated transparent all-graphene gas sensor with endurance to humidity and mechanical bending. *ACS Nano* **9**, 10453-10460, doi: 10.1021/acsnano.5b04680 (2015).

[12] Lu, G. *et al.* Toward practical gas sensing with highly reduced graphene oxide: A new signal processing method to circumvent run-to-run and device-to-device variations. *ACS Nano* **5**, 1154-1164, doi: 10.1021/nn102803q (2011).

[13] Sudibya, H. G., He, Q., Zhang, H. & Chen, P. Electrical detection of metal ions using filed-effect transistors based on micropatterned reduced graphene oxide films. *ACS Nano* **5**, 1990-1994, doi:10.1021/nn103043v (2011).

[14] Park, S. J. *et al.* Ultrasensitive flexible graphene-based field-effect transistor (FET)-type bioelectronic nose. *Nano Lett*ers **12**, 5082-5090, doi: 10.1021/nl301714x (2012).

[15] Labroo, P. & Cui, Y. Flexible graphene bio-nanosensor for lactate. *Biosensors and Bioelectronics* **41**, 852-856, doi: 10.1016/j.bios.2012.08.024 (2013).

[16] Pang, Y. *et al.* Flexible, highly sensitive, and wearable pressure and strain sensors with graphene porous networks structure. *ACS Applied Materials & Interfaces* **8**, 26458-26462, doi: 10.1021/acsami.6b08172 (2016).

[17] Chun, S. *et al.* A graphene force sensor with pressure-amplifying structure. *Carbon* **78**, 601-608, doi: 10.1016/j.carbon.2014.07.051 (2014).

[18] Sadasivuni, K. K. *et al.* Transparent and flexible cellulose nanocrystal/reduced graphene oxide film for proximity sensing. *Small* **11**, 994-1002, doi: 10.1002/smll.201402109 (2015).

[19] Lee, S. *et al.* A transparent bending-insensitive pressure sensor. *Nature Nanotechnology* **11**, 472-479, doi: 10.1038/NNANO.2015.324 (2016).

[20] Romano, M. S. *et al.* Carbon nanotube-reduced graphene oxide composite for thermal energy harvesting applications. *Advanced Materials* **25**, 6602-6606, doi:10.1002/adma.201303295 (2013).

[21] Han, S., Wu, D., Li, S., Zhang, F. & Feng, X. Porous graphene materials for advanced electrochemical energy storage and conversion devices. *Advanced Materials* **26**, 849-864, doi: 10.1002/adma.201303115 (2014).

[22] Ali, Md. A. *et al.* Tunable bioelectrodes with wrinkled-ridged graphene oxide surfaces for electrochemical nitrate sensors. *RSC Advances* **6**, 67184-67195, doi: 10.1039/c6ra09621b (2016).

[23] Wang, Q., Hong, W. & Dong, L. Graphene "microdrums" on a freestanding perforated thin membrane for high sensitivity MEMS pressure sensors. *Nanoscale* **8**, 7663-7671, doi: 10.1039/c5nr09274d (2016).

[24] Ali, Md. A. *et al.* Microfluidic immune-biochip for detection of breast cancer biomarkers using hierarchical composite of porous graphene and titanium dioxide nanofibers. *ACS Applied Materials & Interfaces* **8**, 20570-20582, doi:10.1021/acsami.6b05648 (2016).

[25] Bolotin, K. I. *et al.* Ultrahigh electron mobility in suspended graphene. *Solid State Communications* **146**, 351-356 (2008).

[26] Xu, K. *et al.* The positive piezo conductive effect in graphene. *Nature Communications* **6**, 8119-8125, doi: 10.1038/ncomms9119 (2015).

[27] Lee, C., Wei, X., Kysar, J. W. & Hone, J. Measurement of the elastic properties and intrinsic strength of monolayer graphene. *Science* **321**, 385-388, doi: 10.1126/science.1157996 (2008).

[28] An, B. *et al.* Three-dimensional multi-recognition flexible wearable sensor via graphene aerogel printing. *Chemical Communications* **52**, 10948-10951, doi: 10.1039/c6cc05910d (2016).

[29] Mannoor, M. S. *et al.* Graphene-based wireless bacteria detection on tooth enamel. *Nature Communications* **3**, 763-772, doi: 10.1038/ncomms1767 (2012).

[30] Jiao, Y. *et al.* Wearable graphene sensors with microfluidic liquid metal wiring for structural health monitoring and human body motion sensing. *IEEE Sensors Journal* **16**, 7870-7875, doi: 10.1109/JSEN.2016.2608330 (2016).

[31] Amjadi, M., Kyung, K.-U., Park, I. & Sitti, M. Stretchable, skin-mountable, and wearable strain sensors and their potential applications: A review. *Advanced Functional Materials* **26**, 1678-1698, doi: 10.1002/adfm.201504755 (2016).

[32] Yang, T. *et al.* Tactile sensing system based on arrays of graphene woven microfabrics: Electromechanical behavior and electronic skin application. *ACS Nano* 9, 10867-10875, doi 10.1021/acsnano.5b03851 (2015).

[33] Park, J. W. & Jang, J. Fabrication of graphene/free-standing nanofibrillar PEDOT/P(VDF-HFP) hybrid device for wearable and sensitive electronic skin application. *Carbon* **87**, 275-281, doi: 10.1016/j.carbon.2015.02.039 (2015).

[34] Tung, T. T. *et al.* Graphene quantum resistive sensing skin for the detection of alteration Biomarkers. *Journal of Materials Chemistry* **22**, 21754-21766, doi: 10.1039/c2jm34806c (2012).

[35] Hou, C. *et al.* Highly conductive, flexible, and compressible all-graphene passive skin for sensing human touch. *Advanced Materials* **26**, 5018-5024, doi: 10.1002/adma.201401367 (2014).

[36] Ho, D. H. *et al.* Stretchable and multimodal all graphene electronic skin. *Advanced Materials* 28, 2601-2608, doi: 10.1002/adma.201505739 (2016).

[37] Wu, C. *et al.* Large-area graphene realizing ultrasensitive photothermal actuator with high transparency: new prototype robotic motions under infrared-light stimuli. *Journal of Materials Chemistry* **21**, 18584-18591, doi: 10.1039/c1jm13311j (2011).

[38] Novoselov, K. S. *et al.* Electric field effect in atomically thin carbon films. *Science* **306**, 666-669, doi: 0.1126/science.1102896 (2004).

[39] Wang, L. *et al.* Simple and large-scale strategy to prepare flexible graphene tape electrode. *ACS Applied Materials & Interfaces* **9**, 9089-9095, doi:10.1021/acsami.6b14624 (2017).

[40] Tehrani, F., Reiner, L. & Bavarian, B. Rapid prototyping of a high sensitivity graphene-based glucose sensor strip. *PLOS One* **10**, 145036-145047, doi :10.1371/journal.pone.0145036 (2015).

[41] Alemán, B. *et al.* Transfer-free batch fabrication of large-area suspended graphene membranes. *ACS Nano* **4**, 4762-4768, doi: 10.1021/nn100459u (2010).

[42] Zhang, L. *et al.* Photocatalytic patterning and modification of graphene. *Journal of the American Chemical Society* **133**, 2706-2713, doi:10.1021/ja109934b (2011).

[43] Sun, Z. *et al.* Towards hybrid superlattices in graphene. *Nature Communications* **2**, 559-564, doi:10.1038/ncomms1577 (2011).

[44] Kuzum, D. *et al.* Transparent and flexible low noise graphene electrodes for simultaneous electrophysiology and neuroimaging. *Nature Communications* **5**, 5259-5269, doi: 10.1038/ncomms6259 (2014).

[45] Bae, S.-H. *et al.* Graphene-based transparent strain sensor. *Carbon* **51**, 236-242, doi: 10.1016/j.carbon.2012.08.048 (2013).

[46] Li, X. *et al.* Large-area synthesis of high-quality and uniform graphene films on copper foils. *Science* **324**, 1312-1314, doi: 10.1126/science.1171245 (2009).

[47] Andrew, M. H. Ng. *et al.* Patterning of graphene with tunable size and shape for microelectrode array devices. *Carbon* **67**, 390-397, doi: 10.1016/j.carbon.2013.10.009 (2014).

[48] Yong, K., Ashraf, A., Kang, P. & Nam, S. Rapid stencil mask fabrication enabled one-step polymer-free graphene patterning and direct transfer for flexible graphene devices. *Scientific Reports* **6**, 24890-24898, doi: 10.1038/srep24890 (2016).

[49] Hofmann, M., Hsieh, Y.-P., Hsu, A. L. & Kong, J. Scalable, flexible and high-resolution patterning of CVD graphene. *Nanoscale* **6**, 289-292, doi: 10.1039/c3nr04968j (2014).

[50] El-Kady, M. F. & Kaner, R. B. Scalable fabrication of high-power graphene micro-supercapacitors for flexible and on-chip energy storage. *Nature Communications* **4**, 1475-1484, doi: 10.1038/ncomms2446 (2013).

[51] Senyuk, B. *et al.* Three-dimensional patterning of solid microstructures through laser reduction of colloidal graphene oxide in liquid-crystalline dispersions. *Nature Communications* **6**, 7157-7164, doi: 10.1038/ncomms8157 (2015).

[52] Lin, J. *et al.* Laser-induced porous graphene films from commercial polymers. *Nature Communications* **5**, 5714-5722, doi:10.1038/ncomms6714 (2014).

[53] Tian, H. *et al.* Scalable fabrication of high-performance and flexible graphene strain sensors. *Nanoscale* **6**, 699-705, doi: 10.1039/c3nr04521h (2014).

[54] Tian, H. *et al.* A graphene-based resistive pressure sensor with record-high sensitivity in a wide pressure range. *Scientific Reports* **5**, 8603-8609, doi: 10.1038/srep08603 (2015).

[55] Das, S. R. *et al.* 3D nanostructured inkjet printed graphene via UV-pulsed laser irradiation enables paper-based electronics and electrochemical devices. *Nanoscale* **8**, 15870-15879, doi: 10.1039/c6nr04310k (2016).

[56] Lee, J. S. *et al.* Wafer-scale patterning of reduced graphene oxide electrodes by transfer-and-reverse stamping for high performance OFETs. *Small* **9**, 2817-2825, doi:10.1002/smll.201300538 (2013).

[57] He, Q. *et al.* Centimeter-long and large-scale micropatterns of reduced graphene oxide films: Fabrication and sensing applications. *ACS Nano* **4**, 3201-3208, doi:10.1021/nn100780v (2010).

[58] Liu, W.-W., Xia, B.-Y., Wang, X.-X. & Wang, J.-N. Exfoliation and dispersion of graphene in ethanol-water mixtures. *Frontiers of Materials Science* **6**, 176-182, doi: 10.1007/s11706-012-0166-4 (2012).

[59] Zheng, W. Surface wetting characteristics of rubbed polyimide thin films. *Polymer Thin Films* Ch. 10 (2010).

[60] Ebnesajjad, S. & Ebnesajjad, C. Surface Treatment of Materials for Adhesion Bonding. *William Andrew Publishing* **2nd ed.,** Ch. 5. (2014).

[61] Kim, H. *et al.* Micropatterning of thin P3HT films via plasma enhanced polymer transfer printing. *Journal of Materials Chemistry* **18**, 3489-3495, doi: 10.1039/b807285j (2008).

[62] Dupont Kapton Summary of Properties, https://www.dupont.com/ content/dam/dupont/products-and-services/membranes-and films/ polyimde films/documents/DEC-Kapton-summary-of-properties. pdf (accessed: March 2017).

[63] Jeon, I.-Y. *et al.* Direct nitrogen fixation at the edges of graphene nanoplatelets as efficient electrocatalysts for energy conversion. *Scientific Reports* **3**, 2260-2267, doi: 10.1038/srep02260 (2013).

[64] Feng, X. *et al.* Three-dimensional nitrogen-doped graphene as an ultrasensitive electrochemical sensor for the detection of dopamine. *Nanoscale* **7**, 2427-2432, doi: 10.1039/c4nr06623e (2015).

[65] Y. R. Jeong, *et al.* Highly stretchable and sensitive strain sensors using fragmentized graphene foam. *Advanced Functional Materials* **25**, 4228-4236, doi:10.1002/adfm.201501000 (2015).

[66] 3M™ Electrically Conductive Adhesive Transfer Tape 9707, https:// multimedia.3m.com/mws/media/536957O/3mtm-electrically-conductive- adhesive-transfer-tape-9707.pdf (accessed: May 2014).

[67] Schnable, P. S. *et al.* The B73 Maize Genome: Complexity, Diversity, and Dynamics. *Science* **326**, 1112-1115, doi: 10.1126/science.1178534 (2009).

[68] Kozbial, A. *et al.* Study on the surface energy of graphene by contact angle measurements. *Langmuir* **30**, 8598-8606 (2014).

[69] Huang, X. D. et al. Surface modification studies of Kapton HN polyimide films. *Polymer International* **52**, 1064-1069, doi: 10.1002/pi.1143 (2003).

[70] Accu Dyne Test, https://www.accudynetest.com/polytable_02.html (accessed: April 2017).

[71] Graphene Supermarket, https://graphene-supermarket.com/Conductive- Graphene-Dispersion-100.html (accessed: January 2017).

CHAPTER 3

HELICAL- SHAPED GRAPHENE TUBULAR SPRING FORMED WITHIN MICROCHANNEL FOR WEARABLE STRAIN SENSOR WITH WIDE DYNAMIC RANGE

A paper published in IEEE Sensor Letters

Seval Oren, Halil Ceylan, and Liang Dong

3.1 Abstract

This paper reports on a helical spring-like piezo resistive graphene strain sensor formed within a microfluidic channel. The helical spring has a tubular hollow structure and is made of a thin graphene layer coated on the inner wall of the channel using an *in situ* microfluidic casting method. The helical shape allows the sensor to flexibly respond to both tensile and compressive strains in a wide dynamic detection range from 24% compressive strain to 20% tensile strain. Fabrication of the sensor involves embedding a helical thin metal wire with a plastic wrap into a precursor solution of an elastomeric polymer, forming a helical microfluidic channel by removing the wire from cured elastomer, followed by microfluidic casting of a graphene thin layer directly inside the helical channel. The wide dynamic range, in conjunction with mechanical flexibility and stretch ability of the sensor, will enable practical wearable strain sensor applications where large strains are often involved.

3.2 Introduction

Many functional nanomaterials and composites have recently been incorporated with elastomer substrates to realize flexible mechanical sensors [1]. These sensors often work by detecting subtle changes in electrical resistivity or permittivity of sensing materials in response to mechanical stimuli. For wearable sensor applications, such as body motion tracking [2], strain

sensors often experience large tensile and compressive strains, and thus require a wide dynamic range, and high flexibility and stretchability [3]. Conventional strain sensors using rigid substrates, however, are unable to meet these requirements. For substrate materials of wearable and flexible strain sensors, polydimethylsiloxane (PDMS) has been demonstrated as a promising elastomer substrate due to high stretchability and simple fabrication. Ecoflex is another substrate candidate material for strain sensors since it can be stretched by over 900% and return to its original state [4]. For sensing materials of wearable and flexible strain sensors, recent advances in nanomaterials have led to many candidates sensing materials in the form of nanoparticles, nanowires and nanotubes, as well as two-dimensional materials [5-15]. Among them, graphene possesses high piezoresistivity, electron mobility and flexibility [10]. As a result, many graphene-based flexible strain sensors have been developed by forming graphene patterns on the surface of elastomer substrate [14, 15] or using graphene-based nanocomposites [16-18].

It should be pointed out that most of the existing graphene-based strain sensors have a planar structure. They are often realized on the surfaces of elastomer substrates. The planar graphene elements tend to break at large strains, even though the elastomer substrate may still remain functional. In addition, most planar graphene sensors are not able to detect compressive strain. In order to enhance the dynamic range of strain sensors, wavy wrinkled micro/nanoscale structures have been realized on the top surfaces of elastomer substrates [16-18]. Carbon nanotube (CNT) array double helices have also been used as the main building block of a sensitive film to form a highly stretchable strain sensor on a thermoplastic elastomer substrate [19].

In this paper, we demonstrate unique design and manufacturing of flexible strain sensors to obtain a wide dynamic range. The central core of the sensor is a helical-shaped tubular hollow

structure made of graphene. The helically structured graphene is formed on the inner surface of a helical channel embedded inside a PDMS substrate. Due to the helical spring-like design, the sensor offers an improved dynamic range of strain along the axis of the spring and also is able to respond to both compression and tension. In addition, unlike other graphene strain sensors manufactured using traditional techniques such as deposition, photolithography and etching, or new methods such as transfer printing, nanoimprint lithography and laser cutting [20-23], our graphene sensor uses a simple molding and refill process to realize *in situ* microfluidic casting of graphene layer directly inside a helical channel.

3.3 Method

Fabrication of the helical tubular graphene strain sensor takes four major steps, including (i) embedding a helical coil into a precursor solution of elastomer (Fig. 3.1a), (ii) realizing a helical channel by removing the coil from cured elastomer (Fig. 3.1b and 3.1c), (iii) *in situ* microfluidic casting of graphene on the inner surface of the helical channel (Fig. 3.1d), and (iv) forming electrical contacts to external circuits. The detail of fabrication process is described below.

Initially, the precursor solution of PDMS was prepared by mixing Sylgard 184 silicone elastomer base and its curing agent (Dow Corning, Auburn, MI) at a weight ratio of 10:1, and then were degassed in a vacuum desiccator for 20 min. Subsequently, a Tin-plated copper metal wire wrapped with a plastic coating (0.5 mm-diameter wrapping wire; Gauge 30) was manually winded around a 2.9 mm-diameter metal rod. The spacing between neighboring helix of the coiled wire was controlled by the alignment marks pre-labelled on the metal rod. The helical coil was taken off the rod, serving as a mold for the helical channel. Subsequently, the mold was fully

immersed in the PDMS precursor solution. Here, the shape of the helical coil was determined by the following equations [24]:

$$L_o = \sqrt{(\pi D)^2 + S^2} \quad (1)$$

$$L_n = NL_o \quad (2)$$

$$L = NS \quad (3)$$

where D, S, L_o, N, L_n, and L correspond to the helix diameter (D = 2.9 mm), the distance between the neighboring helix (S = 1.9 mm), the circumference of each helix (L_o = 9.3 mm), the number of helix (N = 6), the total length of the coil in flat mode (L_n = 55.8 mm), and the straight end-to-end length of the coil (L = 11.4 mm). The helical coil was supported by two clips at its two ends before the PDMS precursor solution was poured over it. After thermally cured on a hotplate at 65 °C for 2 h, the cured PDMS embedded with the helical coil was placed in acetone for 2 h. As a result, the plastic wrap was partially dissolved by acetone, allowing easy pulling of the coil out of the PDMS. Therefore, a helical channel was obtained inside the elastomer. It should be noted that if a metal coil alone (without a plastic wrap) was used as the mold of the helical channel, it would be difficult to pull out the coiled metal due to a large friction between the metal and surrounding PDMS. On the other hand, a plastic wire alone (without a metal core) is not easy to be shaped into a coil. When serving as the mold, the plastic wire may be broken inside the PDMS during pulling.

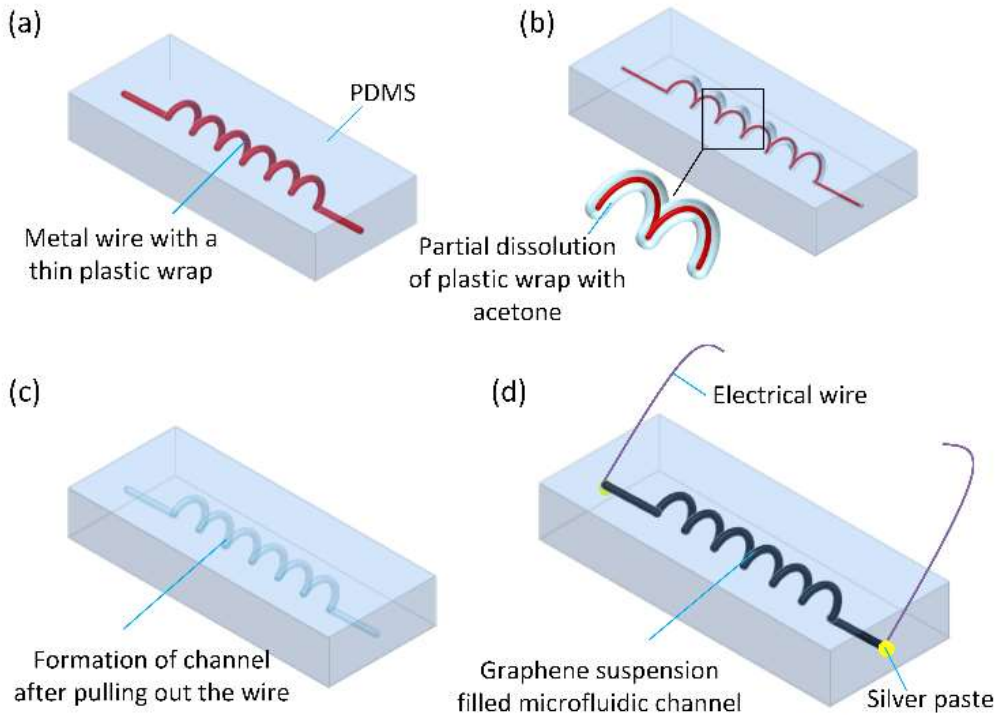

Figure 3.1 Schematic representation of the fabrication process for the helical-shaped tubular graphene strain sensor.

Next, the *in situ* microfluidic casting approach was used to obtain a graphene layer on the inner wall of the helical channel. Here, aqueous solutions of graphene suspensions (20 mg/ml) were prepared by dispersing 20 mg graphene nanoplatelets (obtained by evaporation of acetate from the graphene dispersion purchased from Graphene Supermarket, Calverton, NY; SKU: UHC-NPD) in a 1 ml mixture of ethanol and deionized water at a volume ratio of 7:3, followed by sonication at room temperature for 400 min. The specific ethanol-to-water volume ratio was chosen because it could provide sufficient dispersion and maximum concentration of graphene nanoplatelets in the mixture (Figure A4, Appendix) [25]. After that, the helical channel was filled by injecting the prepared graphene suspension solution into the channel using a medical syringe (National Target; 10 ml volume). After drying at room temperature for 10 min and then at 90 °C for 5 min, a graphene layer (1.45 ± 0.24 µm) was casted on the inner surface of the

channel. This *in situ* fabrication process was repeated twice to ensure a full graphene coverage on the inner wall. Next, electrical contacts of the graphene with two tin copper wires (Gauge 20) were realized with silver paste at the two ends of the channel. For comparison, a counterpart sensor with a straight channel was manufactured using the same fabrication process. The straight channel had the same diameter (0.5 mm) and end-to-end length (11.4 mm) as the helical channel.

3.4 Results and Discussion

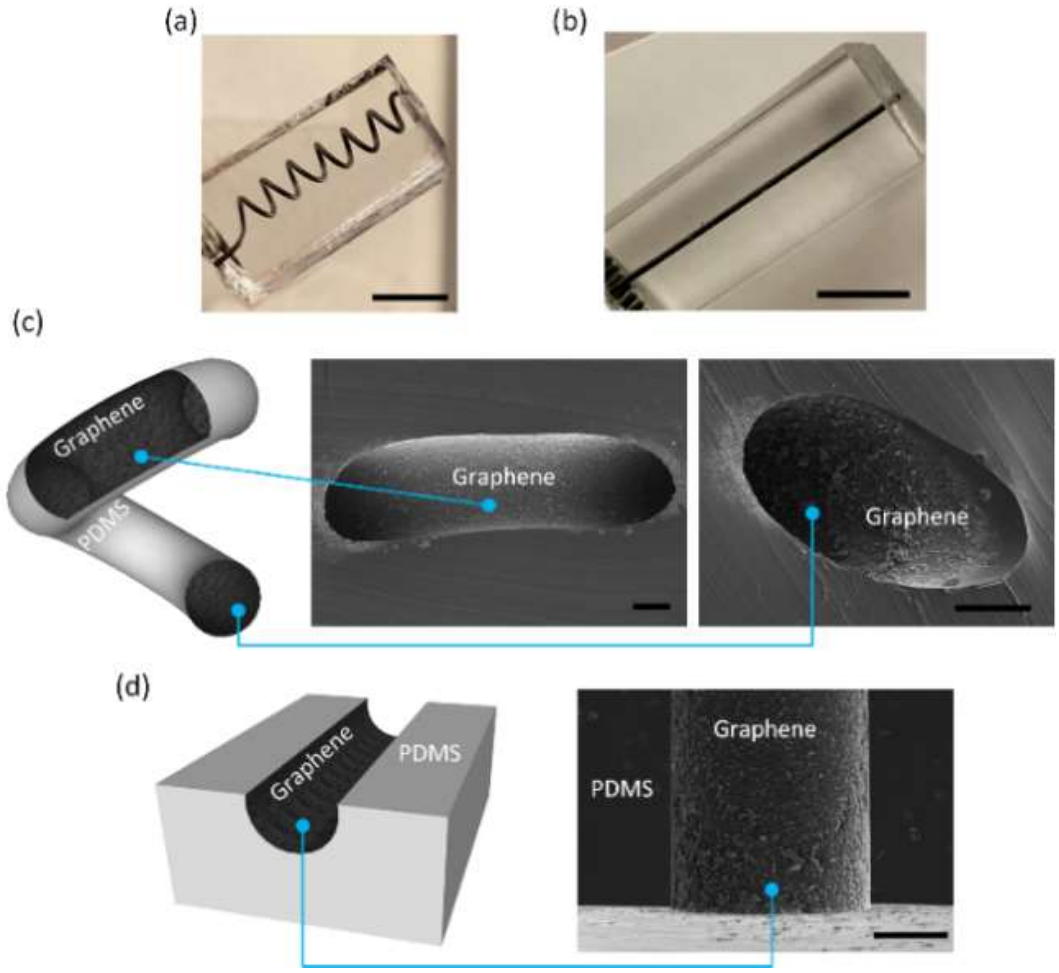

Figure 3.2 (a, b) Photos of the fabricated tubular helical (a) and straight (b) graphene sensors. Scale bars represent 4 mm. (c, d) SEM images of the graphene coated inner surface of the helical (c) and straight (d) channels. Schematic for the helical and straight channels are shown to the left of (c) and (d), respectively. Scale bars represent 200 μm.

Fig. 3.2a and 3.2b show the fabricated helical and straight graphene sensors, respectively. Scanning electron microscopy (SEM) images in Fig. 3.2c and 3.2d demonstrate the formation of the graphene film on the inner walls of the channels. Because the graphene suspension solution contained 70% volume fraction of ethanol, the liquids could rapidly evaporate at 90 °C before the graphene nanoplatelets settled down in a direction, thus allowing casting a graphene layer on the inner wall in all radial directions.

To assess the mechanical properties of the sensors, the sensors were mounted on home-made clamps. Different levels of tension and compression were applied along the length direction of the sensors using a fully programmable motorized stage (LX-4000; Applied Scientific Instruments, Eugene, OR). The initial electrical resistances of the helical and straight sensors were 6 MΩ and 2.7 MΩ, respectively. A LCR meter (AT2817A; Applent Instruments, Jiangsu, China) was adopted to measure and record the resistance responses of the sensors to the applied strains. Fig. 3.3 presents the time-lapse images of the helical sensor when acting as a spring in response to different levels of compression and tension.

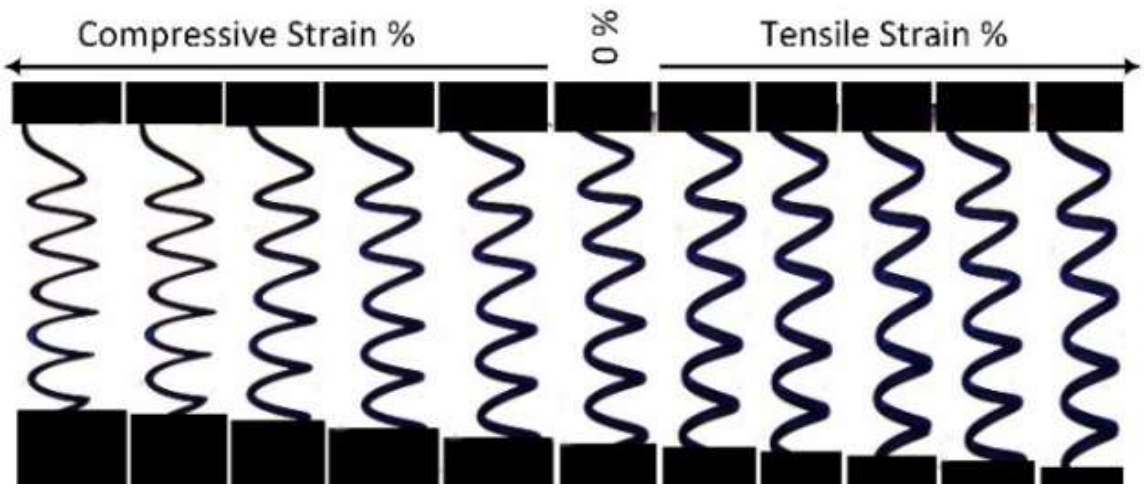

Figure 3.3 Time-lapse images of the helical sensor under compression (left) and tension (right).

The testing of the sensor demonstrated some distinct features of the helical sensor when responding to tensile and compressive strains along the axis of the helical structure. Fig. 3.4a shows that the relative resistance changes (ΔR/R) of the helical and straight sensors increase almost linearly with applied tensile strains. The helical sensor could sustain to increasing tension up to 20% strain with a gauge factor of GF = 6.7 ± 0.27 (obtained from the slope of the linear fitting curve). In contrast, the straight sensor provided a higher GF = 42.8 ± 1.5 but could respond only up to 9% of tensile strain, beyond which the sensor would unrecoverable fail. The compression experiment also demonstrated that the helical design allowed extending the dynamic range of compressive strain measurements. Similarly, based on the slope of the fitting curve in Fig. 3.4b, the GF of the helical sensor was found as 5.16 ± 0.3 under compression up to 24% strain, while the straight sensor showed little sensitivity to applied compressive strains.

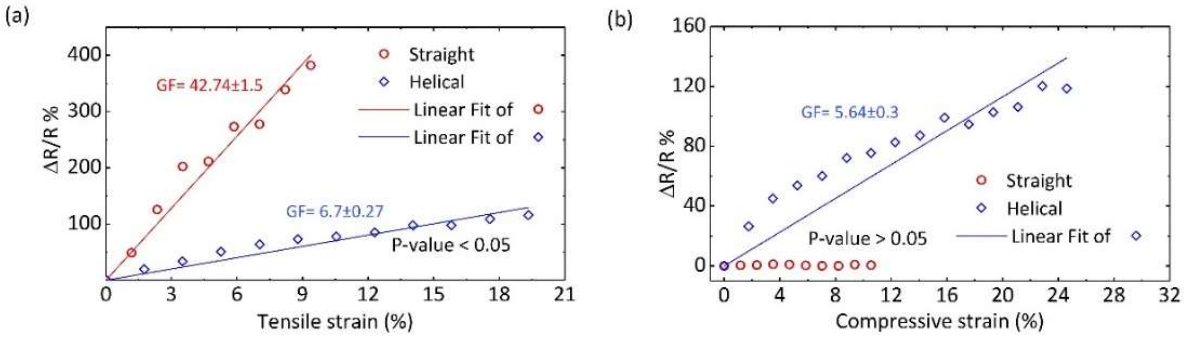

Figure 3.4 Relative resistance changes of the helical and straight sensors under applied tensile (a) and compressive (b) strains.

Next, to verify stability and reversibility of the helical sensor, the sensor was repeatedly loaded and unloaded for thirty cycles (Fig. 3.5). Here, 16% and 8% tensile strains, each in a triangular waveform, were applied to the helical and straight sensors, respectively, in the loaded state. Upon relaxation, the sensors returned to their initial resistance values, indicating good reversibility of the sensors. In addition, the helical and straight sensors exhibited a response time

of ~2.7 s and ~1.1 s to the applied 16% and 8% tensile strains, respectively. The hysteretic behaviours of both the sensors were also investigated, during which the helical and straight sensors were stretched at the rate of 3.5% s^{-1}, and then were released back to their initial positions at the same rate. Fig. 3.6 shows that the helical sensor exhibited a lower hysteresis than the straight sensor.

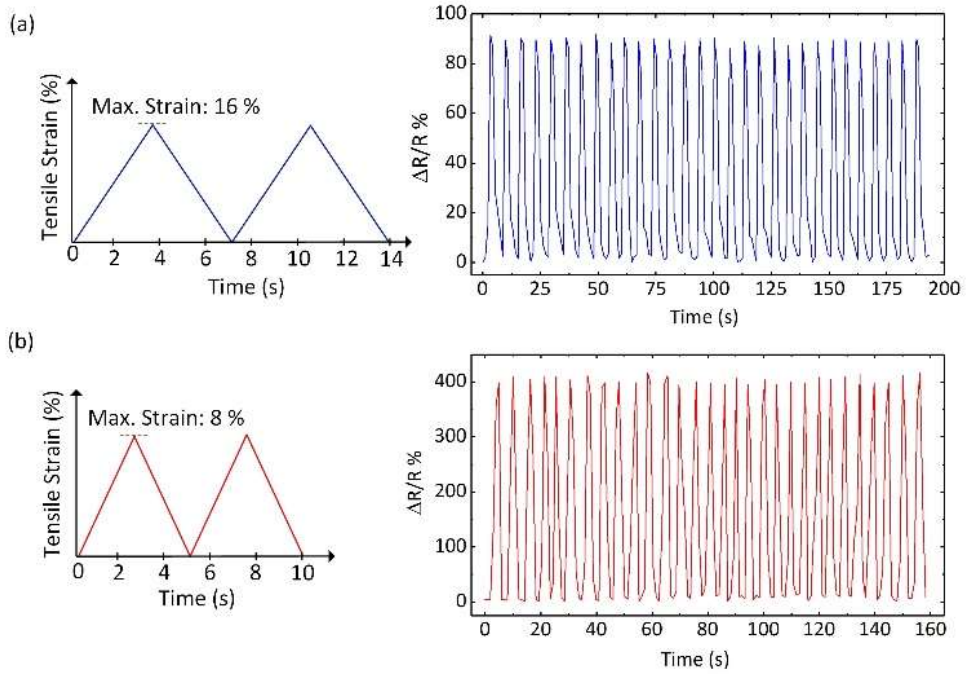

Figure 3.5 Relative resistance changes of the helical (a) and straight (b) strain sensor responding to the repetition of thirty loading and unloading cycles. 16% and 8% tensile strains in triangular waveform were applied to the helical and straight sensors. The applied tensile strains are shown to left of the corresponding response plots.

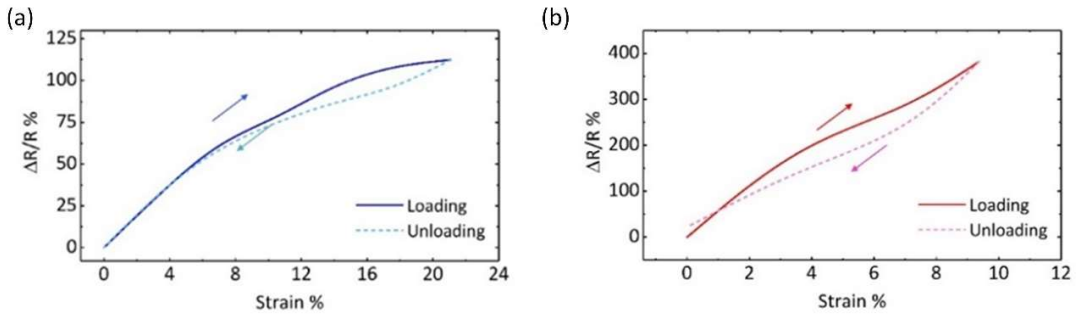

Figure 3.6 Hysteresis of the helical sensor (a) and straight sensor (b).

There is much room to optimize the design of the sensor to achieve both high sensitivity and wide dynamic range. For example, the critical parameters for the design of helical coil are determined by the following equations [26, 27]:

$$F = k\Delta l \tag{4}$$

$$k = \frac{Gd^4}{8ND^3} \tag{5}$$

where F, Δl, k, G, and d refer to the applied force, the force-induced change in the straight end-to-end length of the coil, the spring constant, the shear modulus of material, and the coil wire diameter, respectively. To increase the mechanical stretchability or dynamic range, one can increase both the diameter and number of helix while decreasing the coil wire diameter. This, however, will result in lowering the spring constant, and thus decreasing the sensitivity of the sensor. Therefore, while this work described here demonstrates proof-of-concept of the helical graphene strain sensor, one important future work is to explore the tradeoff between the sensitivity and stretchability of the device through systematic structural optimizations. In addition, other sensing nanomaterials, such as CNTs, may possibly be introduced into the channels to realize helical sensors, with tailored mechanic-electrical properties. Although the previously reported strain sensor with the CNT array based double helices [19] exhibited higher stretchability than our sensor, it is nontrivial to realize the complex double helical nanostructures to build the sensor, and also it is unclear so far whether or not that sensor can respond to both tensile and compressive strains. Lastly, we believe that by accurately positioning aqueous graphene suspension solutions at different locations inside the channel [28] or selectively treating the surface chemical properties of the channel [29], it is possible to realize complex sensor structures inside the channel.

3.5 Conclusions

We have demonstrated a novel helical-shaped tubular graphene strain sensor for the detection of large mechanical strains. This sensor is uniquely structured and manufactured in a way that allows a large dynamic range from 24% compressive strain to 20% tensile strain. The *in situ* microfluidic casting method is unique, simple and allows easy coating of a graphene layer on the inner wall of the helical channel in all radial directions. The wide dynamic detection range, along with mechanical flexibility and stretchability, will benefit many wearable strain sensor applications such as real-time motion capture.

3.6 Acknowledgements

This work was supported in part by the Iowa Highway Research Board and the Iowa Department of Transportation, and in part by the PSI Faculty Scholar Program at the Iowa State University. S.O. thanks the Turkish Council of High Education and Anadolu University for partial financial support. The authors also thank Drs. Kasthurirangan Gopalakrishnan, Peter Taylor, Sunghwan Kim for discussions.

3.7 References

[1] Amjadi, M., Kyung, K., Park, I. & Sitti, M. Stretchable, skin-mountable, and wearable strain sensors and their potential applications: A review. *Advanced Functional Materials* **26**, 1678-1698, doi **:**10.1002/adfm.201504755 (2016).

[2] Jiao, Y. *et al.* Wearable graphene sensors with microfluidic liquid metal wiring for structural health monitoring and human body motion sensing. *IEEE Sensors Journal* **16**, 7870-7875, doi:10.1109/JSEN.2016.2608330 (2016).

[3] Park, S. J., Kim, J. Chu, M. & Khine, M. Highly flexible wrinkled carbon nanotube thin film strain sensor to monitor human movement. *Advanced Materials Technologies* **1**, 1600053-1600061, doi:10.1002/admt.201600053 (2016).

[4] Yang, S. *et al.* From flexible and stretchable meta-atom to metamaterial: A wearable microwave meta-skin with tunable frequency selective and cloaking effects. *Scientific Reports* **6**, 21921-21929, doi: 10.1038/srep21921 (2016).

[5] Lee, J. *et al.* A stretchable strain sensor based on a metal nanoparticle thin film for human motion detection. *Nanoscale* **6**, 11932-11939, doi:10.1039/c4nr03295k (2014).

[6] Yi, L. *et al*. Nanoparticle monolayer-based flexible strain gauge with ultrafast dynamic response of acoustic vibration detection. *Nano Research* **8**, 2978-2987, doi: 10.1007/s12274-015-0803-1 (2015).

[7] Yao, S. & Zhu, Y. Wearable multifunctional sensors using printed stretchable conductors made of silver nanowires. *Nanoscale* **6**, 2345-2352, doi:10.1039/C3NR05496A (2014).

[8] Amjadi, M. *et al.* Highly stretchable and sensitive strain sensor based on silver nanowire-elastomer nanocomposite. *ACS Nano* **8**, 5154-5163, doi: 10.1021/nn501204t (2014).

[9] Amjadi, M., Yoon, Y. & Park, I. Ultra-stretchable and skin-mountable strain sensors using carbon nanotubes-Ecoflex nanocomposties. *Nanotechnology* **26**, 375501-375512, doi:10.1088/0957-4484/26/37/375501 (2015).

[10] Wang, Q., Hong, W. & Dong, L. Graphene 'microdrums' on a freestanding perforated thin membrane for high sensitivity MEMS pressure sensors. *Nanoscale* **8**, 7663-7671, doi: 10.1039/C5NR09274D (2016).

[11] Li, X. *et al.* Stretchable and highly sensitive graphene-on-polymer strain sensors. *Scientific Reports* **2**, 395-401, doi:10.1038/srep00870 (2012).

[12] Chun, S., Choi, Y. & Park, W. All-graphene strain sensors on soft substrate. *Carbon* **116**, 753-759, doi:10.1016/j.carbon.2017.02.058 (2017).

[13] Boland, C. *et al.* Sensitive, high-strain, high-rate bodily motion sensors based on graphene–rubber composites. *ACS Nano* **8**, 8819-8830, doi: 10.1021/nn503454h (2014).

[14] Bae, S.-H. Graphene-based transparent strain sensor. *Carbon* **51**, 236-242, doi:10.1016/j.carbon.2012.08.048 (2013).

[15] Wang, B., Lee, B.-K. Kwak, M.-J. & Lee, D.-W. Graphene/polydimethylsiloxane nanocomposite strain sensor. *Review of Scientific Instruments* **84**, 105005-105009, doi:10.1063/1.4826496 (2013).

[16] Khang, D. Y., Jiang, H., Huang, Y. & Rogers, J. A. A stretchable form of single-crystal silicon for high-performance electronics on rubber substrates. *Science* **311**, 208-212, doi: 10.1126/science.1121401 (2006).

[17] Qi, Y. *et al.* Enhanced piezoelectricity and stretchability in energy harvesting devices fabricated from buckled PZT ribbons. *Nano Letters* **11**, 1331-1336, doi: 10.1021/nl104412b (2011).

[18] Wang, Y. *et al.* Super-elastic graphene ripples for flexible strain sensors. *ACS Nano* **5**, 3645-3650, doi: 10.1021/nn103523t (2011).

[19] Li, C. *et al.* Flexible CNT-array double helices strain sensor with high stretchability for motion capture. *Scientific Reports* **5**, 15554-15562, doi: 10.1038/srep15554 (2015).

[20] Ng, A. *et al.* Patterning of graphene with tunable size and shape for microelectrode array devices. *Carbon* **67**, 390-397, doi:10.1016/j.carbon.2013.10.009 (2014).

[21] Yong, K., Ashraf, A., Kang, P. & Nam, S. Rapid stencil mask fabrication enabled one-step polymer-free graphene patterning and direct transfer for flexible graphene devices. *Scientific Reports* **6**, 24890-24898, doi: 10.1038/srep24890 (2016).

[22] Jeong, J. W. *et al.* High-resolution nanotransfer printing applicable to diverse surfaces via interface-targeted adhesion switching. *Nature Communications* **5**, 5387-,5399, doi: 10.1038/ncomms6387 (2014).

[23] Hofmann, M., Hsieh, Y.-P., Hsu, A. L. & Kong, J. Scalable, flexible and high-resolution patterning of CVD graphene. *Nanoscale* **6**, 289-292, doi: 10.1039/c3nr04968j (2014).

[24] Balanis, C. Antenna Theory - Analysis and Design (3rd Edition), John Wiley & Sons.

[25] Liu, W.-W., Xia, B.-Y., Wang, X.-X. & Wang, J.-N. Exfoliation and dispersion of graphene in ethanol-water mixtures. *Frontiers of Materials Science* **6**, 176-182, doi:10.1007/s11706-012-0166-4 (2012).

[26] Atanackovic, T. M. & Guran, A. Hooke's Law in Theory of elasticity for scientists and Engineers. *Birkhauser* **Ch 3**, 85-111 (2000).

[27] Acxesspring.com, https://www.acxesspring.com/find-spring-constant-k-units-calculator.html

[28] Dong, L. & Jiang, H. Selective formation and removal of liquid microlenses at pre-determined locations within microfluidics through pneumatic control. *Journal of Microelectromechanical Systems* **17**, 381-392, doi:10.1109/JMEMS.2007.912702 (2008).

[29] Yang, H. & Dong, L. Selective nanofiber deposition using a microfluidic confinement approach. *Langmuir* **26**, 1539-1543, doi: 10.1021/la903988w (2009).

CHAPTER 4

TRACKING OF WATER MOVEMENT DYNAMICS INSIDE PLANTS USING LEAF SURFACE HUMIDITY SENSORS

A paper published in 12th International Conference on Nano/Micro Engineered and Molecular Systems (IEEE NEMS, 2017)

Seval Oren, Zhaokui Wang, Xinran Wang, Shawana Tabassum, Yueyi Jiao, Byron J. Montgomery, Nathan Neihart, Colton M. McNinch, Patrick S. Schnable, and Liang Dong

4.1 Abstract

This paper reports on a simple method to track water transport inside the plant by using multiple graphene oxide (GO) based relative humidity sensors. The sensor was formed on an adhesive polyimide film by selectively coating a GO layer on top of gold interdigitated electrodes and subsequently peeling the whole device structure off from a pre-coated polydimethylsiloxane temporary layer. To allow easy installation of the sensor at the leaf of plant, a simple assembly fixture was designed. The present measurement method provides information on how water moves within the plant that is associated with water use efficiency, an important selection trait to evaluate crop quality. In addition, the device can be adhered to other target surfaces due to its flexible and adhesive features.

4.2 Introduction

Water stress adversely affects plant growth and productivity [1]. Selection of plants with improved tolerance to increasing water stress is one of the major objectives in the breeding crops. Quantification of water use efficiency (WUE) requires sensors to determine water transport from the soil into the plant and then leaves the plant. In the past decades, soil moisture sensors have been well developed. However, there are not many cost-effective, high-

performance sensors available to monitor water transpiration process that regulates water contents in the plant.

High osmotic pressure on the hair roots of plants causes water to be absorbed from soils. The cohesion force in the tiny tubes of roots leads to a continuous column of water from roots to leaves. Transpiration is the physiological process of water transportation in the plant and giving off vapor through the leaf stomata. Plants have the capability to regulate transpiration level to optimize internal temperature for continuous metabolic functions. Plants reduce water loss by closing the stomata and at the same time allowing in carbon dioxide and releasing oxygen to perform photosynthesis. When the stomata are opened, water vapors escape from leaves, increasing the local humidity level at the leaf surface. On the other hand, the closure of stomata leads to reducing water evaporation, thus lowering the humidity value (Fig. 4.1). Because transpiration is a critical process for plants to be alive, selection of plants with improved tolerance to increasing water stress is one of the major objectives in the breeding crops.

Graphene and its related materials (e.g., graphene oxide or GO) have attracted increasing interests for use in a number of applications owed to exceptional optical, electrical, mechanical, and chemical properties [2]. The chemical structure of GO is often described as a graphene sheet bonded to oxygen in the form of carboxyl, hydroxyl, or epoxy groups [3]. These functional groups provide GO with high hydrophilicity, allowing the intercalation of different types of molecules (especially, polar molecules) [4]. It was reported that structural and mechanical properties of GO are strongly affected by atmospheric water vapor. Borini et. al. reported an ultrafast GO-based sensor to track the variation of moisture level in a user's breath [5]. Yao et al. reported a quartz crystal microbalance-based relative humidity (RH) sensor using a GO coating

[6]. In addition, Zhang et. al. demonstrated another high-performance RH sensor based on a new nanocomposite of GO and polyelectrolyte [7].

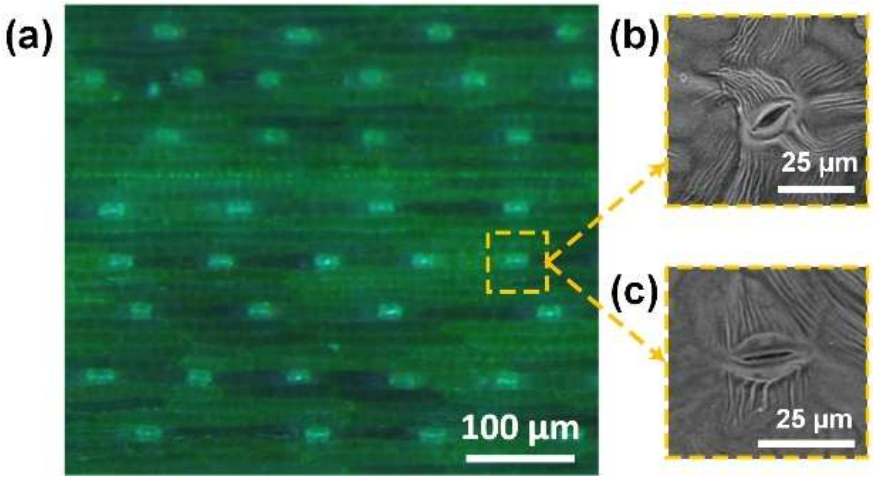

Figure 4.1 (a) Optical images of maize leaf. (b,c) SEM images of opened (b) and closed (c) leaf stomata of maize (Zea mays) genotype B73.

This paper reports on the development of a novel flexible RH sensor formed on an adhesive polyimide film to realize dynamic tracking of water transport from the lower to upper leaves of the plant. Because water up-taken by the plant arrives at different leaves at different time points, it is possible to track water transport inside the plant using multiple sensitive RH sensors mounted at the leaves upon irrigation. To our knowledge, this kind of simple measurement method has not been reported.

4.3 Device Principle and Design

The RH sensor is formed by selective coating of a 500-nm-thick GO layer on top of gold interdigital electrodes (IDEs) (Fig. 4.2a). The sensor operates based on changing resistance and capacitance of the device in response to different environmental RH levels. Fig. 4.2b shows the equivalent circuit models of the GO-based RH sensor when exposed to different RH environments. The bulk impedance (Z_{GO}) of GO consists of a resistor (resistance: R_{GO}) and a

capacitor (capacitance: C_{GO}). According to ref. [7], at low RH, only few water molecules are adsorbed on the surface of GO film resulting in a low coverage of water on the film surface and thus an insufficient proton (H^+)-electron exchange between the GO and the adsorbed water molecules. In this case, charge transfer resistance (R_{ct}) is very high (more than 100 MΩ). When the RH level rises, more water molecules are adsorbed on the surface of GO film, and protons arising from the hydroxyl group of GO sheet are bonded to the excess adsorbed water molecules to form Hydronium (H_3O^+). This, in turn, leads to an increase in charge carrier density, thus decreasing the value of R_{ct} [8]. As the RH level increases further, the absorbed water molecules can facilitate diffusion of charge carriers into the GO film through the strong interaction between water and H_3O^+ ions. This diffusion process will result in formation of Warburg impedance ($Z_{Warburg}$) at the interface between the GO film and the electrode below the film.

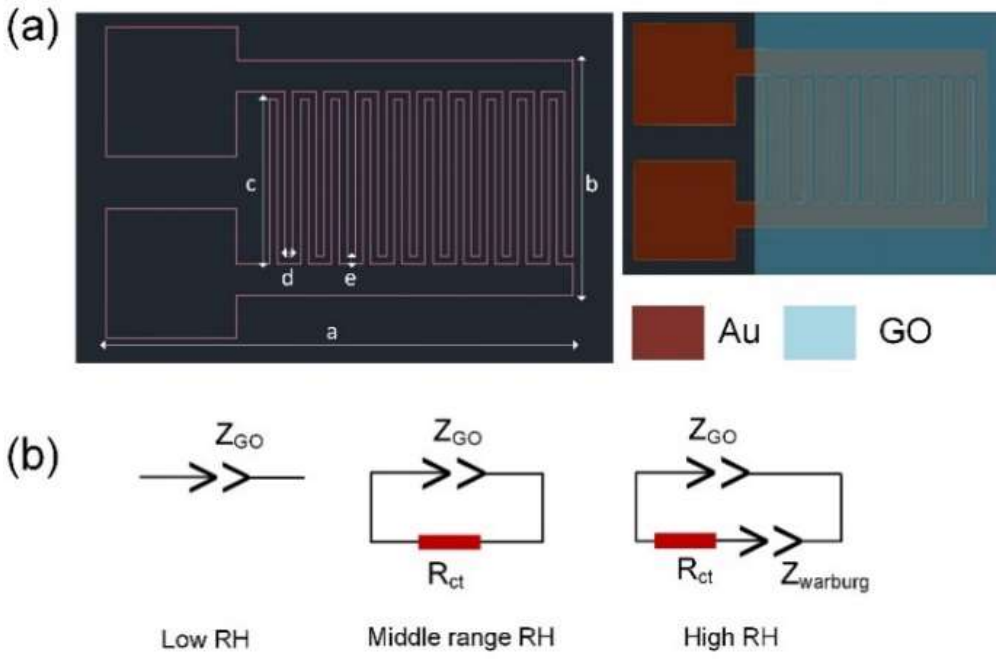

Figure 4.2 (a) Physical dimensions of sensor. In mm size of a= 4 mm, b=2 mm, c=1.43 mm, d=e=0.067 mm. (b) Equivalent circuit of GO-based moisture sensor under different RH levels.

4.4 Device Fabrication and Installation

The fabrication of the proposed RH sensor involved two major procedures, including the formation of Au IDEs on a stand-alone adhesive polyimide film, and the selective coating and patterning of GO layer on the surface of IDEs. First, a 200-μm-thick polydimethylsiloxane (PDMS) layer was spin-coated on a 3-inch silicon wafer as a temporary substrate and thermally cured at 70 ºC for 1 hr. The precursor solution of PDMS was formed by mixing PDMS monomer and curing agent at a 10:1 weight ratio. Following that, a 100 μm-thick adhesive polyimide film (3DMakerworld, Kapton tape) was adhered to the PDMS layer. Next, the Au IDEs (Fig. 4.3a) were formed using conventional evaporation, photolithography, and wet chemical etching methods, all performed on the surface of the polyimide layer. The Au layer used here was 75 nm thick. Then, a 500 nm- thick GO layer was selectively formed and patterned on the surface of IDEs using the spray coating and lift-off process. In this step, AZ photoresist was first coated on the polyimide film and exposed under ultraviolet (UV) light with a desired mask. Then, the IDEs were treated with O_2 plasma to make the surface hydrophilic. Subsequently, the whole surface of the device was coated with GO using a spinning assisted spray-coating process at room temperature. The setup for this coating method is shown in Fig. 4.4. Two main parts were used in the setup, including an airbrush (Badger 350, Badger Air-Brush) which utilizes compressed air as a carrier gas, and a step motor spinner (Nanotec-SMCI33-1) able to rotate the wafer to achieve uniform coating of the prepared GO suspension solution. The major processing parameters of this method include the vertical distance between the airbrush and the substrate (9.6 cm), the pressure of air source (45 psi), and the spinning speed of the substrate (10 rpm). By using this method, the GO dispersion can spread uniformly from the center towards the edges of a substrate without any noticeable spilling over. After the GO film was formed, the AZ photoresist was

stripped off with acetone. Thus, the selective patterning of GO on the IDEs was realized. Finally, the adhesive polyimide film containing the sensor structures was gently peeled off from the PDMS layer. Fig. 4.3a displays the schematic of the fabrication processes for manufacturing the proposed RH sensors. Fig. 4.3b and 4.4c show the fabricated devices.

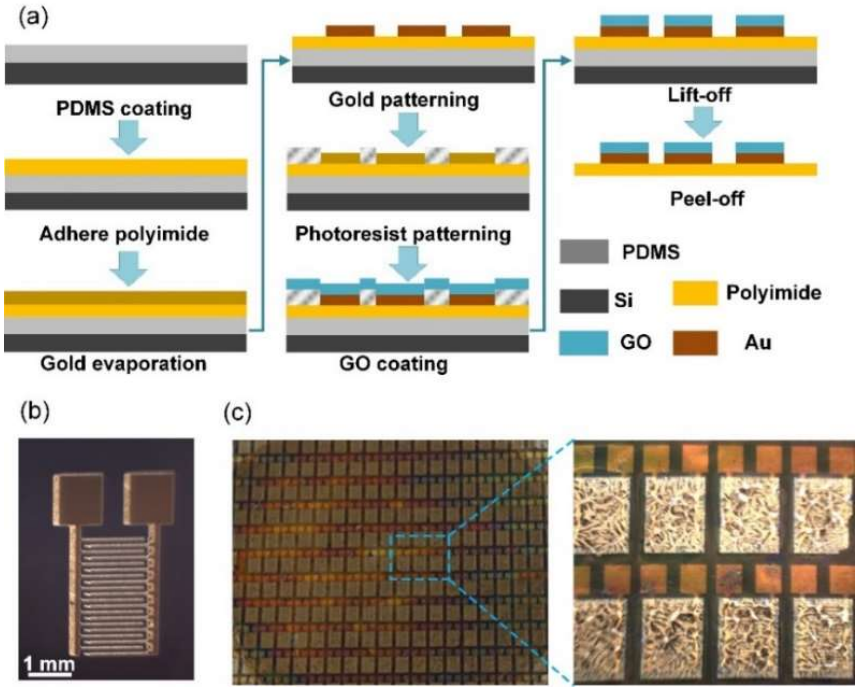

Figure 4.3 (a) Process flow for the RH sensor. (b) Optical image of a single IDE. (c) Optical image of the IDEs coated with the patterned GO film.

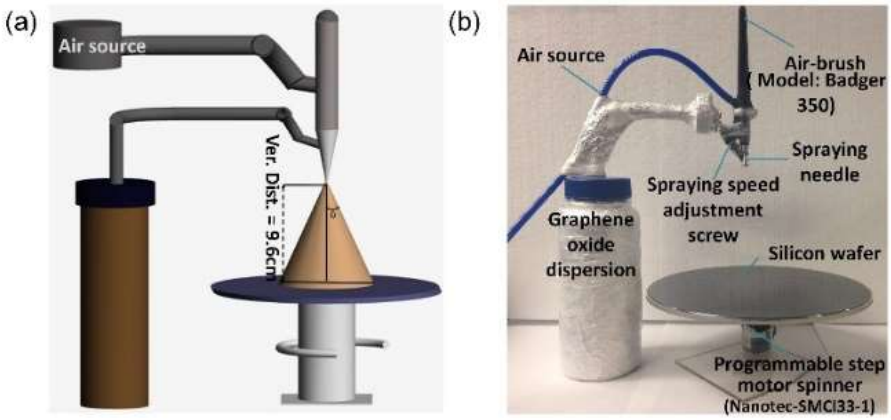

Figure 4.4 (a) Schematic representation of the GO film formation on Si wafer by SSC method (b) The real setup for the proposed SSC method.

Fig. 4.5a and 4.5b show a schematic representation and an optical image for the installation of the RH sensor at the leaf. A 1-mm-deep chamber was formed in an acrylic glass. The sensor was directly adhered to the bottom of the chamber. Four small breathing holes (1 mm diameter) were punched to avoid the accumulation of water vapor inside the chamber. The chamber was fixed on the back of leaf with the help of two light-weight plastic clamping slabs and two plastic screws. There was also a small air gap between the top of the chamber and the slab. This allowed the leaf to grow normally even during long-time monitoring. The clamping slabs were hanged on stable rods via thin lines to avoid possible damages to the leaf. Customized printed circuit board was designed to read out the sensor output signals (Fig. 4.5c).

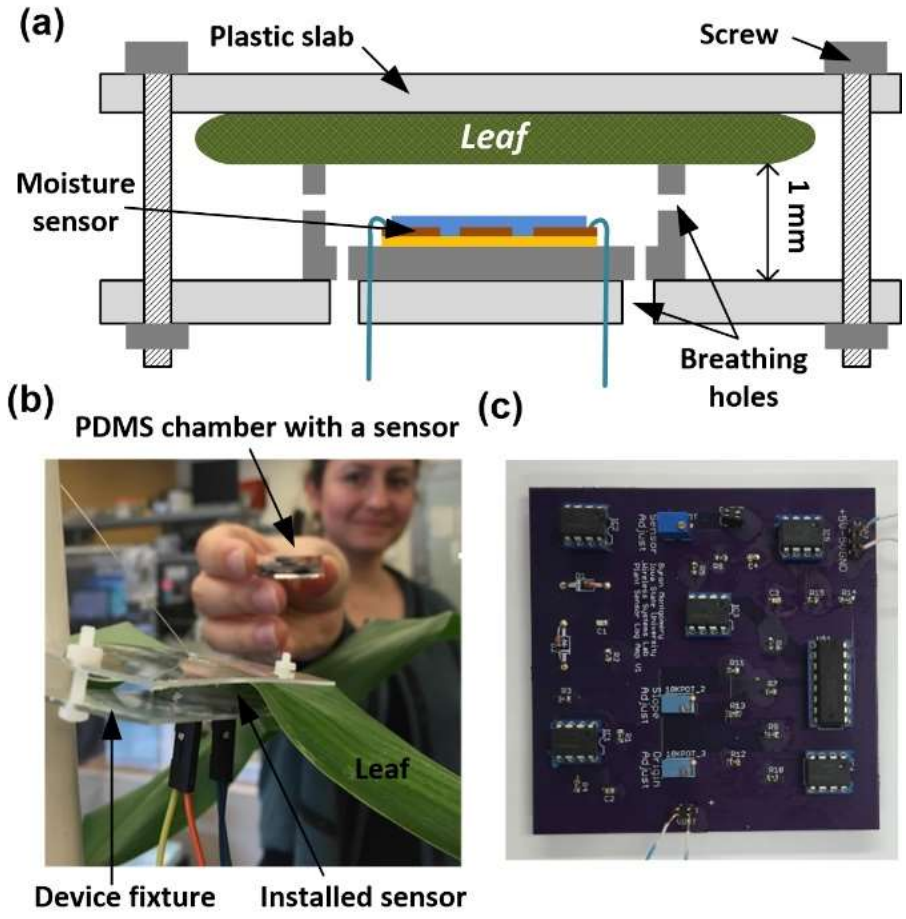

Figure 4.5 (a) Schematic and (b) photography of the device installation at the back of the leaf. (c) Customized printed circuit board for signal readout and processing.

4.5 Experimental Results

Fig. 4.6 shows the resistance and capacitance of the sensor as a function of RH at different operation frequencies. First, in the tested RH range from 22 to 96% RH, with increasing RH value, the resistance reduced, and the capacitance increased, while the total impedance of the sensor decreased. The higher impedance at the lower RH may be associated with the fact that there is no sufficient amount of water molecules absorbed by the GO film, thus making it hard to accelerate the transportation of ions [2]. At the higher RH levels, adequate water molecules are adsorbed by the GO film and diffused into it, thus increasing the charge carrier density and decreasing the impedance [7]. Second, in the RH range below 40% RH, the sensor exhibited less sensitive to changing RH at higher operation frequencies. It should be noted that at high frequencies, the direction of electric field changes so fast that the adsorbed water molecules at the GO surface are not able to catch up with the alternating rate of the applied electric field, due to its large relaxation time [2]. However, in the range above 40% RH, no obvious differences in sensitivity were observed for different operation frequencies. Therefore, the low frequency of 100 Hz was chosen for the sensor to measure RH in the tested range.

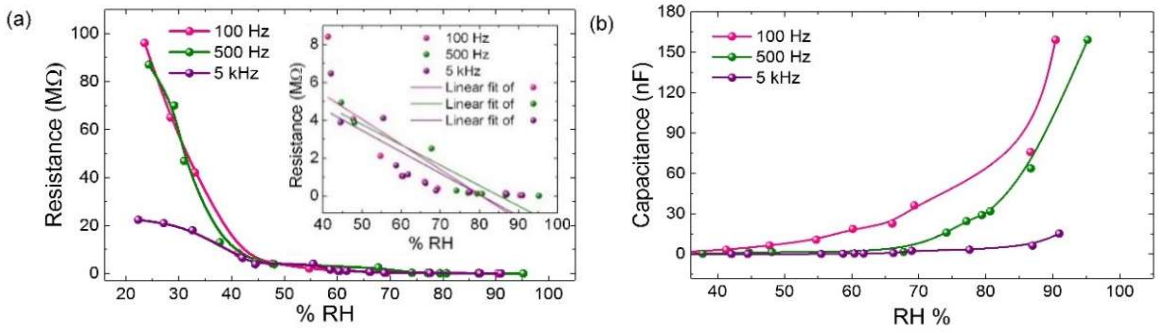

Figure 4.6 (a) Resistance and (b) capacitance of the sensor as a function of RH at different operation frequencies.

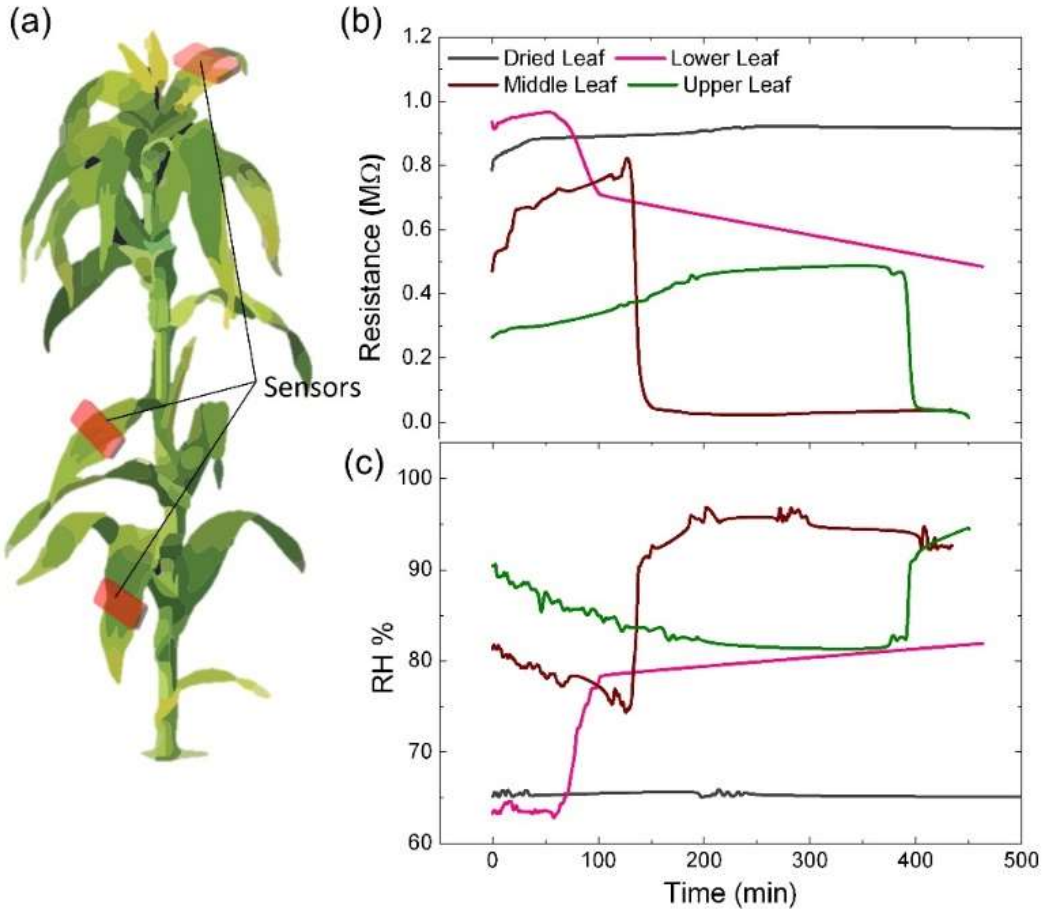

Figure 4.7 (a) Three GO-based humidity sensors installed at different locations of a corn plant. Real-time monitoring of leaf surface humidity after the plant is irrigated. (b) Resistance vs. time tracking (c) RH vs. time tracking.

To demonstrate the concept of using multiple RH sensors to track water transport from one to another leaf, we installed three sensors at three leaves of a 7-week old maize plant (Inbred B73). Fig. 4.7a depicts the schematic of placing the three sensors at the low, the middle, and the top leaves of the plant. The plant with the sensors was irrigated at 5 minutes after the sensor measurements started. Fig. 4. 7c demonstrates the real-time monitoring of leaf-surface RH using the sensors installed at three leaves. Only resistance measurement was taken in this experiment at the frequency of 100 Hz (Fig. 4.7b). Before the plant was not irrigated, there was not significant

resistance drop. After the irrigation, the three sensors exhibited obvious resistance drops at different time points. More specifically, the low and middle sensors presented resistance reduction and thus RH increase at ~55 min and ~135 min, respectively. Therefore, transport of water from the low leaf to the middle one took ~80 min. However, the sensor installed at the top leaf responded distinctly at ~400 min, indicating that the plant required a longer time of ~265 min to transport water from the tested middle leaf to the top one.

4.6 Conclusions

The flexible GO-based RH sensor has been developed on an adhesive polyimide thin film by selectively coating and patterning GO at the surface of Au IDEs and subsequently peeling the device off from a temporary PDMS film. We have also demonstrated a simple but effective method to track water transport inside the plant via real-time monitoring of RH variations at the surfaces of different leaves of the plant. This low-cost method will facilitate studying of water transpiration and transport dynamics in the plant.

4.7 Acknowledgements

This work was supported by the National Science Foundation under grant DBI-1331390, the Iowa Corn Promotion Board, and the Plant Sciences Institute at Iowa State University. S.O. thanks, Turkish Council of High Education and Anadolu University in Turkey for financial support.

4.8 References

[1] Osakabe, Y., Osakabe, K., Shinozaki, K. & Tran, L.-S. P. Response of plants to water stress. *Front Plant Science* **5**, 86-94, doi:10.3389/fpls.2014.00086 (2014).

[2] Yao, Y. *et al.* The effect of ambient humidity on the electrical properties of GO films. *Nanoscale Research Letters* **7**, 363-370, doi: 10.1186/1556-276X-7-363 (2012).

[3] Mkhoyan, K. A. *et al.* Atomic and electronic structure of graphene-oxide. *Nano Letters* **9**, 1058-1063,doi: 10.1021/nl8034256 (2009).

[4] Bujans, F.B., Cerveny, S. Alegria, A. & Colmenero, J. Soprtion and desorption behavior of water and organic solvents from graphite oxide. *Carbon* **48**, 3277-3286, doi:10.1016/j.carbon.2010.05.023 (2010).

[5] Borini, S. *et al.* Ultrafast graphene oxide humidity sensors. *ACS Nano* **7**, 11166-11173, doi: 10.1021/nn404889b (2013).

[6] Yao, Y., Chen, X., Guo, H. & Wu, Z. Graphene oxide thin film coated quartz crystal microbalance for humidity detection. *Applied Surface Science* **257**, 7778-7782, doi: 10.1016/j.apsusc.2011.04.028 (2011).

[7] Zhang, D., Tong, J., Xia, B. & Xue, Q. Ultrahigh performance humidity sensor based on a layer by layer self-assembly of graphene oxide/polyelectrolyte nanocomposite film. *Sensors and Actuators, B: Chemical* **203**, 263-270, doi:10.1016/j.snb.2014.06.116 (2014).

[8] Agmon N. The Grotthuss mechanism. *Chemical Physics Letters* **244**, 456-462 (1995).

CHAPTER 5

CONCLUSIONS AND OUTLOOK

5.1 Conclusions

The main target of this thesis is to investigate cost-effective, simple, and large-scale patterning and transferring methods of graphene-based nanomaterials to develop flexible electronics platform and wearable devices. Graphene is envisioned to open a new era in flexible electronics due its remarkable properties. It makes it possible to fabricate foldable, stretchable and highly flexible devices, sensors and more other products which are ready to take place in the markets. Therefore, inexpensive, large-scale, and simple patterning and transferring techniques for flexible and wearable electronics have advantageous over traditional ones. The recent literature on graphene-based nanomaterial patterning and transferring techniques and related applications was reviewed. Based on the literature review, the pros and cons described in recent studies have been determined and a new perspective for graphene-based patterning and transferring methods were proposed. The investigations described in this thesis are related to concepts of flexible strain, pressure, and RH sensor fabrication based on a novel tape-based cost-effective patterning and transferring technique, an *in situ* microfluidic casting method, and a novel selective-coating technique for graphene-based nanomaterials.

In Chapter 2, a simple, high-resolution, and scalable method was developed for patterning and transferring graphene-based nanomaterials onto various types of tape to realize flexible graphene microsensors. The method involves drop-casting a graphene film by graphene suspension onto a prepatterned PDMS surface containing negative features, applying Scotch tape to remove the excess graphene from the nonpatterned areas of the PDMS surface, then transferring the patterned graphene from the inside of the negative features at the PDMS surface

onto a target tape. The method utilizes the work of adhesion at the interface between two contacting materials as determined by their surface energies to pattern graphene on a PDMS substrate and transfer it onto a target tape. Once PDMS negative patterns are formed via conventional soft lithography, only adhesive tapes are required to produce graphene patterns with feature resolution of a few microns. This technology will open a new route for low-cost, simple, and scalable production of graphene-based sensors on tape.

In Chapter 3, a helical spring-like piezo-resistive graphene strain sensor formed within a microfluidic channel was developed for the detection of large mechanical strains. A thin graphene layer is coated on the inner wall of the helical channel in all radial directions using an *in situ* microfluidic casting method. Fabrication of the sensor consists of embedding a helical thin metal wire with a plastic wrap into a precursor solution of an elastomeric polymer, forming a helical microfluidic channel by removing the wire from cured elastomer, and microfluidic casting of a thin graphene layer directly inside the helical channel. The helical shape allows the sensor to flexibly respond to both tensile and compressive strains over a wide dynamic detection range, from 24% compressive strain to 20% tensile strain. The wide dynamic range, in conjunction with mechanical flexibility and stretch ability of the sensor, will enable practical wearable strain sensor applications such as real-time motion capture.

In Chapter 4, a flexible GO-based RH sensor on an adhesive polyimide thin film was developed by selectively coating and patterning GO at the surface of Au IDEs. A simple but effective method has been demonstrated to track water transport inside the plant via real-time monitoring of RH variations at the surfaces of different leaves of the plant using GO-based RH sensors. This low-cost method provides information on how water moves within the plant that is associated with water use efficiency, an important selection trait when evaluating crop quality.

5.2 Outlook

The future prospects of wearable and flexible sensors include a search for appropriate applications for each developed fabrication method and improving the information obtained from sensors (i.e., sensitivity, wider dynamic range, multifunctional sensing ability). For all developed sensors in this thesis, the electrical connection between the sensor and data logger was achieved using electrical wires, resulting in some measurement issues such as signal instability and difficulties in handling of the wires when many sensors are tested at the same time. Future work includes development of a wireless unit to make reading out data from the sensor by more straight-forward and faster way. The methods introduced in this thesis can also be utilized in the fabrication of different types of functional materials-based sensors on different substrates to expand the range of possible applications including; bio-sensing and electrochemical sensing.

REFERENCES

[1] Yeo, H.-W. *et al.* Multifunctional epidermal electronics printed directly onto the skin. *Advanced Materials* **25,** 2773-2778, doi: 10.1002/adma.201204426 (2013)

[2] Drack, M. *et al.* An imperceptible plastic electronic wrap. *Advanced Materials* **27,** 34-40, doi: 10.1002/adma.201403093 (2015).

[3] Yoon, S., Sim, K. J. & Cho, H.-Y. A flexible and wearable human stress monitoring patch. *Scientific Report*s **6**, 23468, doi: 10.1038/srep23468 (2016).

[4] Dollar, M. A. & Howe, D. R. A robust compliant grasper via shape deposition manufacturing. *IEEE/ASME Transactions on Mechatronics* **11,** 154-161, doi: 10.1109/TMECH.2006.871090 (2006).

[5] Yamada, T. *et al.* A stretchable carbon nanotube strain sensor for human-motion detection. *Nature Nanotechnology* **6,** 296-301, doi: 10.1038/NNANO.2011.36 (2011).

[6] Zardetto, V., Brown, M. T., Reale, A. & Carlo, D. A. Substrates for flexible electronics: A practical investigation on the electrical, film flexibility, optical, temperature, and solvent resistance properties. *Polymer Physics* **49**, 638-648, doi: 10.1002/polb.22227 (2011).

[7] Taptimthong, P., Rittinger, J., Wurz, C. M. & Rissing L. Flexible magnetic writing / reading system: Polyimide film as flexible substrate. *Procedia Technology* **15**, 230-237, doi: 10.1016/j.protcy.2014.09.076 (2014).

[8] Chou, N., Yoo, S. & Kim, S. Fabrication of stretchable and flexible electrodes based on pdms substrate. *MEMS 2012*, 247-250 (2012).

[9] Eom, H.-S. & Lim, S. RF stretcable sensor using flexible substrate and eutectic gallium-indium. *Proceedings of ISAP2016,* 996-997 (2016).

[10] Soni, R., Raveendran, A. & Kurungot, S. Grafoil–Scotch tape-derived highly conducting flexible substrate and its application as a supercapacitor electrode. *Nanoscale* **9**, 3593-3600, doi: 10.1039/c7nr00281e (2017).

[11] Kang, Y. D. *et al.* Scalable microfabrication procedures for adhesive-integrated flexible and stretchable electronic sensors. *Sensors* **15**, 23459-23476, doi:10.3390/s150923459 (2015).

[12] Fujiwara, K., Shimasaki, H., Morimoto, K. & Kuwahara, N. Studies on a polyester fabric substrate of the feed line to a flexible slot antenna. *Proceeding of Asia-Pasific Microwave Conference 2014*, 456-458 (2014).

[13] Balde, M., Jacquemoud-Collet, F., Vena, A. & Sorli B. Wet microelectronic technologies on paper substrate for flexibleelectronic applications. *Sensors and Actuators A:Physical* **240**, 118-125, doi:10.1016/j.sna.2015.09.037 (2016).

[14] Liao, X. *et al.* Flexible and highly sensitive strain sensors fabricated by pencil drawn for wearable monitor. *Advanced Functional Materials* **25**, 2395-2401, doi:10.1002/adfm.201500094 (2015).

[15] Amjadi, M., Kyung, U.-K., Park, I. & Sitti, M. Stretcable, skin-mountable, and wearable strain sensors and their potential applications: A review. *Advanced Functional Materials* **26**, 1678-1698, doi: 10.1002/adfm.201504755 (2016).

[16] Kenry, Yeo, C. J. & Lim, T. C. Emerging flexible and wearable physical sensing platforms for healthcare and biomedical applications. *Microsystems&Nanoengineering* **2**, 16043, doi:10.1038/micronano.2016.43 (2016).

[17] Choi, Y.-J., *et al.* Advances in 2D/3D printing of functional nanomaterials and their applications. *ECS Journal of Solid State Science and Technology* **4**, 3001-3009, doi:10.1149/2.0011504jss (2015).

[18] Do, N. T. & Visell, Y. Stretchable, twisted conductive microtubules for wearable computing, robotics,electronics, and healthcare. *Scientific Reports* **7**, 1753, doi: 10.1038/s41598-017-01898-8 (2017).

[19] Ashjaran, A. & Oshaghi, H. Graphene as single layer of carbon atoms: Perusal on structure, properties and applications. *Research Journal of Pharmaceutical, Biological and Chemical Sciences* **5**, 327-335, Issn: 0975-8585 (2014).

[20] Wang, Q., Hong, W. & Dong, L. Graphene "microdrums" on a freestanding perforated thin membrane for high sensitivity MEMS pressure sensors. *Nanoscale* **8***,* 7663 (2016).

[21] Ali, Md. A., Mondal, K., Jiao, Y., Oren, S., Xu, Z., Sharma, A. & Dong, L. Microfluidic immuno-biochip for detection of breast cancer biomarkers using hierarchical composite of porous graphene and titanium dioxide nanofibers. *ACS Applied Materials Interfaces*, **8**, 20570-20582, doi: 10.1021/acsami.6b05648 (2016).

[22] Allen, J. M., Tung, C. V. & Kaner, B. R. Honeycomb carbon: a review of graphene. *Chemical reviews*, **110**, 132-145, doi: 10.1021/cr900070d (2009).

[23] Lee, M. S., Kim, H.-J. & Ahn, H.-J. Graphene as a flexible electronic material: mechanical limitations by defect formation and efforts to overcome. *Materials Today,* **18**, 336-344, doi:10.1016/j.mattod.2015.01.017 (2015).

[24] Ren, Y. & Zhu, C. An improved method for transferring graphene grown by chemical vapor deposition. *NANO:Brief Reports and Reviews,* **7**, 1150001-1150006, doi:10.1142/S1793292011500019 (2012).

[25] Pirkle, A., *et. al.* The effect of chemical residues on the physical and electrical properties of chemical vapor deposited graphene transferred to SiO_2. *Applied Physics Letters,* **99**, 122108-122111, doi: 10.1063/1.3643444 (2011).

[26] Her, M., Beams, R. & Novotny, L. Graphene transfer with reduced residue. *Physics Letters A,* **377**, 1455-1458, doi:10.1016/j.physleta.2013.04.015 (2013).

[27] Aleman, B., *et. al.* Transfer-free batch fabrication of large-area suspended graphene membranes. *ACS Nano,* **4**, 4762-4768, doi: 10.1021/nn100459u (2010).

[28] Kuzum, D., *et. al.* Transparent and flexible low noise graphene electrodes for simultaneous electrophysiology and neuroimaging. *Nature Communications,* **5**, 5259, doi: 0.1038/ncomms6259 (2014).

[29] Hofmann, M., Hsieh, P.-Y., Hsu, L. A. & Kong, J. Scalable, flexible and high resolution patterning of CVD graphene. *Nanoscale,* **6**, 289-292, doi: 10.1039/c3nr04968j (2013).

[30] Khang, Y.-D., Jiang, H., Huang, Y. & Rogers, A. J. A stretchable form of single-crystal silicon for high-performance electronics on rubber substrates. *Science,* **311**, 208-212 (2006).

[31] Zhang, Q., *et. al.* Carbon-nanotube-array double helices. *Angewandte Chemie International Edition,* **49**, 3642-3645, doi: 10.1002/anie.200907130 (2010).

[32] Yao, Y., Chen, X., Zhu, J., Zeng, B., Wu, Z. & Li, X. The effect of ambient humidity on the electrical properties of graphene oxide films. *Nano Express*, **7**, 363-370, doi: 10.1186/1556-276X-7-363 (2012).

[33] Borini, *et. al.* Ultrafast graphene oxide humidity sensors. *ACS Nano,* **7**, 11166-11173, doi:10.1021/nn404889b (2013).

[34] Zhao, L.-C., Qin, M. & Huang, A.-Q. Humidity sensing properties of the sensor based on graphene oxide films with different dispersion concentrations. *Sensors, IEEE,* doi: 10.1109/ICSENS.2011.6126968 (2011).

[35] Yao, Y., Chen, X., Guo, H. & Wu, Z. Graphene oxide thin film coated quartz crystal microbalance for humidity detection. *Applied Surface Science,* **257**, 7778-7782, doi:10.1016/j.apsusc.2011.04.028 (2011).

[36] Zhang, D., Tong, J., Xia, B. & Xue, Q. Ultrahigh performance humidity sensor based on layer-by-layerself-assembly of graphene oxide/polyelectrolyte nanocomposite film. *Sensors and Actuators B,* **203**, 263-270, doi:10.1016/j.snb.2014.06.116 (2014).

[37] Yao, Y., Chen, X., Guo, H., Wu, Z. & Li, X. Humidity sensing behaviors of graphene oxide-silicon bi-layer flexible structure. *Sensors and Actuators B,* **161**, 1053-1058, doi: 10.1016/j.snb.2011.12.007 (2012).

[38] Ghany Abdel, A. N., Elsherif, A. S. & Handal, T. H. Revolution of graphene for different applications: State-of-the-art. *Surfaces and Interfaces,* **9**, 93-106, doi:10.1016/j.surfin.2017.08.004 (2017).

[39] Kumar, A. & Lee, H. C. Synthesis and biomedical applications of graphene:present and future trends. *Advances in Graphene Science,* Chapter 3, doi: 10.5772/55728 (2013).

[40] Li, X. *et. al.* Large-area synthesis of high-quality and uniform graphene films on copper foils. *Science,* **324**, 1312-1314, doi:10.1126/science.1171245 (2009.

[41] Mattevi, C., Kim, H. & Chhowalla, M. A review of chemical vapour deposition of graphene on copper. *Journal of Materials Chemistry,* **21**,3324-3334, doi: 10.1039/c0jm02126a (2011).

[42] Lee, Y. *et. al.* Wafer-scale synthesis and transfer of graphene films. *Nano Letters,* **10**, 490-493, doi:10.1021/nl903272n (2010).

[43] Sun, Z. *et. al.* Towards hybrid superlattices in graphene. *Nature Communications,* **2**, 559, doi:10.1038/ncomms1577 (2011).

[44] Tian, H. *et. al.* A graphene-based resistive pressure sensor with record-high sensitivity in a wide pressure range. *Scientific Reports,* **5**, 8603, doi: 10.1038/srep08603 (2015).

[45] Das, R. S. *et. al.* 3D nanostructured inkjet printed graphene via UV-pulsed laser irradiation enables paper-based electronics and electrochemical devices. *Nanoscale,* **8**, 15870-15879, doi: 10.1039/c6nr04310k (2016).

[46] Lee, S. J. *et. al.* Wafer-scale patterning of reduced graphene oxide electrodes by transfer-and-reverse stamping for high performance OFETs. *Small,* **9**, 2817-2825, doi:10.1002/smll.201300538 (2013).

[47] He, Q. *et. al.* Centimeter-long and large-scale micropatterns of reduced graphene oxide films: Fabrication and sensing applications. *ACS Nano,* **4**, 3201-3208, doi:10.1021/nn100780v (2010).

[48] Lee, C., Wei, X., Kysar, W. J. & Hone, J. Measurement of the elastic properties and intrinsic strength of monolayer graphene. *Science*, **321**, 385-388, doi:10.1126/science.1157996 (2008).

[49] Wang, J., Ma, F., Liang, W. & Sun, M. Electrical properties and applications of graphene, hexagonal boron nitride (h-BN), and graphene/h-BN heterostructures. *Materials Today Physics,* **2**, 6-34, doi:10.1016/j.mtphys.2017.07.001 (2017).

[50] Patel, K. & Tyagi, K. P. Multilayer graphene as a transparent conducting electrode in silicon heterojunction solar cells. *AIP Advances,* 5, 077165-077176, doi:10.1063/1.4927545 (2015).

[51] Goosey, M. A short introduction to graphene and its potential interconnect applications. *Circuit World,* **38**, 83-86, doi:10.1108/03056121211222309 (2012).

[52] Jiao, Y. *et. al.* Wearable graphene sensors within microfluidic liquid metal wiring for structural health monitoring and human body motion sensing. *IEEE Sensors Journal,* **16**, 7870-7875, doi: 10.1109/JSEN.2016.2608330 (2016).

[53] Nakamura, A., Hamanishi, T., Kawakami, S. & Takeda, M. A piezo-resistive graphene strain sensor with a hollow cylindrical geometry. *Materials Science and Engineering B,* **219**, 20-27, doi10.1016/j.mseb.2017.02.012 (2017).

[54] Mkhoyan, A. K. *et. al.* Atomic and electronic structure of graphene-oxide. *Nano Letters,* **9**, 1058-1063, doi: 10.1021/nl8034256 (2009).

[55] Bujans-Barroso, F., Cerveny, S., Alegria, A. & Colmenero, J. Sorption and desorption behavior of water and organic solvents from graphene oxide. *Carbon,* **48**, 3277-3286, doi:10.1016/j.carbon.2010.05.023 (2010).

[56] Wang, L., Zhang, Y. Y., Yang, H., Miao, L. & Song, Y. Simple and large-area strategy to prepare flexible graphene tape electrode. *Applied Materials and Interfaces,* **9**, 9089-9095, doi:10.1021/acsami.6b14624 (2017).

[57] Li, C. *et. al.* Flexible CNT-array double helices strain sensor with high stretchability for motion capture. *Scientific Reports*, **5**, 1554, doi:10.1038/srep15554 (2015).

[58] Kalita, H., Palaparthy, S. V., Baghini, S. M. & Aslam, M. Graphene quantum dot soil moisture sensor. *Sensors and Actuators B,* **233**, 582-590, doi:10.1016/j.snb.2016.04.131 (2016).

[59] Hornero, G., Gaitan-Pitre, E. J., Finetti-Serrano, E., Casas, O. & Areny-Pallas, R. Anovel low-cost smart leaf wetness sensor. *Computers and Electronics in Agriculture,* **143**, 286-292, doi:10.1016/j.compag.2017.11.001 (2017).

[60] Afzal, A., Duiker, W. S. & Watson, E. J. Leaf thickness to predict plant water status. *Biosystems Engineering,* **156**, 148-156, doi:10.1016/j.biosystemseng.2017.01.011 (2017).

[61] Seelig, D.-H., Wolter, A. & Schroder, G.-F. Leaf thickness and turgor pressure in bean during plant desiccation. *Scienta Horticulturae,* **184**, 55-62, doi:10.1016/j.scienta.2014.12.025 (2015).

[62] Atherton, J. J., Rosamond, C. M. & Zeze, A. D. A leaf-mounted thermal sensor for the measurement of water content. *Sensors and Actuators A,* **187**, 67-72, doi:10.1016/j.sna.2012.06.021 (2012).

[63] Hadjiloucas, S., Karatzas, S. L. & Bowen, W. J. Measuremnts of leaf water content using terahertz radiation. *IEEE Transaction on Microwave Theory and Techniques,* **47**, 142-149 (1999).

[64] Jones, G. H. & Leinonen I. Thermal Imaging for the study of plant water relations. *Journal of Agricultural Meteorology,* **59**, 205-217 (2003).

APPENDIX SUPPORTING INFORMATION

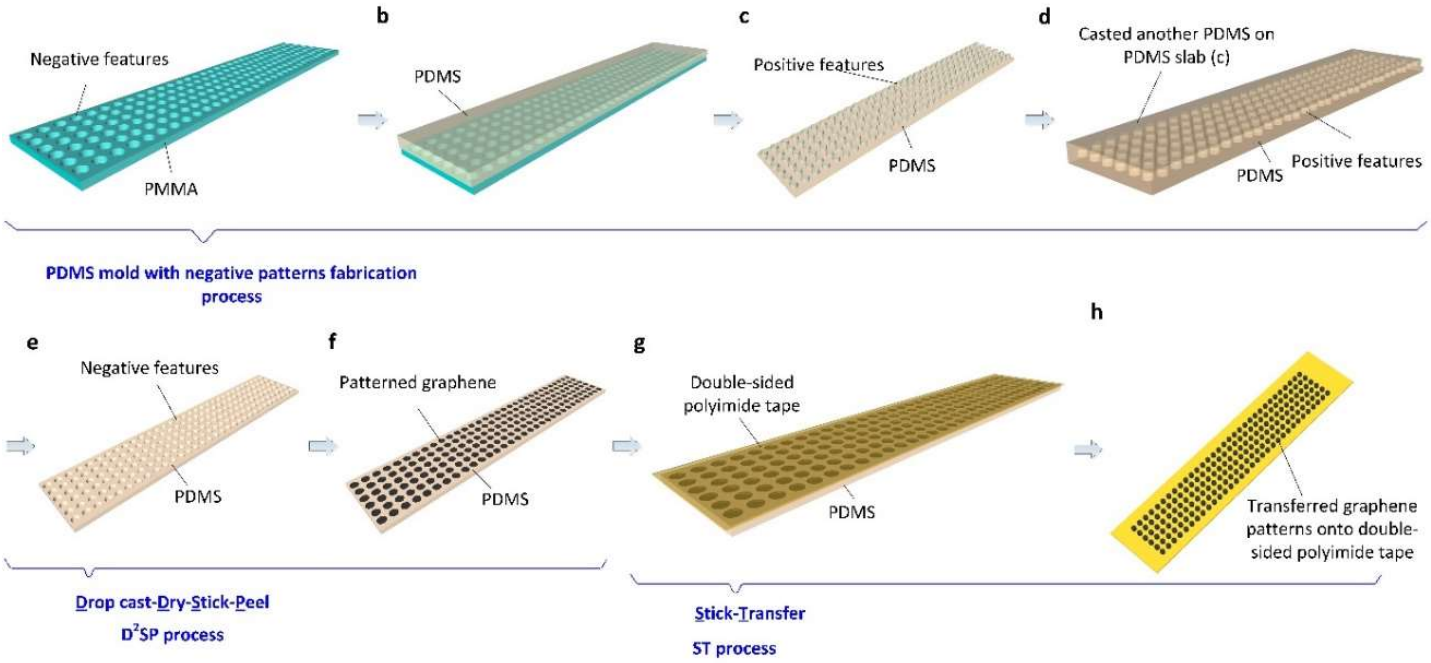

Figure A1. A schematic representation of the formation of graphene patterns on a 1-meter long polyimide tape. (a) Negative features created on a ¼-inch thick poly (methyl methacrylate) or PMMA sheet using a high-precision CNC milling machine. (b) PDMS precursor solution poured over and cured on the patterned PMMA sheet. (c) PDMS mold with positive features peeled off from the PMMA surface. (d) PDMS precursor solution poured over and curved on the PDMS mold with positive features formed in (c). (e) PDMS mold with negative features peeled off from the mold formed in (d). (f) Graphene patterns formed inside the negative patterns at the PDMS surface using the D^2SP method. (g) A double-sided polyimide tape adhered onto the PDMS surface containing the negative patterns. (h) Graphene patterns transferred onto the double-sided polyimide tape and then covered by non-adhesive liner.

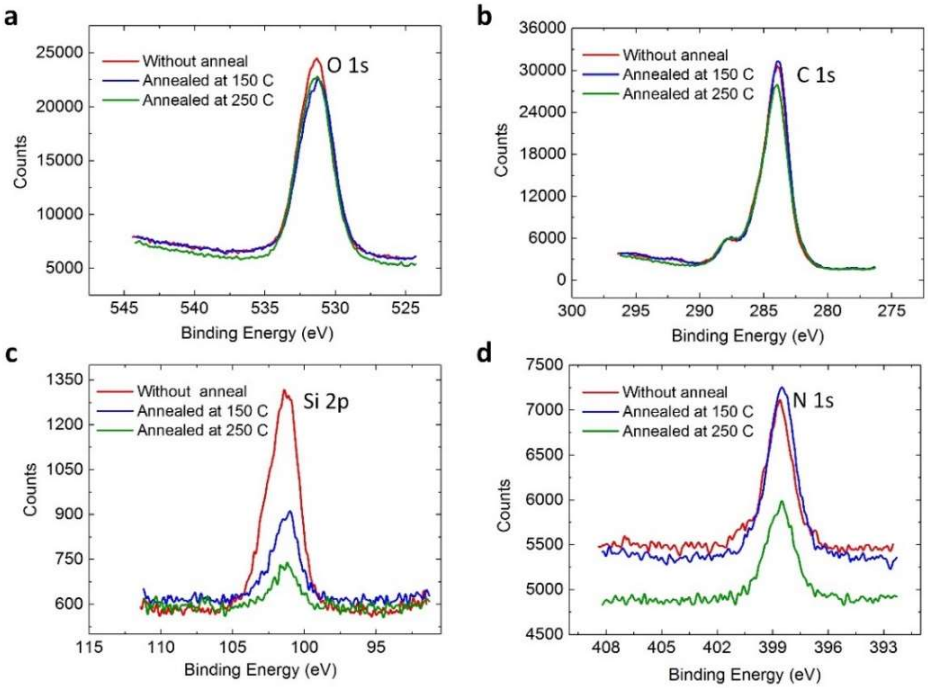

Figure A2. XPS high-resolution spectra of the graphene patterns on a polyimide tape without thermal treatment and annealed at 150 °C and 250 °C for 180 min. (a) O 1s. (b) C 1s. (c) Si 2p. (d) N 1s.

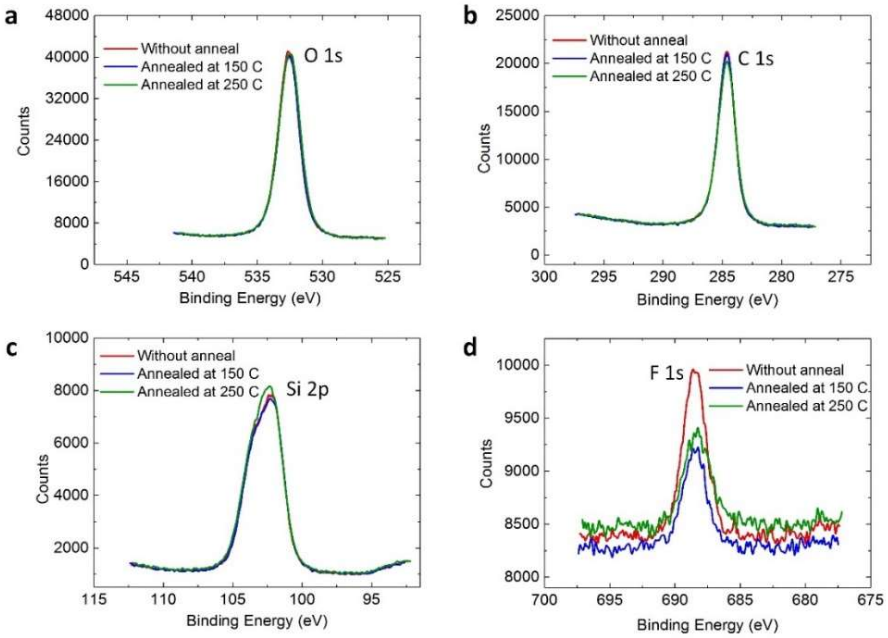

Figure A3. XPS high-resolution spectra of the polyimide tape alone, without thermal treatment and annealed at 150 °C and 250 °C for 180 min. (a) O 1s. (b) C 1s. (c) Si 2p. (d) F 1s.

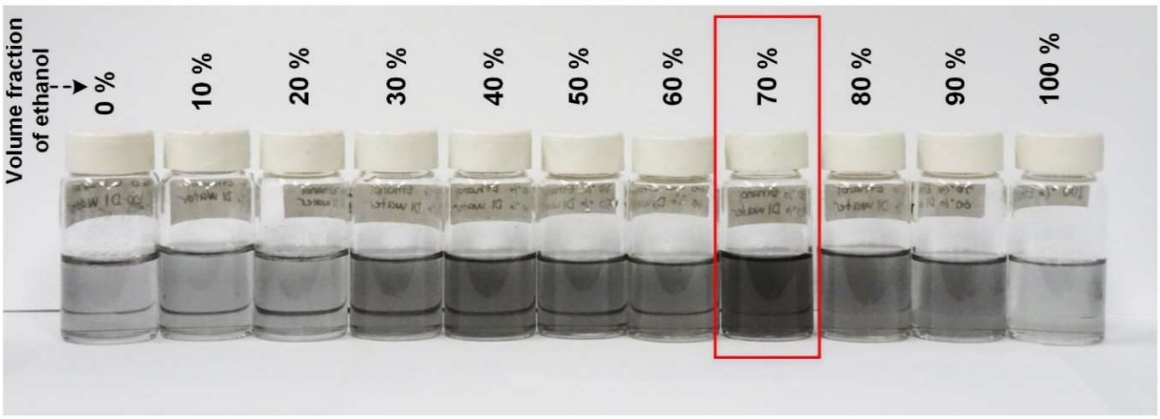

Figure A4. Optical images of graphene dispersions in ethanol and distilled water (DI) mixture with different volume fraction ratios of ethanol.

Essentially, adhesion is achieved due to the molecular contact and surface force formed over the interfacial surface of two materials [60]. Work of adhesion is defined as the energy required to separate two bonded materials by repelling surface force and damaging molecular contact at the interface between two contacting materials, as determined by their surface energies [59]. Removal of the excess graphene from the PDMS surface using a tape in the D^{2}SP process, and subsequent transferring of the formed graphene patterns from the PDMS channel onto a target tape in the ST process result from having the difference of the work of adhesion at the interface of the graphene-tape and the graphene-PDMS. Table A1 presents the surface energies of the materials and work of adhesion (calculated by using Equation 1) when they are bonded with graphene. In our method, for the D^{2}SP process, because $W_{\text{Graphene-PDMS}}$ (55.8 mJ·m^{-2}) < $W_{\text{Graphene-Scotch}}$ (75.8 mJ·m^{-2}; note: the Scotch tape used here use a synthetic rubber adhesive), it is possible to peel off the excess graphene from the PDMS surface. Further, for the ST process, the requirements of $W_{\text{Graphene-PDMS}}$ (55.8 mJ·m^{-2}) < $W_{\text{Graphene-Polyimide}}$ (93.9 mJ·m^{-2}) and $W_{\text{Graphene-PDMS}}$ (55.8 mJ·m^{-2}) < $W_{\text{Graphene-Scotch}}$ (73.9 mJ·m^{-2}; note: the Scotch tape used here has an acrylic adhesive which is also used at the 3M™ and aluminum foil tapes) are also met, thus ensuring the successful transfer of the patterned graphene onto the polyimide, Scotch, 3M™ and aluminum foil tapes.

Table A1. Surface energies of different materials and work of adhesion at the interfaces between two contacting materials utilized in this work

Materials	Surface energy ($mJ \cdot m^{-2}$)			Work of adhesion ($mJ \cdot m^{-2}$)
	γ	γ^{d}	γ^{p}	$W_{A\text{-}B}$
PDMS [61]	19.8	19	0.8	
Graphene [68]	51.6	43.5	8.1	
Polyimide tape [69]	46	44	2	
Scotch tape (Synthetic rubber adhesive) [70]	33.6	33.6	0	
Scotch tape (Acrylic adhesive) [70]	30.2	28.9	1.3	
3M™ conductive tape (Acrylic adhesive) [70]				
Aluminum foil tape (Acrylic adhesive) [70]				
Graphene – PDMS				55.8
Graphene – Polyimide tape				93.9
Graphene – Scotch tape (Synthetic rubber adhesive)				75.8
Graphene– Scotch, 3M™, or Aluminum foil tape (Acrylic adhesive)				73.9